

Portable Thermoelectric Refrigerator

By

Cassandra Beck
Joshua DiMaggio
Ryan Gelinas
Zachary Wilson

Mechanical Engineering Department

California Polytechnic State University

San Luis Obispo

2018

STATEMENT OF DISCLAIMER

Since this project is a result of a class assignment, it has been graded and accepted as fulfillment of the course requirements. Acceptance does not imply technical accuracy or reliability. Any use of information in this report is done at the risk of the user. These risks may include catastrophic failure of the device or infringement of patent or copyright laws. California Polytechnic State University at San Luis Obispo and its staff cannot be held liable for any use or misuse of the project.

Table of Contents

ABSTRACT	5
1.0 INTRODUCTION	5
2.0 BACKGROUND	5
2.1 PATENT RESEARCH	9
2.2 TECHNICAL LITERATURE RESEARCH	9
3.0 OBJECTIVES	11
4.0 CONCEPT DESIGN DEVELOPMENT	13
4.1 DESIGN VARIABLES	13
4.2 DECISION MATRIX	15
4.3 THEORETICAL ANALYSIS	16
4.3.1 CORRUGATE	17
4.3.2 PELTIER HEAT TRANSFER	18
4.3.3 INSULATION	18
5.0 FINAL DESIGN	19
5.1 DESCRIPTION AND LAYOUT	19
5.2 CORRUGATION DESIGN	20
5.3 PELTIER DESIGN	22
5.4 INSULATION DESIGN	24
5.5 CONTROL DESIGN	24
5.5.1 CONTROLLER DESIGN	26
5.5.1.1 PID CONTROLLER	26
5.5.1.2 ANTI-WINDUP SCHEME	27
5.5.2 FILTER DESIGN	29
5.5.2.1 DIGITAL FILTER DESIGN	29
5.5.2.2 KALMAN FILTER DESIGN	30
5.5.3 COMPARISON OF RESULTS	32
5.5.4 FINAL DESIGN	33
5.6 COST ANALYSIS	33
5.7 MATERIAL AND SIZE DECISIONS	34
5.8 SAFETY, REPAIRS, AND MAINTENANCE	34
6.0 MANUFACTURING PLAN	34
6.1 CORRUGATED WALLS	35
6.1.1 STEP BY STEP MANUFACTURING	35
6.1.2 AEROGEL CORRUGATE WALL	38
6.1.3 LID	38

6.2 PELTIER/HEATSINK STACK	39
7.0 DESIGN VERIFICATION PLAN	40
7.1 STRENGTH TESTING	40
7.2 PELTIER ARRANGEMENT TESTING	42
7.3 PELTIER HEAT TRANSFER TESTING	47
7.4 INSULATION TESTING	49
7.4.1 Experimentation	49
7.4.1.1 Fabrication	49
7.4.1.2 Experimental Setup	50
7.4.1.3 Experimental Results	52
7.4.2 Results	54
7.4.2.1 Thermal Analysis and Results	54
A detailed sample analysis can be found in Appendix C.	56
3.5.3.2.2 Results and Discussion	56
7.5 CONTROLS TESTING	57
7.6 PROTOTYPE TESTING	57
8.0 PROJECT MANAGEMENT	60
9.0 CONCLUSION AND RECOMMENDATIONS	61
REFERENCES	62
APPENDIX A: QFD	64
APPENDIX B: Decision Matrices	65
APPENDIX C: Preliminary Insulation Hand Calculations	71
APPENDIX D: Drawing Package	75
APPENDIX E: Simulation Code	82
APPENDIX F: Project Budget	97
APPENDIX G: FMEA	98
APPENDIX H: Safety Hazard Checklist	99
APPENDIX I: Risk Assessment	101
APPENDIX J: Operators' Manual	102
APPENDIX K: Design Verification Plan & Report	103
APPENDIX L: Gantt Chart	104

ABSTRACT

This project created a versatile thermoelectric refrigerator that can be used via a wall outlet. The product is durable and effective. The refrigerator is functional in any ambient temperature, and uses thermoelectric cooling, and work from a standard 120V power outlet. By understanding existing products' limitations and strengths, this project produced a product that outperforms what's currently on the market. Many of the existing products' operating temperature is dependent on the ambient temperature of the surroundings, which is a large drawback. Additionally, most of them take a long time to reach their lowest temperature, around 3 hours. One team member, Josh DiMaggio, did research with the Cal Poly Physics department over the Summer of 2017 on the effectiveness of Peltier devices in refrigeration. Josh discovered that when Peltiers are thermally in series they can create a much larger temperature difference. A Peltier is a thermoelectric cooling device, therefore satisfying the design requirement. Key design challenges included the following: heat transfer through the insulation, power draw, thermodynamic efficiency, structure strength, intuitive interface, along with other crucial factors. Following design, the refrigerator was built, tested, and the preliminary analysis was validated against the test results. There are plenty of existing patents regarding thermoelectric cooling, but only a few like what this project achieved. The final design is presented in this document.

1.0 INTRODUCTION

Throughout the world, refrigeration is a critical means for storing food and perishable resources. Although a vapor-compression cycle is an excellent means of refrigeration, a device that utilizes this cycle can be expensive and difficult to maintain. Another means of refrigeration, thermoelectric cooling, employs the use of a phenomenon known as the Peltier Effect—which requires no working fluid. This project team has been tasked with designing, testing, and manufacturing a refrigeration device that makes use of this effect. The main design objectives of this project are to create a lightweight, compact refrigerator that is inexpensive and reliable.

2.0 BACKGROUND

Current refrigerators that use Peltier devices as the only source of cooling typically have a standard design. Most have one or two Peltier devices, each with a large heatsink and fan on the hot side and a smaller heatsink and fan on the cold side. For some designs, the fans were on top of the heat sinks, and for others the fans were adjacent. Since most refrigerators are similar, a CPU refrigerator was ordered to deconstruct and observe typical internals. This is the bare bones of most refrigerators, with 2 Peltiers, 2 heat sinks, and 2 fans, the layout can be seen in Figure 2.1.

One of the refrigerators that was baselined, the Igloo Iceless TEC Refrigerator, had an interesting design; on the cold side heat sink, there was an added 2-inch cube protrusion. Its sole purpose was to accommodate the geometry of the rest of the refrigerator. Without this added metal, which makes the fin array much less efficient, the heatsink is not in contact with the cold side of the Peltier, hindering heat transfer. This was documented as an inefficient design which was avoided for this project. A photo of the cold side setup can be seen in Figure 2.2.

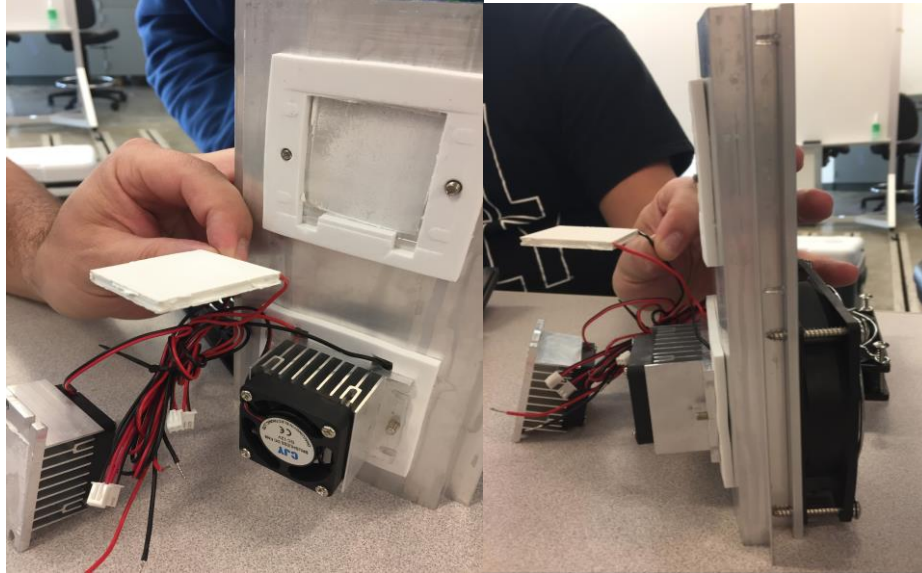


Figure 2.1. On the left is a photo of the cold side of the Peltier, the right photo is a side view of the setup with the top Peltier's fans removed. Side view of the CPU refrigerator, from left to right the setup is cold side fan, cold side heat sink, thermoelectric grease, foam insulation, Peltier, hot side heat sink (much larger than cold side), large fan.

A Peltier/Fan setup that is in an actual cooler design can be seen in Figure 2.2, the inside of the Igloo.



Figure 2.2. Cold side of Peltier setup in the igloo iceless.

The Igloo refrigerator plugs into the 12V outlet in a car, with 6A current draw, and there is an optional 120V adapter that can be purchased if the user desires to use the refrigerator with a wall outlet. This versatility in design was noted and has been incorporated into the design presented in this document. The Igloo refrigerator only uses one Peltier in the lid of the refrigerator and can get to 36°F below ambient. It does, however, take 3 hours empty to achieve this. This became one of the design goals for the new design: reach operating temperature faster than 3 hours, ideally in under 1. The primary insulation used is polystyrene. The predominant customers of this product, as seen in its Amazon reviews, are truck drivers, travelers on road trips, and people keeping personal medicines cold. [1] The main product requirements extrapolated from these reviews include portability, large cooling space, and long life. Figure 2.3 shows the hot side of the Peltier setup, with fan and heatsink adjacent to each other. The only thing resembling a temperature control used in the Igloo is a thermostat sensor that will limit current from flowing to the

Peltier if the temperature becomes too high. This sensor is a safety measure and can be seen in the picture with a yellow wire running to it, screwed into the bottom of the heatsink. Noting this low level of tuneability in the refrigerator, the final design of the refrigerator presented in this document contains fine tune control, with the user able to control chamber temperature down to the degree.



Figure 2.3. Hot side of Peltier setup in the Igloo Iceless Refrigerator.

Another refrigerator that was ordered was the BESTEK 30-quart car refrigerator, which plugged into the 12V outlet in a car. This “refrigerator” has both a heating and a cooling setting, with claims of cooling 45°F below ambient, or up to 140°F for its heating setting. This was a benefit of this design over the Igloo, and the versatility of use led to brainstorming that has driven the design documented in this paper to include a freezing section, cooling section, and the potential to also be made into a heater. This heater/refrigerator draws 4A of current from the 12V source, and weighs 12.8 lb. This device also only uses one Peltier. Some limitations of the products taken apart include: no temperature control, temperature ratings are dependent on ambient temperature, thermal insulation on the sides of the Peltiers is minimal, and usually only one Peltier is used. Noting these limitations, superior design goals have been set for this new design and have been discussed with respect to the competition. Plenty of models of similar car thermoelectric refrigerators are available on Amazon, including the Koolatron and Coleman Powerchill. [2]

Wine refrigerators, such as the Vinotemp V16TEDS also frequently use thermoelectric cooling because it is quiet and doesn’t vibrate like a typical compressor refrigeration design. Many designs using Peltiers have temperature ratings in degrees below ambient, which works well for something which will be stored in a home as the ambient temperature is generally regulated by a thermostat. Unlike the cheaper refrigerators, most wine refrigerators have a temperature control interface, so the user can specify the exact temperature. [3] This adds benefit for the user and has been incorporated into the final design documented in this paper.

Thermoelectric cooling is used in hospital applications, like the Helmer Scientific MLR102 [4]. Research was performed in depth to find information and specifications on these types of hospital thermoelectric refrigerators, however bounded limited results. An interesting thing about the Helmer model is that it claimed to be more energy efficient than a normal refrigerator. From the preliminary research, it appears that TEC cooling is less efficient than normal refrigeration methods.

Over the summer Josh was tasked with furthering the research with the physics department under Dr. Peter Schwartz. The Physics department was analyzing the performance and efficiency of thermoelectric refrigerators and a simple prototype was created, see Figure 2.4, to understand the application of the research. Using mostly recycled materials and a straightforward design, the device achieved freezing

temperatures with relatively small current inputs. Getting to freezing temperatures was accomplished by putting a Peltier back to back with another Peltier to double the possible temperature change.

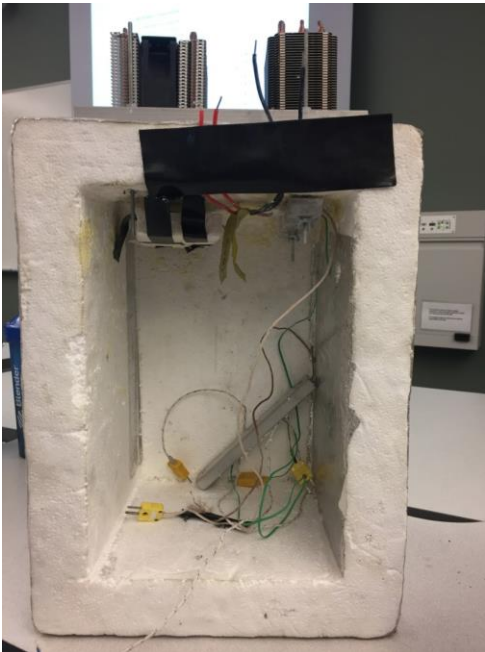


Figure 2.4. Picture of Josh’s summer project. Current configuration is two Peltiers (not stacked) each with a heat pipe fin array to use for heat dissipation from the hot side.

A lot of data was analyzed to determine the greatest efficiency achievable when operating at such low temperatures, which can be seen in Figure 2.5.

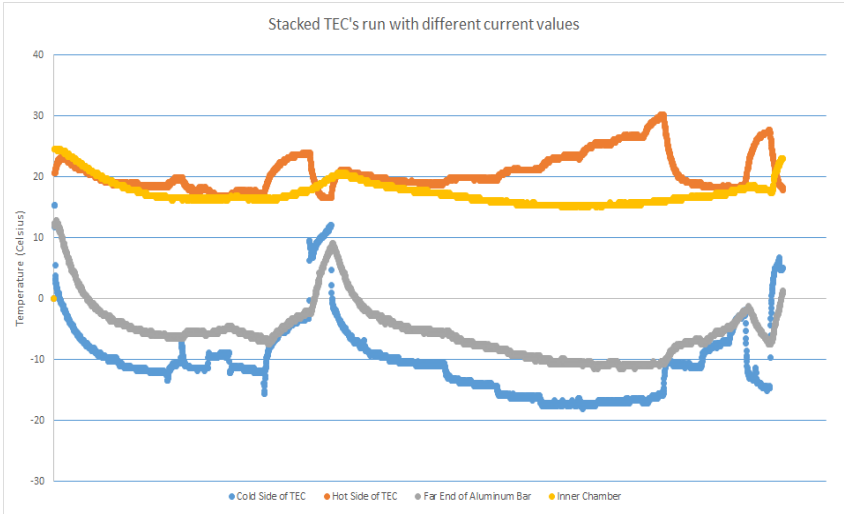


Figure 2.5. Temperature data collected as a result of stacking Peltiers and supplying different currents to each the hot and cold side Peltiers.

The key limiting factor was the heat extraction, due to limited heatsink capabilities. Past a certain threshold, when current was supplied the system it caused it to become oversaturated with heat and a divergence of temperature was observed, and the become an oven. This first test provides many areas for improvement, including: improving the insulation and creating a more durable test device. The Peltier

closest to the inside of the refrigerator is referred to as being on the “cold side” and the Peltier closest to the outside of the refrigerator is referred to as being on the “hot side”. This nomenclature is based upon the heat flow, the Peltier on the outside will physically be hotter than the one on the inside of the refrigerator. The data acquired from the stacked Peltier tests can be seen in Figure 2.5. In the first part of graph, up to the first peak, the hot Peltier is held fixed at 3 amps, while the cold side Peltier is changed from 1-5 amps until it diverges, and the heat extractor is saturated. The next part is where the cold side of the Peltier is held fixed at 3 amps, while the hot side Peltier is changed from 1-8 amps, where 5 amps acted with the largest change in temperature.

2.1 PATENT RESEARCH

There are many patents regarding thermoelectric cooling, some dating back as far as the 1950s. Few employ Peltiers as the primary source of heat extraction, in fact many of the patents used a standard refrigeration cycle’s cool side as the hot side of the Peltier. This design essentially had a thermoelectric freezer and a refrigerant run refrigerator. Other patents found used Peltiers for creative methods of making clear ice. Very few of the patents that were researched employed Peltier stacking as was proposed in the previous section—which made it a good candidate for further research in the scope of this design.

Table 2.1. List of patents relevant to the project.

Patent Number	Inventor/Company and Date	Description
9,759,472	Whirlpool Co. - 12/13/2012	Clear ice maker that utilizes TEC, vibrates ice tray as warm airflow contacts top of water.
9,714,784	Whirlpool Co. - 12/3/2012	Uses the fresh food compartment as the hot side of a TEC module and cools a freezer compartment.
RE39,287	Medical Products Inc. - 7/19/2001	A temperature-controlled cabinet system for use in an ambulance.
US5188286A	William E. Pence IV - 2/23/1993	Temperature control using Peltier elements thermally in series.
US2984077A	Harold V. Gaskill - 10/24/1958	Strips of thermoelectric material with an insulating material between them. Using the properties to create cooling with the first material adjacent to the former, and another set-in series to have a cooling effect.

2.2 TECHNICAL LITERATURE RESEARCH

To create a refrigerator, it is important to research insulation types and methods of cooling the Peltier device itself. Currently Peltiers are only around 10-15% efficient, making the insulation a critical part of the design. The efficiency of the Peltiers is another area that can be researched, as well as the maximum temperature difference that can be achieved across a single Peltier. Research done by Cal Poly students under Dr. Peter Schwartz showed the most effective current rates to flow through specific models of Peltiers to get the highest temperature difference. [5] Refrigerators typically use a type of foam insulation or vacuum insulation panels. The main premise behind the vacuum insulation panels is to reduce heat transfer through conduction and radiation. Vacuum panels can be difficult to keep protected, however, as they must be completely waterproof, and cannot be punctured if the vacuum is to be maintained. The

service life is also extremely variable, with a range of 5-25 years. [6] The material used for insulation also becomes very important, as reducing pore size to a Nano level largely decreases the heat transfer due to conduction. One particular material that was looked into was aerogel, which is silica in which the gelatinous components have been extracted and replaced with air, making it a very light yet effective insulator. Aerogel pores can be as small as 5 nm. [7] Aerogel is brittle, however with reinforcement it may be an excellent choice for this application.

Since Peltiers cool by transferring the heat across them, the coldest temperature they can achieve is limited by the heat extraction on the hot side. There are a variety of Peltiers, that all have different maximum ΔT ratings, with the larger temperature changes being more expensive. Overall, water cooling was found to be the most effective, followed by air cooling. Heat pipes within heatsinks on the hot side of the Peltiers was the most effective at dissipating the heat. Heat pipes are easy to use because the cooling is passive. Forced convection from the Peltier to water was the second most effective way of cooling, followed by natural convection. [8] This same finding was found for air forced and natural convection. Fans and pumps have drawbacks however because they introduce moving components into the system, and no moving parts is one of the main advantages of Peltier cooling. A 3D chart of the findings for temperature and efficiency can be seen in Figure 2.6. For this design a combination of the top two most effective cooling methods has been employed using a water -cooled radiator and fan combination.

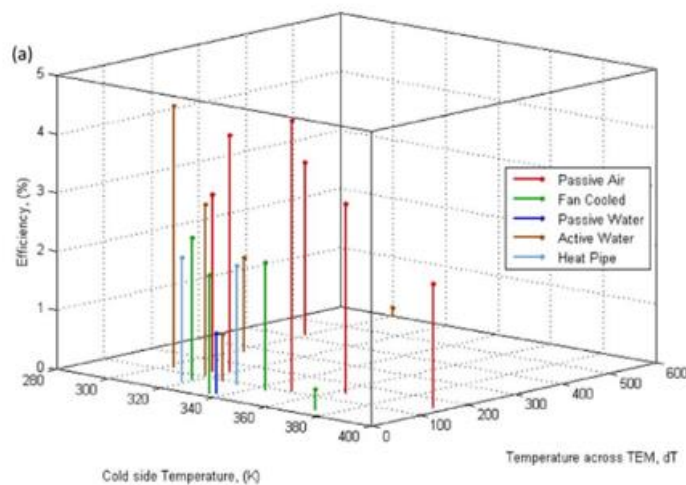


Figure 2.6. This plot shows the results of all the types of cooling tested in the research. [8]

Research published in the Journal of Heat and Mass Transfer shows data from Peltiers in combination. This research found that Peltiers in series can achieve a larger temperature difference than Peltiers in parallel. Further research into stacking Peltiers showed that running different currents through each of the Peltiers can increase the temperature change further, by finding the most efficient current for each. The research also showed that stacking the Peltiers in a pyramid shape as seen in Figure 2.7 produces even larger temperature drops. [9] For this design, Peltiers in series are used, however in initial design stages there were limitations as to how much heat could be transferred from one Peltier to the next, and in some cases did not provide beneficial results. Moving forward, Peltiers that have been manufactured with several semiconductor layers in series will be used. While this does not allow for independent current control it greatly increases the rate of heat transfer between each layer.

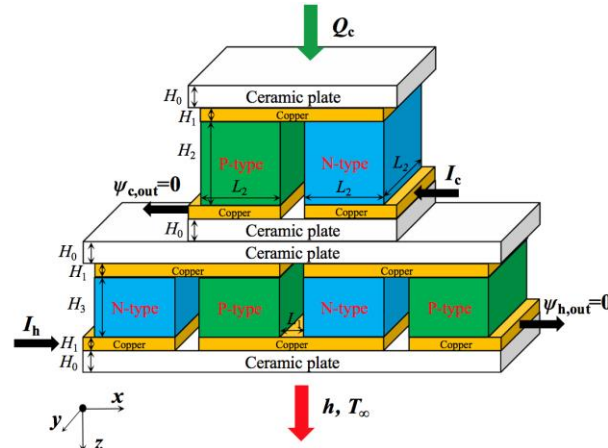


Figure 2.7. Schematic of the two-stage TEC unit. [9]

3.0 OBJECTIVES

The research conducted for this project, goals of the project, engineering specifications, planned design tactics, and communication with the sponsor will be discussed below.

Based on research and communication with the customer, the most important customer needs have been identified. For this product, it is highly desirable for it to be easy to use, portable, and have a low cost. The customer requires that the product has cooling and heating capabilities with a variable temperature setting and a user-friendly interface. In addition, the product must be able to utilize power from a 120V wall outlet. The Problem Statement that defines the scope and goals of this project is as follows:

The goal of this project is to develop a versatile method of refrigeration that can be used by many different people. The product should be cost effective and utilize green materials because the current market has poor quality options that do not meet needs economically or for performance.

A list of engineering specifications was generated based on experience and research as well as customer requirements, displayed in Table 3.1.

Table 3.1. Detailed description of engineering specifications.

Spec. #	Parameter Description	Requirement or Target (units)	Tolerance	Risk	Compliance
1	Capable of Freezing	-10°F	±1°F	L	T, I
2	Maximum Temperature	130°F	Maximum	M	T, I
3	Weight	<30 lb.	±1 lb.	M	T, I

4	Size	≥ 30 quarts	Minimum	L	A
5	Cost	< \$250	Maximum	L	A
6	Temperature Control Speed	30 min	± 2 min	M	T
7	Compressive Loading	400 lb.	Minimum	H	T, I
8	Variable Temperature Range	-10°F to 130°F	± 5°F	M	T, I, S
9	Non-Toxic Materials	-	-	H	A
10	Easy to clean	-	-	L	I
11	Green Design	-	-	M	A
12	Internal Battery	10,000 mAh	± 100 mAh	L	A
13	Works with 12V car power output or solar panels	-	-	L	A, T
14	Capable of Heating	130°F	±1°	M	A
15	Easy User Interface	-	-	L	S
16	Bluetooth (V5)	-	-	L	S

Below is a list of the above specifications with detailed descriptions accompanying them.

- Capable of Freezing - The goal of this project is ultimately to design a product that can reach freezing temperatures, specifically around -10°F

- Maximum Temperature - To ensure that the system doesn't reach potentially dangerous temperatures, the temperature must be regulated with a maximum allowable temperature.
- Weight - The product must be easily lifted by a wide range of people and must not have a potentially dangerous weight.
- Size - The product must have a reasonable amount of storage space.
- Cost - The product must be reasonably priced so that it may be used by many worlds of people.
- Temperature Control Speed - Comparable products have very slow response times, this product must have a response time of about 20 minutes.
- Compressive Loading - The frame of the product must be able to support at least 400 pounds so that it doesn't collapse or break while under a load.
- Variable Temperature Range - A temperature range of -10°F to 130°F is desired to provide cooling as well as heating.

To determine what components of the design were the most important a QFD was created. The QFD specifies who the customers of this product are, the customer's requirements, engineering specifications, also shown in Table 2, and the specific targets to measure whether the design meets the engineering specifications. The full QFD matrix can be seen in Appendix A. In the QFD, current products on the market were compared to the engineering specifications to see how they compared to the design goals of this project. All the current products met, at best, half of the specifications. This shows there is a substantial portion of the market with needs that are unmet, where the design discussed here could flourish.

During this project, there were a multitude of factors that were considered. An important attribute of the project was how much heat transfer will occur between the inside of the refrigerator and the surroundings. This was based on the properties of the insulation as well as the sealing of the refrigerator. The refrigerator needs to be affordable and have a green design, which controlled what packaging and insulation was used. Research into aerogel, silicone, rice hulls, and hemp was conducted to experimentally determine their thermal conductivity when at the design temperatures for the refrigerator. The insulation selected for this application was aerogel as it has the lowest thermal conductivity. For the heat transfer at the Peltier itself a water-cooled radiator has been selected after conducting tests using the standard heat sink and fan and finding it to be an insufficient mode of heat dissipation for this application.

Due to the high performance, multiple layered semiconductor Peltier devices selected the power supply is a crucial design consideration. The system has been designed for use with a 120V standard wall outlet to ensure the Peltiers and fans receive enough power and can cool the chamber in 60 minutes, one of the main design goals of this project—giving it a large advantage over competitor's products.

4.0 CONCEPT DESIGN DEVELOPMENT

To determine the optimal design for this project, many designs were considered. The considered designs are discussed in the following sections.

4.1 DESIGN VARIABLES

To select the best overall design for the refrigerator each component needed to be analyzed to determine the best option for each. These main components are: insulation type, Peltier type and arrangement, wall material and design, size, and lid sealing.

The Peltiers are made up of an arrangement of semiconductors. Each Peltier is rated for a different maximum current; however, it is not the most important factor in determining the amount of heat it can displace. The size becomes increasingly important as the Peltiers are stacked. Stacking arrangements include multiple Peltiers in series or Peltiers in a pyramid shape. Stacking is a more complicated

phenomenon than the simple single Peltier system. As research has shown, temperature difference is not a simple linear model when it comes to the arrangement of Peltiers. This design variable was iterated during testing to determine the most appropriate style and model. According to research and data received from the Physics department, stacking Peltiers in series produced the largest temperature difference. After testing the Peltier configurations, it was determined that the stacked Peltiers were not performing as well as recorded in previous studies. The solution to this was to purchase a multi-stage Peltier model from totech. This provides the same effect as a Peltier stack but with better heat transfer between the stages, which was likely what was causing the tested configuration to perform so inefficiently.

This relates to another important aspect of the heat transfer design--the size and design of the heat sinks. In the results that were taken from the Peltiers the ambient inside air of the refrigerator has a vastly different time constant than the cold side of the Peltier and optimizing the design of the refrigerator includes minimizing this difference. Types and sizes of heat sinks in conjunction with fans were tested and it was determined that a CPU cooler would provide the largest heat transfer rate from the hot side of the Peltier.

The wall material is another one of the decisions that was mostly based on accessibility to composite structures themselves. The idea for plastic injection molding like other refrigerators however good, is a more industrial style of design solution. Access to new research out of the composites lab at Cal Poly allows for more flexibility of structural design. Although plastic injection molding is typically used, it doesn't mean that it is the best option for this application. For this refrigerator design, only one will be made, and there needs to be a good amount of space in the walls for whichever insulation is chosen. Because most refrigerators use an air gap or some foam, the proper way to make space and to also have strength is to corrugate the composite material. Several common shapes can be seen in Figure 3.16. There are many different shapes in which material can be corrugated. To determine the best corrugation style, one of the papers coming from research done in the composites lab on Cal Poly's campus by Riley Hilliker, Jalen Mano, Isaac Blundell and Eltahry Elghandour was used [10].

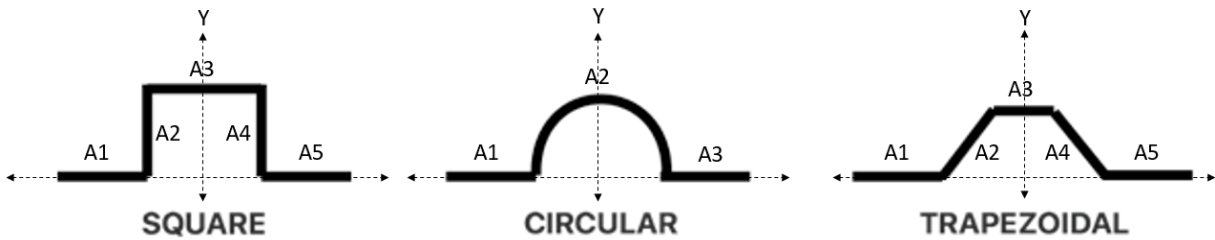


Figure 4.1. Original axis and sections used in analysis by section

Although the square shape was considered due to the ease of insulation installment, ultimately the trapezoidal shape was chosen for ease of manufacturing. The main difference between the shapes is their structural performance, with the trapezoidal shape being able to withstand a larger load. Both maximum loads of are well above the design criteria however, so it was not a factor for selection.

Size was selected based on a variety of factors, most notably the portability factor. To accomplish a key aspect of the problem statement, portability and adaptability, a smaller area will be easier to cool with less power and be lighter when moving it in and out of a car and or space. Size decisions were also made qualitatively based on the research from the existing products and customer feedback on those products. The size is additionally constrained by the size of the back seat in a car and where the fan outlet and inlets were going to be placed. All these factors were considered together, even though there is no one solution as to how it should be solved, the size was chosen to be 8 square feet.

A lid design solution that has been seen in a lot of current product is a bezel that comes down from the lid into the space, with a seal along the top. A similar design has been used here. The refrigerator will also be structurally sound to withstand someone sitting on it or using it as a stool.

4.2 DECISION MATRIX

Using the main ideas from the Pugh matrices, seen in Appendix B, decision matrices were developed to compare these ideas. Table 4.1 is a list of the different combinations of the top decisions for each element, to create 10 ideas for an overall model.

Table 4.1. Possible design ideas for the Peltier refrigerator.

Combinations	Peltier Placement	Control Location	Lid	Insulation	Structural
1	Lid	LCD on side	Hinged	Aerogel	Rounded inside corners
2	Ends	LCD on lid	Off	Rice hulls	Sharp corners
3	One side	LCD on side	Hinged	Fiberglass	Soft corners
4	Ends	LCD on side	Hinged	Aerogel	Sharp corners
5	One side	LCD on side	Off	Aerogel	Rounded inside corners
6	Ends	LCD on side	Slide	Fiberglass	Sharp corners
7	Lid	LCD on side	Off	Aerogel	Sharp corners
8	Ends	LCD on lid	Hinged	Fiberglass	Soft corners
9	Ends	LCD on side	Off	Rice hulls	Soft corners
10	One side	LCD on lid	Slide	Rice hulls	Rounded inside corners

Table 4.2 shows the combinations from Table 3 compared to the engineering specifications from the house of quality, as seen in Appendix A. Using weighted analysis for each specification combinations 4 and 7 were determined to be the best. To create a more unique product, combination 4 was selected.

Table 4.2. Decision matrix comparing the combinations formed in Table 3.

Decision Matrix Analysis							
Engineering Specs:	Capable of Freezing	Maintain Temp Unplugged	Compressive Loading	Weight	Size	Cost	Totals
Weights:	5	1	3	4	3	1	
1	5	5	5	5	4	1	78
2	3	3	5	4	5	5	69
3	4	4	5	3	4	3	66
4	5	5	5	5	5	1	81
5	5	5	5	5	4	1	78
6	4	4	5	3	5	3	69
7	5	5	5	5	5	1	81
8	4	4	5	3	4	3	66
9	3	3	5	4	4	5	66
10	3	3	5	4	4	5	66

4.3 THEORETICAL ANALYSIS

Engineering analysis techniques have been utilized to predict the behavior of the different components of the product. Analysis such as Finite Element Analysis was used to support the design of the structural aspects of this project and determine likely areas of failure. The theoretical thermal analysis for the Peltiers was determined by plots of heat transfer, input current, and coefficient of performance versus temperature difference on tetch's website. Further heat transfer analysis was conducted for other areas of the refrigerator design.

4.3.1 CORRUGATE

A finite element analysis was done to determine the locations of the stress concentrations on the corrugated panels. As seen in Figure 4.2, there will be a stress concentration where the moment is the largest at the edge of a cut corrugated panel. This will not be an issue as there will be an angle that connects the cut sides to each other to form a right angle of the box itself. However, for clarity sake, the FEA does point out where the concentrations will be, and nothing to point out on the distributed lid and or bottom of the box itself.

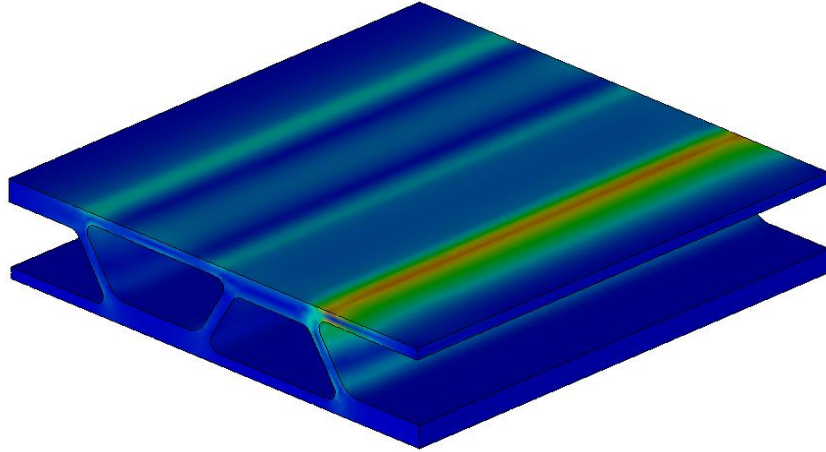


Figure 4.2. FEA distributed load along the top of a corrugated panel.

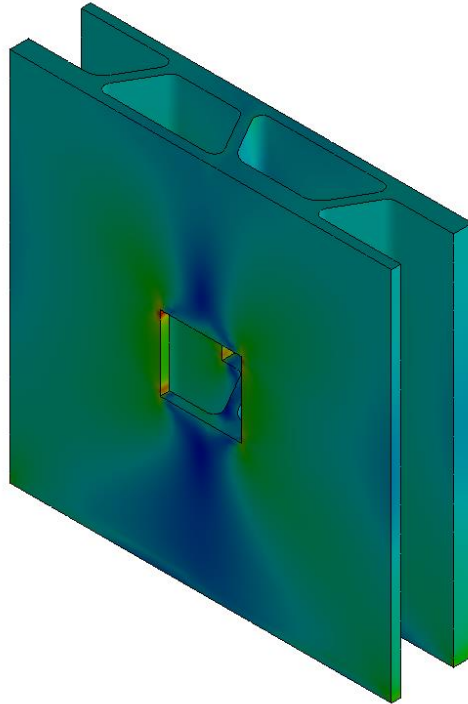


Figure 4.3. Square cutout representing the access for the Peltier stack to protrude and the heat to be extracted through.

Figure 4.3 shows the FEA of the wall of the box as seen from a top down compressive load as predicted for use. From the figure you can see that at the edges of the square cutout will have a stress concentration,

however from testing, the walls were overbuilt to easily account for these loads. Testing was also done on corrugated samples to prove the strength of two-layer fiberglass corrugated structures.

4.3.2 PELTIER HEAT TRANSFER

In order to determine the performance of the refrigerator with the Peltiers ordered a MATLAB script was written to produce a plot of the total heat transfer out of the refrigerator, shown in Figure 4.3.

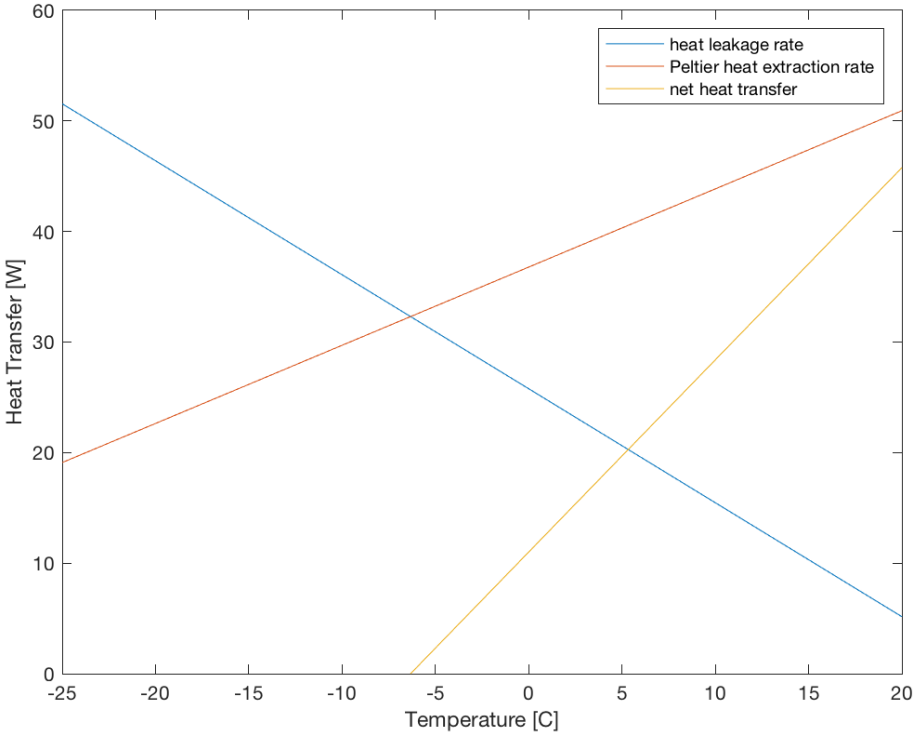


Figure 4.3. Plot of the heat transfer out of the refrigerator versus temperature.

The operating range of this refrigerator is 0 to 20°C, so Figure 4.3 provides a prediction of the net heat transfer out of the refrigerator accounting for the heat leakage into the refrigerator and the heat transfer out of refrigerator by the Peltiers. This plot shows what is anticipated, the heat transfer rate will be much larger when the difference in temperature between the chamber and ambient is closer together. It also shows that with the current design, the refrigerator will be unable to reach the 10°F goal, as the Peltiers and heat leakage will reach an equilibrium.

4.3.3 INSULATION

Most coolers and refrigerators use polystyrene or polyurethane to insulate them. There are many other materials that have not been investigated for use in this type of application. A basic heat transfer analysis using the thermal resistance approach through one wall for temperatures ranging from -10F to 77F, standard ambient, produced a comparison of the top choices for insulation. The new types of insulation analyzed were: silica aerogel, fiberglass batting, cellulose, and rice hulls. These results were plotted against the results of polyurethane and polystyrene which serve as a basis for comparison to current production refrigerators. The results of this analysis can be seen in Figure 4.4 and the hand calculations can be found

in Appendix C. The size of the refrigerator has a linear relationship with how much heat is transferred, and therefore the refrigerator should be kept to the minimum size possible for the engineering specifications.

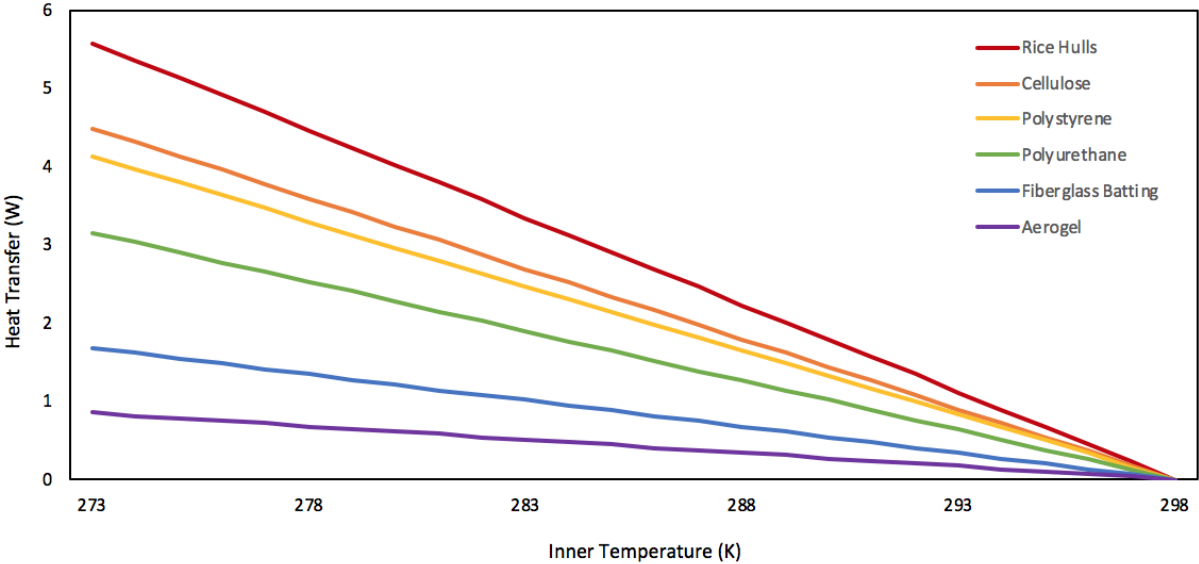


Figure 4.4. Heat transfer modeled through one wall of the refrigerator versus inside temperature of the refrigerator. Thermal conductivities determined through research papers. [\[6\]](#) [\[11\]](#) [\[12\]](#) [\[13\]](#) [\[14\]](#)

5.0 FINAL DESIGN

The analysis and testing that was run to determine the optimal design for the refrigerator will be discussed below.

5.1 DESCRIPTION AND LAYOUT

The concept CAD model of the design that was chosen, created in SolidWorks, is displayed below in Figure 5.1. All key components of the design are shown qualitatively in the model, with descriptions below. The model shown below demonstrates the integration of all the elements and their respective locations. A complete drawing package can be found in Appendix D.

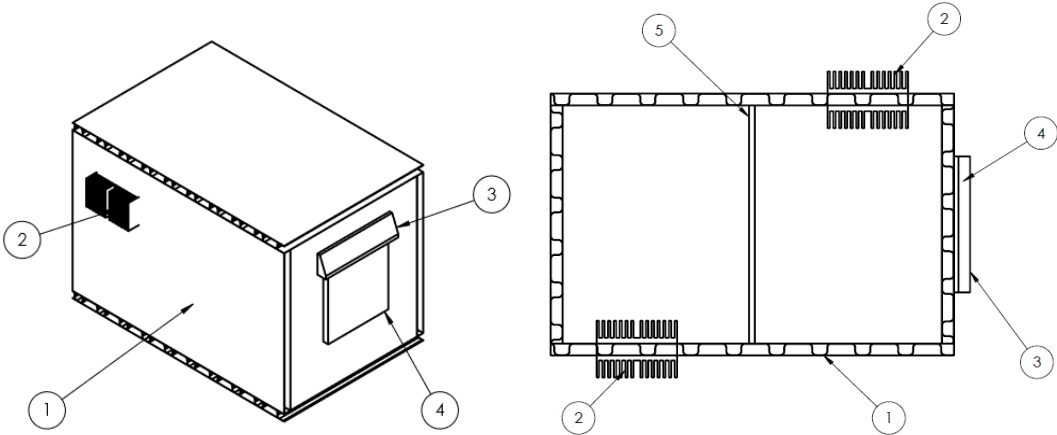


Figure 5.1. Concept CAD Model displaying all key components to be implemented. Isometric view (left) and top section view (right).

1. The square-shaped fiberglass corrugation pattern initially chosen to be used in this design. The air pockets were filled with Aerogel material to provide insulation, while the fiberglass corrugation provides support.
2. Peltier stack, heatsink, and fan combination. Two Peltier stacks were used to accomplish the desired heat transfer rate, as predicted by experimental data. CPU fans and heat sinks were selected to properly circulate the air to provide adequate heat transfer.
3. User interface including a keypad and an LCD screen displaying the desired temperatures and the actual temperatures of each chamber. This was not built into this design but is kept to show how the controls could be integrated in a future build.
4. Module containing the necessary electronics as well as a MicroPython board regulating the controls and current flow to each device.
5. Removable insulated partition separating the two chambers allowing for two different temperatures.

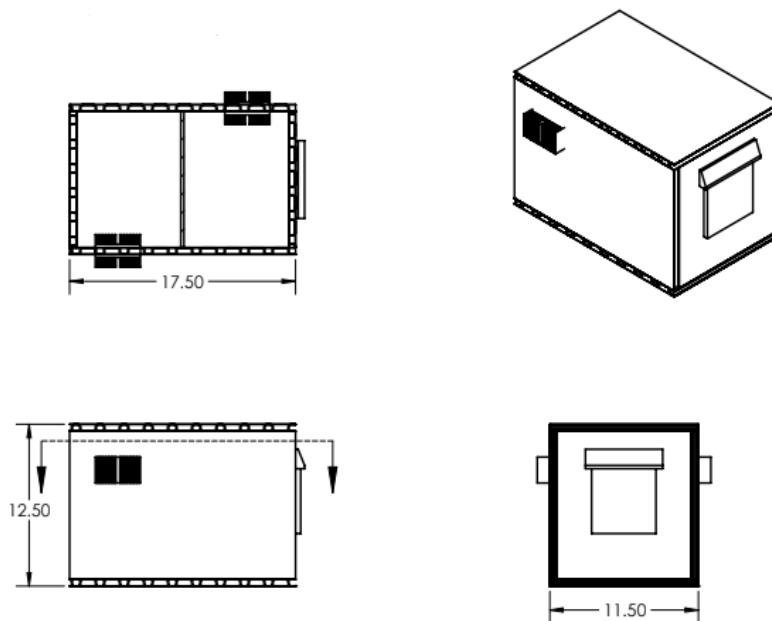


Figure 5.2. Isometric view of refrigerator showing wall dimensions.

5.2 CORRUGATION DESIGN

The choice of using corrugation was made for both strength and insulating properties. If you separate two planes by a web you get a small I-beam. As known from statics and strength of materials classes, separating the plates more will lead to more strength. Also known from heat transfer courses that air is a great insulator, known also from common refrigerators in practice. If a layer of air is trapped, i.e. (jackets, refrigerators, refrigerators, building walls, etc.) then the insulating properties go up as per section 4.3.3 of this report.

Initially a square design had been chosen, which would have been simpler to add insulation to, however in practice the manufacturing was a lot harder to do. The square design has almost vertical walls that when curing composites can be a hassle to have complete contact with the form, the mold can be seen in Figure 5.3. Because the corrugation will be much stronger than the intended design specs, a trapezoidal shape was selected. Using a trapezoid yields the same air space, just a little more complicated to put the insulation into. The Aerogel that was chosen is semi fibrous but will still be very sufficient to fulfill the insulating needs and goals.

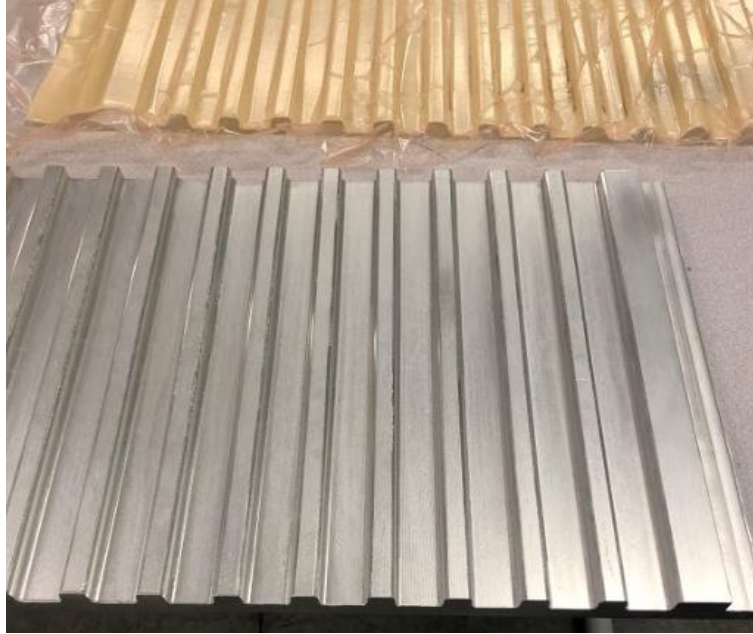


Figure 5.3. Square corrugated structure manufacturing test, concept proven impractical.

As you can see in the photo above, the structure is very close to exactly square and forming the fiberglass to sit exactly in the mold is very difficult in practice, so this shape was not used. A trapezoidal shape was used as shown in Figure 5.4.



Figure 5.4. Trapezoidal shape being prepared with carbon fiber

As shown in Figure 5.4, the trapezoidal shape fits in the mold and releases much easier because of the relief angles. Thus, the trapezoid shape was chosen for this design. A cross section with dimensions of the shape can be seen in Figure 5.5.

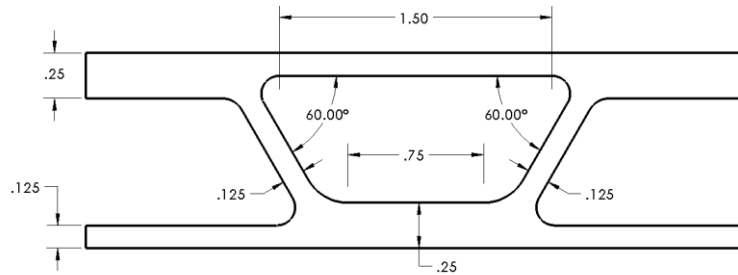


Figure 5.5. Trapezoidal dimensions in inches for corrugated structure.

As Figure 5.5 shows, the corrugated structures are built with three separate pieces then epoxied together to make a corrugated panel. With the corrugation being cured independently, the relief angle you can see is much greater with the trapezoidal shape than the square shape, this creates better manufacturability.

5.3 PELTIER DESIGN

The ordered Peltiers were multi-stage models from tetch. A multi-stage module is one in which there are multiple layers of semiconductors within one Peltier. This provides the same benefits for heat transfer as the stacked Peltier configurations researched in this paper without the limitations of heat transfer between the two modules. The particular model ordered, TE-2-(127-127)-1.15, has two stages of semi-conductors of different thicknesses. Figure 5.6 shows a schematic of the module, where it can be seen the thicker of the two stages is on the cold side.

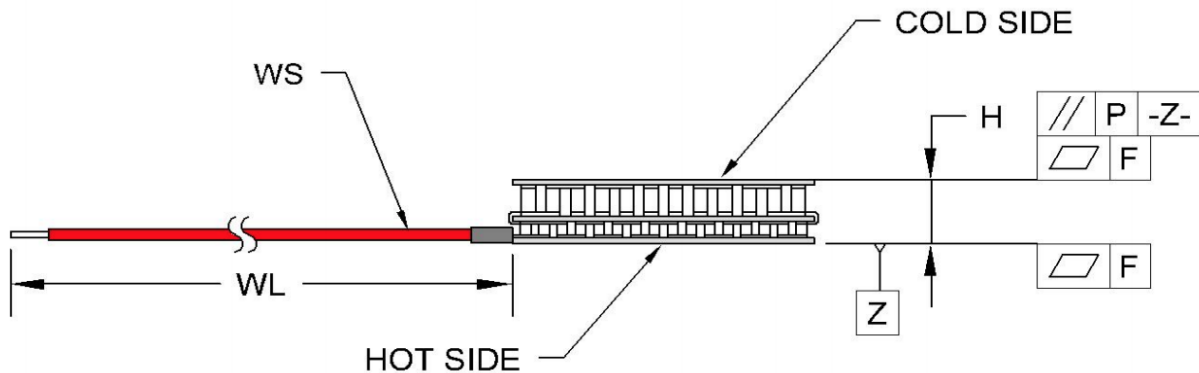


Figure 5.6. Tetch model TE-2-(127-127)-1.15 schematic. [15]

The refrigerator runs two of these Peltier devices in order to achieve desired temperatures within the refrigerator. Upon analyzing provided thermal plots for the Peltier device, 4.5A was selected as the operating current. As can be seen in Figure 5.7, 4.5A is the current required at 12V for the smallest temperature differences, and it drops down to 4A for subsequently larger differences. As the temperature inside the chamber becomes lower the amperage will be reduced to reflect the optimum current for that temperature difference. However, it is likely that the input will always be 4.5A because the maximum temperature difference we expect for the refrigerator is about 60°F, or 15°C.

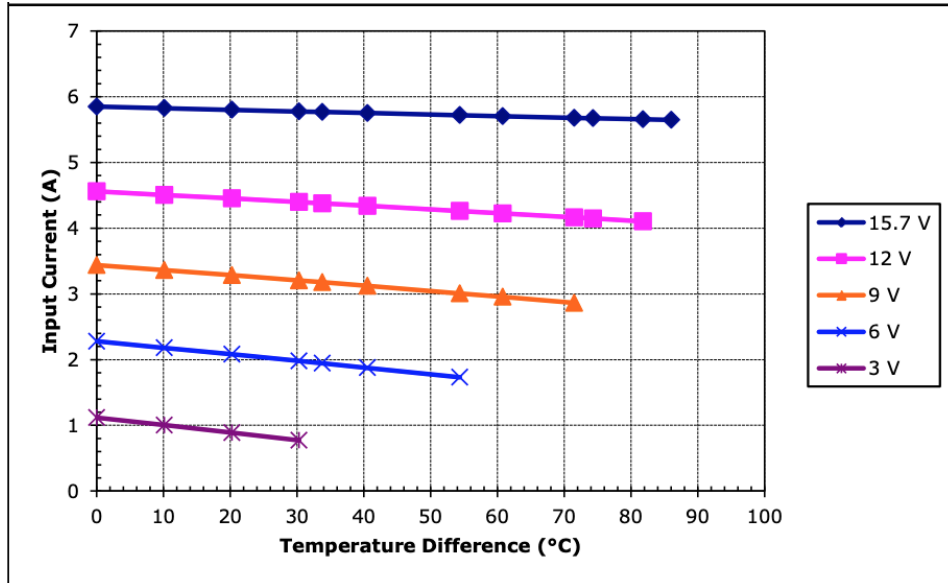


Figure 5.7. Provided input current versus temperature difference for ttech Peltier model TE-2-(127-127)-1.15. [15]

Similarly, the heat removed can be estimated by Figure 5.8. For 12V and 15°C the anticipated heat removed is 24W.

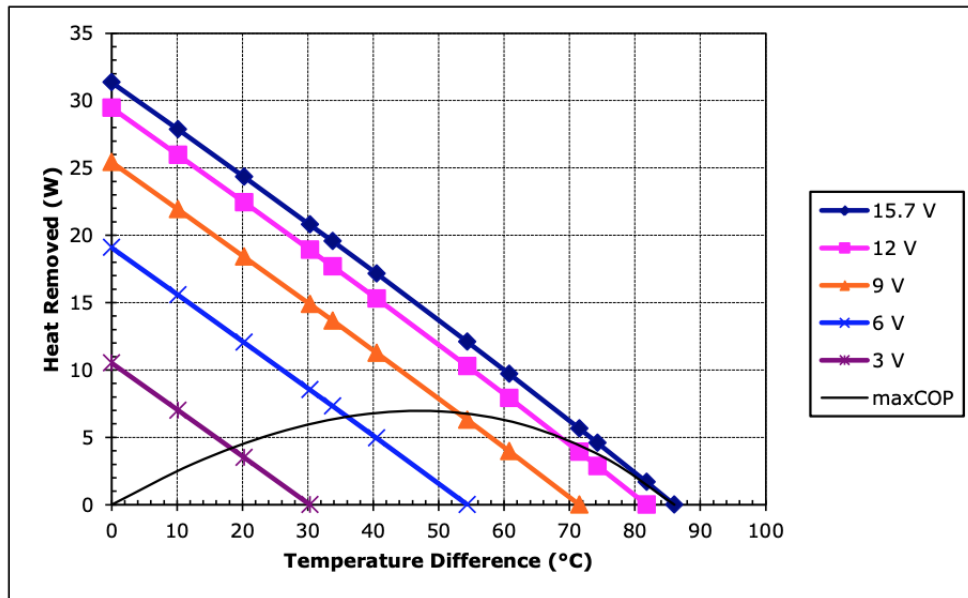


Figure 5.8. Provided heat transfer data versus temperature difference for ttech Peltier model TE-2-(127-127)-1.15. [15]

In order to maximize the heat dissipated from the hot side, which ensures maximum performance of the Peltier, model H60 CPU cooler was purchased from Corsair. The interface to the Peltier is a copper plate with pre-applied thermal paste for the best conductivity to the CPU cooler. The heat is then transferred to coolant which runs through piping from the backside of the Peltier interface through a radiator equipped with a fan which cools the coolant before it returns to the Peltier interface. As previous research showed, water-cooled forced convection was the most efficient method of heat extraction for the Peltiers.

Additionally, it utilizes a similar system to that used in a full-size Refrigerator, with the added fan to increase convection levels. Figure 5.9 shows the front and back views of the CPU cooler.



Figure 5.9 Front and back images of the Corsair series H60 CPU cooler. [16]

The radiator/fan component of the refrigerator was fixed perpendicular to the walls of the refrigerator to supply the cooling air supply. This configuration allows for the best air movement through the system.

5.4 INSULATION DESIGN

Aerogel was selected as the insulation for the refrigerator as it outperformed other tested and researched materials, with a thermal conductivity of 0.0305 W/mK in the temperature range 0°C to 30°C, which is the designed temperature difference across the walls of the refrigerator. The aerogel was cut and installed in the space left in the wall by the corrugate, Figure 5.10 shows the aerogel installed in the wall.



Figure 5.10. Top view of two glued walls, with aerogel installed.

5.5 CONTROL DESIGN

To design a robust controller, a simulation was run to determine the response of the system using time constants and system gains determined from experimental data. These values are displayed in Table 5.1.

Table 5.1. Tabulated system time constants and gains from experimental data.

System	Time Constant (min)	System Gain (-)
Peltier Element Temperature	6.1667	9.5667
Inner Chamber Temperature	13.417	0.5234

The system was modeled as two first order systems, in which the Peltier element system served as the input to the inner chamber model. Process noise and measurement noise was included in the simulation as a random Gaussian distribution that made the inner chamber temperature vary by $\pm 1^\circ\text{F}$. A simple PID controller was used as the initial control law, with an electrical current being the actuated signal sent to the Peltier element model. The system model included a saturation block that limited the actuated current to 6A. The results of this simulation can be seen in Figures 5.11 and 5.12. In this simulation, the ambient temperature was 90°F and the desired inner chamber temperature was 22°F .

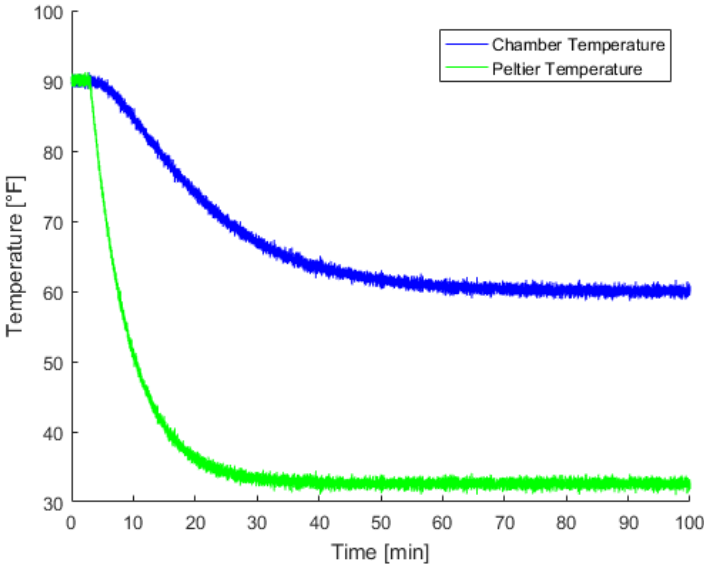


Figure 5.11. System response with original system gains.

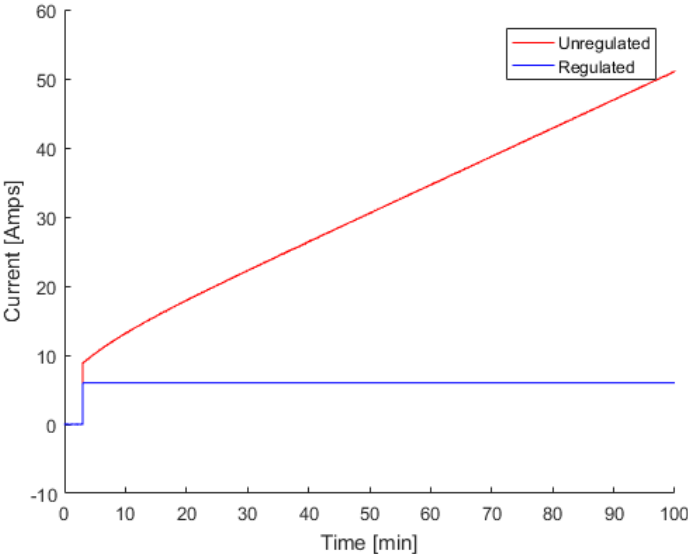


Figure 5.12. Unregulated and regulated actuator signal with original system gains.

The results of the simulation indicated that the time constants of the system were adequate, but the current system gains only allowed the inner chamber to reach a temperature 30°F below the ambient temperature. In addition, the actuator signal immediately saturates and diverges. This result indicates that the gains of the physical system currently do not meet the design requirements. Table 5.2 shows the new system

parameters that will achieve the design requirements. These new parameters will be used in the simulation to properly design the control law.

Table 5.2. New system time constants and gains used to design the controller.

System	Time Constant (min)	System Gain (-)
Peltier Element Temperature	6.1667	18.0
Inner Chamber Temperature	13.417	0.75

Multiple control schemes and filters were considered to control the system and to filter the feedback signal, which will be discussed below.

5.5.1 CONTROLLER DESIGN

The two controller designs considered will be discussed below. These will include a simple PID controller and a PID controller with an Anti-Windup scheme. The results of the simulations indicate that the optimal controller design for this system is a PID controller with an Anti-Windup scheme.

5.5.1.1 PID CONTROLLER

Figure 5.13 shows the block diagram of a simple PID controller that was tested in the simulation. The error signal was fed through the proportional, integral, and derivative branches shown in the block diagram, and fed through a saturation block before being sent through the system model.

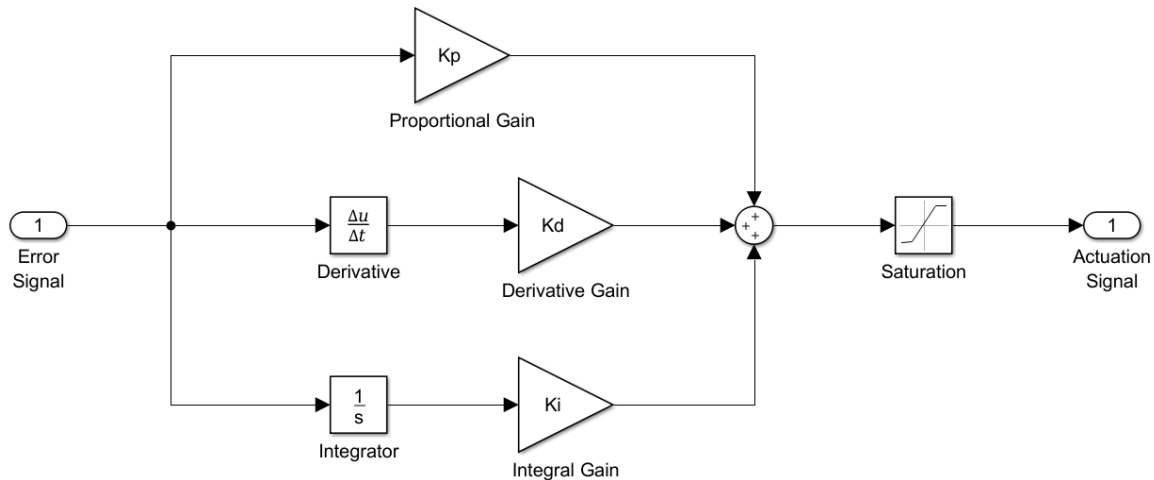


Figure 5.13. Block diagram of simple PID controller with a saturation block.

The results of the simulation with this controller can be seen in Figures 5.14 and 5.15. Again, the ambient temperature for this simulation was 90°F and the desired chamber temperature was 22°F.

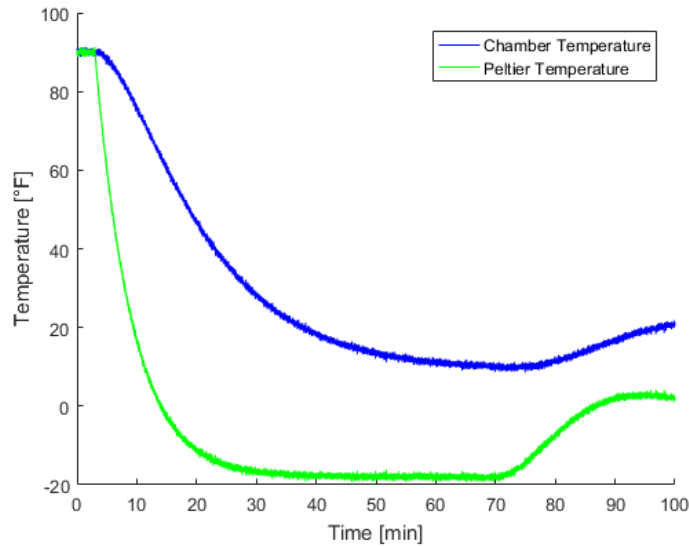


Figure 5.14. System response with a simple PID controller.

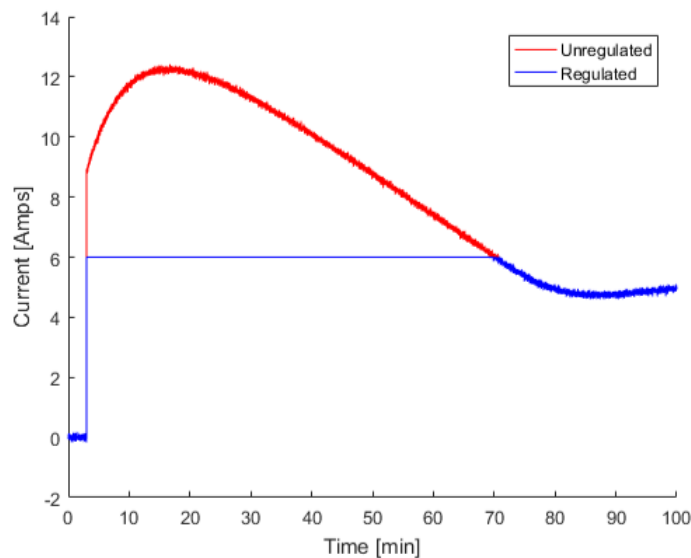


Figure 5.15. Unregulated and regulated actuator signal with a simple PID controller.

Due to the very slow response of the system, the actuator signal saturates immediately. This causes the error to accumulate because of the integral branch of the PID controller. Because an excessive amount of error accumulates, it takes a long time for the controller to realize that the desired temperature has been reached. This causes the temperature to overshoot the desired value and then reaches the desired value after the error de-accumulates. The overshoot is undesirable; thus, a more advanced controller is required to dissuade the system from saturating for extended periods of time.

5.5.1.2 ANTI-WINDUP SCHEME

Figure 5.16 shows a block diagram of a PID controller with the addition of an Anti-Windup scheme. In addition to the three branches of the PID controller, another feedback loop is incorporated. The difference between the saturated and unsaturated signals is taken and subtracted from the integral branch of the PID controller. This minimizes the error accumulation during the times the actuated signal is saturated.

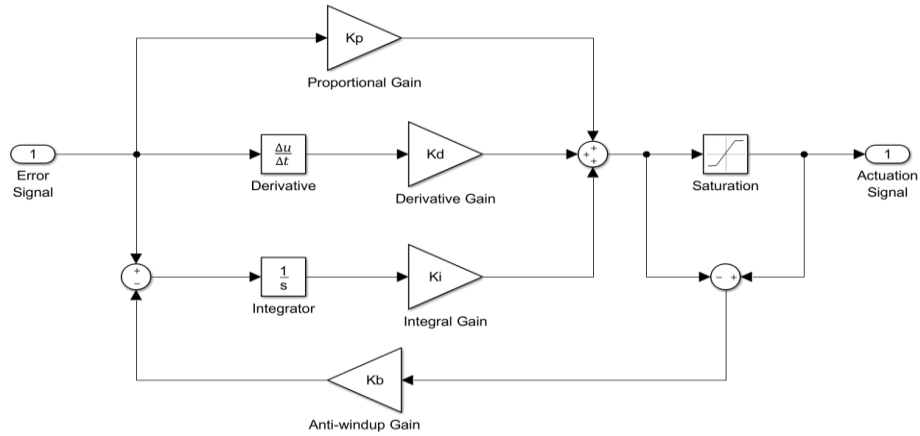


Figure 5.16. Block diagram of a PID controller with an Anti-Windup scheme.

The simulation was run with the same ambient and desired temperature settings as the previous, with the Anti-Windup scheme discussed above. Figures 5.17 and 5.18 show the improved response of the system due to the Anti-Windup scheme.

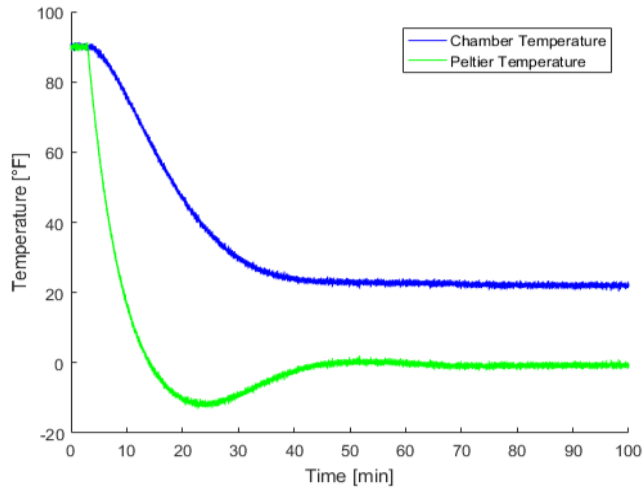


Figure 5.17. System response with a PID controller with an Anti-Windup scheme.

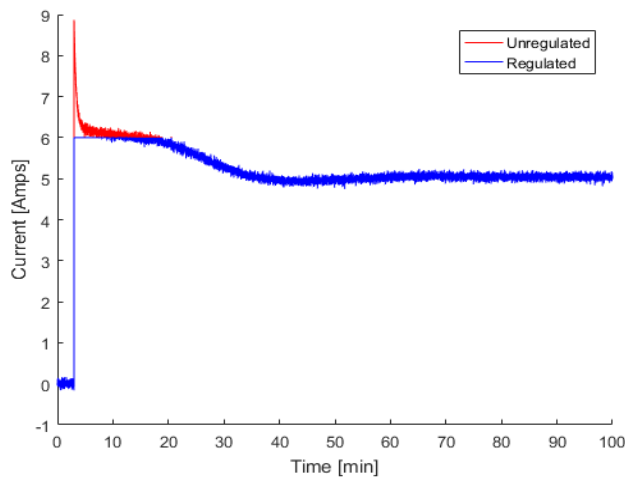


Figure 5.18. Unregulated and regulated actuator signal with a simple PID controller.

The results clearly indicate that the error buildup is quickly corrected by the Anti-Windup scheme. The inner chamber temperature no longer overshoots and reaches steady state at the desired value of 22°F. Based on the response of the simulated system, this controller design was deemed proficient and will be incorporated in the final design.

In this simulation, it was found that the addition of derivative control did not improve the response of the system. Because the system saturates immediately, any added effort to the actuator signal during the transient response due to derivative control has no effect on the results. Thus, proportional control, integral control, and the Anti-Windup scheme were the only necessary components to incorporate in this design.

5.5.2 FILTER DESIGN

The three filter designs that were considered will be discussed below. These include a digital filter, and two different iterations of a Kalman Filter. Due to the noisy nature of thermocouples that will be used in the actual system to measure data, it was deemed necessary to use a Kalman Filter for this design.

5.5.2.1 DIGITAL FILTER DESIGN

The first filter that was considered for this system was a low-pass digital filter that served to filter the high-frequency noise that was assumed to be present in the system. This is incorporated by taking the noisy signal as the input to the differential equation displayed in Equation 5.1,

$$x_k = \frac{\tau_f}{\tau_f + \Delta t} x_{k-1} + \frac{\Delta t}{\tau_f + \Delta t} u_k \quad (5.1)$$

where τ_f is the time constant of the filter, Δt is the discrete time step of the simulation, and u_k is the noisy signal. The response of the system is shown below in Figures 5.19 and 5.20, with a filter time constant of 5 seconds and a timestep of 0.5 seconds.

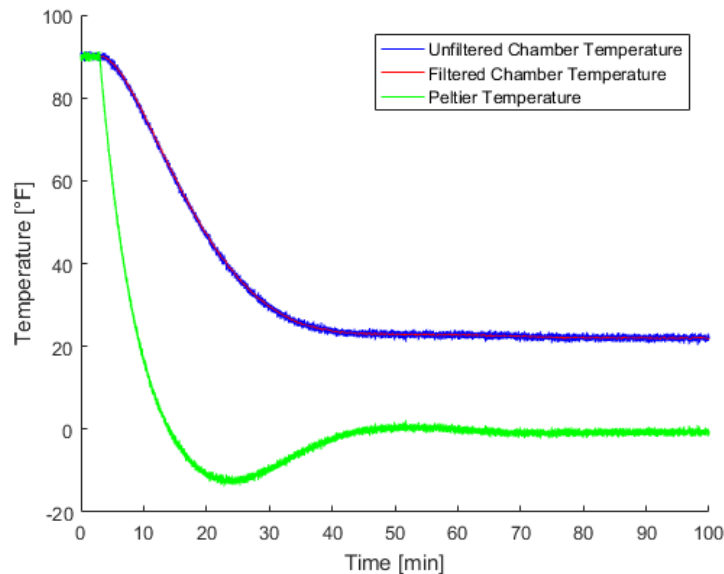


Figure 5.19. System response with the addition of a digital filter.

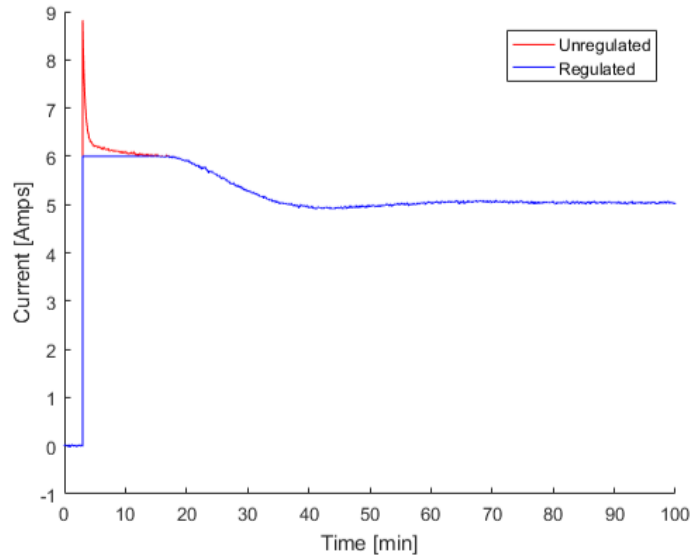


Figure 5.20. Unregulated and regulated actuator signal with the addition of a digital filter.

The addition of the digital filter does not have any significant effect on the system response. However, the actuated signal as well as the feedback signal sent to the controller is much less noisy. While these results are adequate, different filter designs were also considered.

5.5.2.2 KALMAN FILTER DESIGN

The Kalman Filter is a robust form of a discrete state estimator that optimizes its own parameters while filtering a noisy signal. The filter works by running a discrete dynamic simulation of the system based on the input to the system and the measured state of the system. A block diagram of the Kalman Filter is displayed in Figure 5.21.

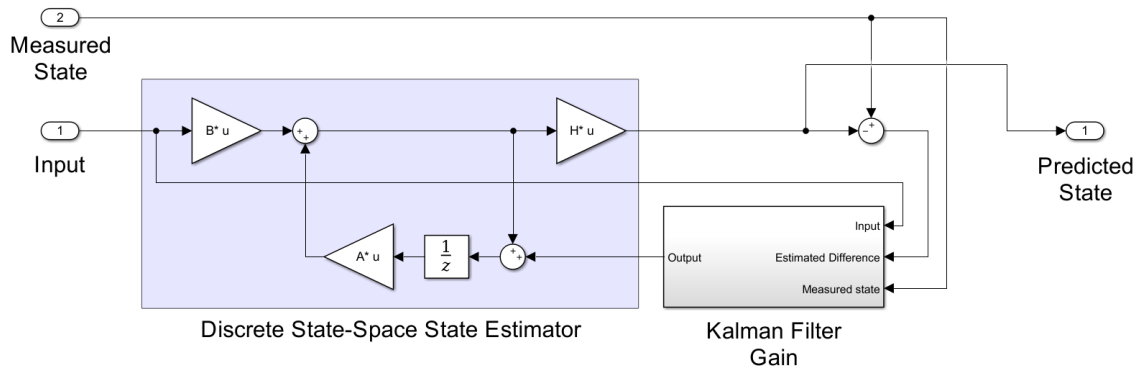


Figure 5.21. Block diagram of a discrete Kalman Filter.

The filter takes the difference between the measured state and predicted state, multiplies that difference by the Kalman gain K_k , and then adds the result into the state estimator seen in Figure 5.27. The Kalman gain is calculated at each time step by the algorithm shown by Equations 5.2 - 5.6.

$$\underline{x}_k^- = A\hat{\underline{x}}_{k-1} + B\underline{u}_k \quad (5.2)$$

$$P_k^- = AP_{k-1}A^T + Q \quad (5.3)$$

$$K_k = P_k^{-1} H^T (H P_k^{-1} H^T + R)^{-1} \quad (5.4)$$

$$\hat{x}_k = \hat{x}_k^- + K_k (z_k - H \hat{x}_k^-) \quad (5.5)$$

$$P_k = (I - K_k H) P_k^- \quad (5.6)$$

In Equations 5.2 - 5.6, the values A , B , and H are the discrete state-space matrices, Q and R are the assumed process and measurement noise variances, u_k is the input to the dynamic simulation, P_k is the Predictor gain of the Kalman Filter, and K_k is the Kalman gain that is optimized by the algorithm.

The first iteration of the Kalman Filter design took the actuator signal as the input to the dynamic simulation. While this resulted in a less noisy filtered signal, the simulation results were still not satisfactory. Thus, a second iteration of the Kalman Filter was created with the output of the Peltier element model taken as the input to the dynamic simulation. This resulted in a signal with very little noise, orders of magnitude less than the previous two filter designs discussed. The results of the simulation with the second iteration of the Kalman Filter is shown in Figures 5.22 and 5.23.

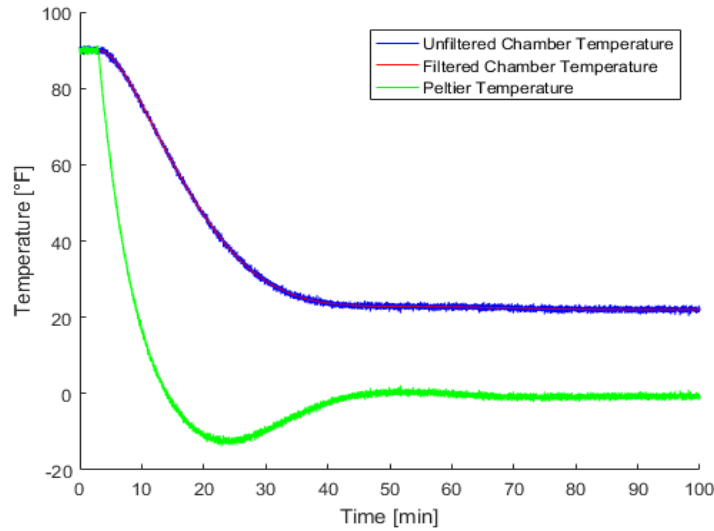


Figure 5.22. System response with the addition of a Kalman Filter

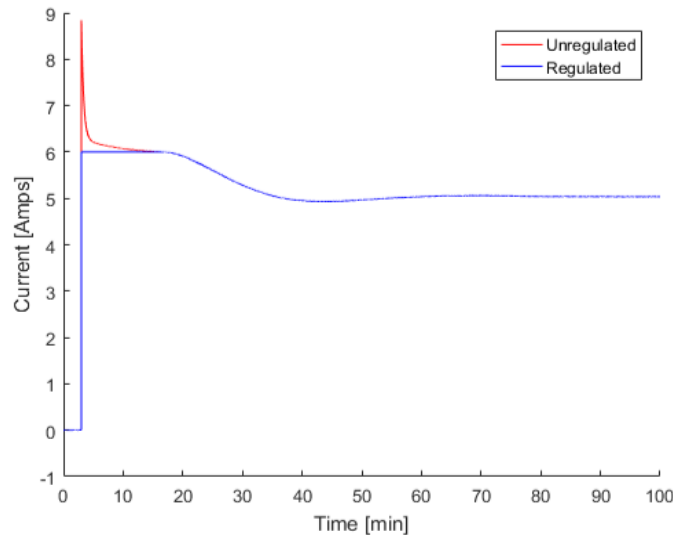


Figure 5.23. Unregulated and regulated actuator signal with the addition of a Kalman Filter.

There are no noticeable differences between the results of this simulation and the previous but comparing the results of the signals being fed back into the controller show significant improvements. The MATLAB code used to run the simulation can be found in Appendix E. Each simulation will be discussed and compared below.

5.5.3 COMPARISON OF RESULTS

Figure 5.24 shows a comparison between the feedback signals for each controller and filter design that was considered. The difference between the original feedback signal and the signal with the Anti-Windup scheme incorporated is evident, while the signals with the different filter designs are less noticeable. However, Figure 5.25 shows the feedback signals and the relative magnitudes of the noise present in each signal.

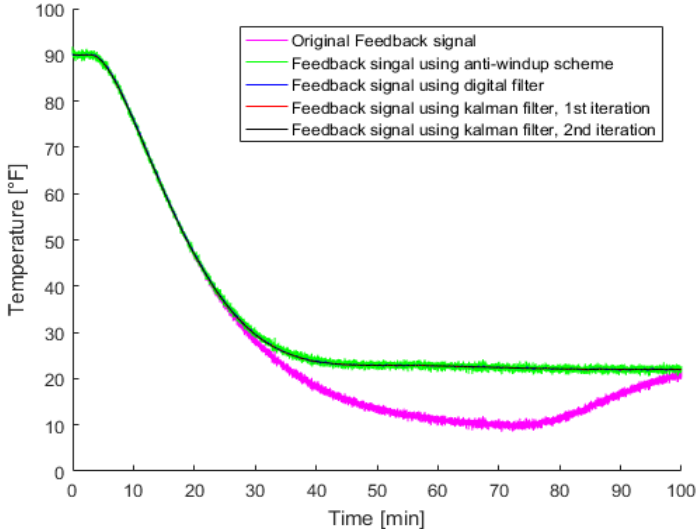


Figure 5.24. Comparison between feedback signals for all designs considered.

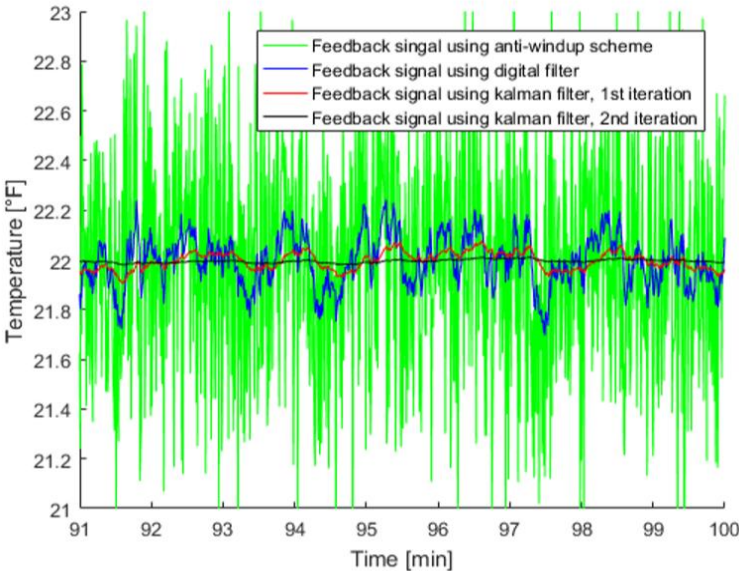


Figure 5.25. Comparison between the noise of each feedback signal.

The feedback signal using the digital filter, while less noisy than the original feedback signal, still has a significant variance. The noise variance is reduced using the first iteration of the Kalman Filter, where the input to the dynamic simulation is the actuator signal. However, the noise variance is reduced even further with the second iteration of the Kalman Filter, where the input to the dynamic simulation is the output of the Peltier element model. Based on these results, the second iteration of the Kalman Filter is the optimal filter choice for this design. In addition to providing a very clean feedback signal, this filtered signal could also be displayed on the LCD screen to provide the user with a very accurate measure of the temperature of the inner chamber.

5.5.4 FINAL DESIGN

The block diagram of the simulation that was used to analyze and design the control and filter schemes can be seen in Figure 5.26. This model takes the difference between the ambient temperature and desired temperature as the input to the system.

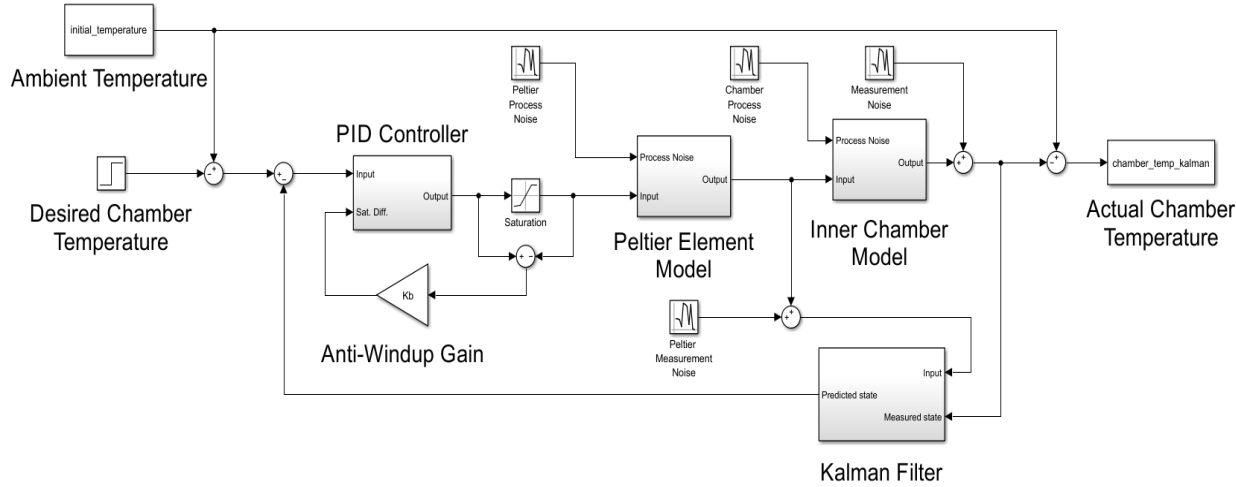


Figure 5.26. Block diagram of system model used for simulation.

The final design incorporates the Anti-Windup scheme discussed above to dissuade the controller from accumulating an excessive amount of error so that the chamber temperature does not overshoot. It also incorporates the second iteration of the Kalman Filter that results in a clean feedback signal to the controller as well as an accurate value of temperature for the inner chamber.

5.6 COST ANALYSIS

To manufacture the refrigerator each assembly that’s been designed will be manufactured and assembled. All the components in the prototype along with their materials and cost can be seen in Figure 5.27. It can also be found in Appendix F.

Indented Bill of Material (BOM)										
Peltier Cooler Assembly										
Assy Level	Part Number	Description				Matl	Vendor	Qty	Cost	Ttl Cost
		Lvl0	Lvl1	Lvl2	Lvl3					
0	100000	Peltier Cooler Assembly								
1	100001	Insulation								
2	100002		Aerogel	Aerogel & Fiberglass		Aspen Aerogels	18	\$ 9.38	\$ 168.84	
2	100003		Styrofoam	Styrofoam		Home Depot	1	\$ 10.72	\$ 10.72	
2	100004		Silicone Caulking	Silicone		Home Depot	1	\$ 13.54	\$ 13.54	
1	101000	Peltier Modules								
2	101001		Multistage Peltiers	Ceramic, semi-conductors		tetech	2	\$ 78.50	\$ 157.00	
2	101002		CPU Cooler	Plastic, water, copper		Amazon	2	\$ 59.77	\$ 119.54	
2	101004		Small Heat Sink	Aluminum		Amazon	2	\$ 5.45	\$ 10.90	
2	101005		Small Fan	Plastic		Amazon	2	\$ 8.36	\$ 16.72	
1	102000	Corrugated Walls								
2	102001		Fiberglass	Fiberglass			1	\$ 70.00	\$ 70.00	
2	102002		Epoxy				1	\$ 30.00	\$ 30.00	
1	103000	Controller								
2	103001		Microcontroller	NUCLEO-L452RE		Mouser Electronics	1	\$ 14.00	\$ 14.00	
2	103002		Current Drivers	MAX1969		Maxim Integrated	2	\$ 18.47	\$ 36.94	
2	103003		Transistors	BC337		SparkFun Electronics	2	\$ 0.50	\$ 1.00	
2	103004		Diodes	Schottky Diode		SparkFun Electronics	2	\$ 0.15	\$ 0.30	
2	103005		Wires	Various		Provided by ME Dept.	1	\$ -	\$ -	
2	103006		Thermocouples	Type-K-Glass Braid Insulated		SparkFun Electronics	4	\$ 13.95	\$ 55.80	
2	103007		LCD Screen	Basic 16x2 Character LCD		SparkFun Electronics	1	\$ 14.95	\$ 14.95	
2	103008		Keypad	Keypad - 12 Button		SparkFun Electronics	1	\$ 3.95	\$ 3.95	
2	103009		Resistors	Various		Provided by ME Dept.	15	\$ -	\$ -	
							Purchased Parts Total:	\$ 724.20		

Figure 5.27. All assemblies, parts, and their cost break-down used in the build.

5.7 MATERIAL AND SIZE DECISIONS

The material was chosen to be fiberglass pre-impregnated with epoxy, as fiberglass is a more inexpensive option when it comes to composites. Most refrigerators are made from plastic, which needs a custom mold to be made which is not feasible for this one-off application. Using a simple weave of fiberglass over under 1x1 pre-preg, then layering in two sheet thick layers. Fiberglass has better insulating properties than carbon fiber and is more cost effective.

Sizing the box was a combination of the available corrugated plate templates, as well as the average size of competing refrigerators. The team decided to make a refrigerator with very similar dimensions to ones that are pre-existing as they size was not flagged as a consumer complaint.

The wall dimensions are 42 X 32 (cm) and 29 X 30 (cm), with a base of 42 X 29 (cm). The 90° angle attachment pieces will be 1 X 1 X 30. This yields a refrigerator at 30 quarts and close to the dimensions of known car refrigerators, easily mobile.

5.8 SAFETY, REPAIRS, AND MAINTENANCE

As this product has no moving parts, it is not expected that maintenance will be required over the lifetime of the refrigerator. No data or analysis has been collected on the potential lifetime of the refrigerator, but with proper use it should last as long as most refrigerators do. The prototype was built fully sealed to avoid buildup of moisture in the insulating panels, and to reduce heat transfer to the surroundings. The refrigerator can withstand compressive loading up to 5000 lbs., therefore using it as a bench or shelf should do no harm to it.

6.0 MANUFACTURING PLAN

The final design was developed through careful consideration of manufacturability and functionality. The use of exotic materials as compared to other refrigerators was a selection based on integrity and function. Much of the build process of this project has been centered around the composite corrugation and insulation. One team member, Josh, works in the composites lab and has access to the tools needed to fabricate the corrugated fiberglass composite walls. Fiberglass pre-impregnated sheets were used to create the corrugated shape and the plates on either side of the corrugation. Figure 6.1 shows the fiberglass sheets in vacuum sealed bags curing in the autoclave. In addition to manufacturing the corrugated walls, top, bottom, and corners were made to bond the pieces to one another.

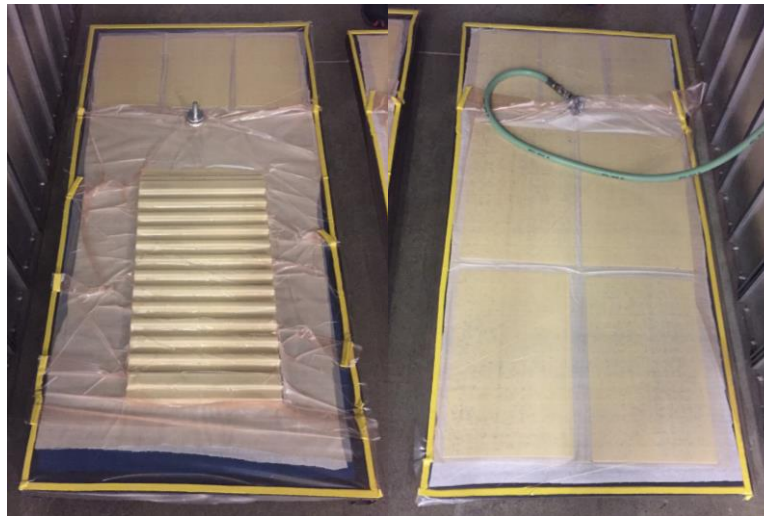


Figure 6.1. Vacuum curing of the corrugation (left) and vacuum curing of the plates (right).

Originally, the plan was to use square cross sectional corrugate, but after learning easier ways to manufacture the corrugated composite sheets, the team decided to use a trapezoidal cross section. The design of the structure can be seen in CAD model drawings in Appendix D.

The structural support and insulation were the main part of fabrication. Most of the other components were purchased. Peltiers, LCD display, microcontroller, heatsinks, and electrical hardware.

6.1 CORRUGATED WALLS

The walls of the refrigerator were constructed from corrugated fiberglass. The molds used in the manufacturing process have already been made and are available for use through the Mechanical Engineering Department. The corrugation shape is trapezoidal. Each sheet constructed was made with two layers of pre-impregnated fiberglass. All four walls and the base were constructed in the same fashion. To make a sheet of corrugated material also called a sandwich panel two side panels and the corrugated structure laid into the mold need to be epoxied together.

6.1.1 STEP BY STEP MANUFACTURING

F1: Step 1

Cut pre-impregnated fiberglass roll into sheets sized to the specifications. Using a simple utility knife and a straight edge with a marked line.

F1: Step 2

Remove one side of film on each fiberglass sheet and place sheet on top of each other in an organized and exact fashion. If removing the blue be very careful as the sheet will try and lift. Make sure to iron out any wrinkles incurred at this stage of the construction as they will continue to be a thorn in the side of the construction if it gets passed the curing stage.

F1: Step 3

If making flat plates set them on a flat plate carefully not bending or any wrinkles in the base layer or the sheets.

C1: Step 4

For the corrugated cores, the molds are pre-made at the dimensions labeled in CDR report. The molds are made from machined aluminum. To prepare the molds for a cure, the previous epoxy or resin must be removed. Using scotch brite and some elbow grease, remove the imperfections exposing just the bare aluminum.

C1: Step 5

Clean the molds off with water and let dry completely. Using mold release film, spray liberally and let dry per the mold release film instructions. Once the plates have plenty of mold release film set them aside to be prepared.

C1: Step 6

Prepare a two layered sheet of fiberglass and make it the width of the roll of fiberglass itself. Because the corrugated structure is a longer by surface area than the flat plates, more is better than less.

C1: Step 7

With the help of a partner, place the fiberglass sheet on top of the mold longways symmetrically. With one side lifted with a partner, slowly insert the glass into the shape of the mold, using tools to place in the mold, and the partner keeping tension as well as helping to stay in the shape. Press firmly working from the middle to one outer edge. Continue this conforming to all the shapes and angles making sure to not wrinkle the fiberglass and have it symmetric in the mold.

C1: Step 8

Make sure the excess fiberglass is carefully cut from the mold and then place on to a prepared plate.

P1: Step 9

Collect a plate at the appropriate size for all pieces to be cured. A metal base is the best, but anything that can have gum tape adhere to it and a vacuum pulled to not buckle.

P2: Step 10

Set up gum tape along the outermost edge of the plate.

P3: Step 11

Cut out a drip layer that extends 2 inches passed the edges of the samples to be cured, place this on the bottom most layer of the plate to be cured.

P4: Step 12

If making flat plates make sure to put a brown breather layer underneath the samples to be cured or they will stick to the blue base layer. If they stick you will have to peel the layer off by hand as it is cured to the fiberglass itself.

P5: Step 13

Place all pieces to be cured on the plate, making sure to leave a 6-inch square area open for a vacuum valve to be placed in the future. When placing the pieces, all flats make sure that there are no wrinkles or exposed edges when it comes to the fiberglass. All contact will adhere to the part of the exposed areas.

P6: Step 14

Once all pieces are arranged, make a brown Teflon coated breather layer over every surface area that is fiberglass. If this step is not done a bad surface area will be there and you will have to peel up all the vacuum bag layer from the cure.

P7: Step 15

Place the back half of a vacuum valve on the open area, put a layer of thick breather material to make a way for air to escape with the vacuum that will be pulled. The purpose of the back to the valve is to properly attach to the bag you are going to make.

P8: Step 16

Prepare a layer of vacuum material that is bigger than the plate and the samples.

P9: Step 17

Attach the vacuum bag in the corners working your way slowly to create a tight seal when the vacuum is pulled. Using gum tape, be wary of corners or features and make an ear (extended piece above the samples at corners to get rid of stress concentrations in the vacuum bag. The ears are best built by a 4-inch loop or so then place in such a way to not have a leak.

P10: Step 18

Set the plate inside the oven and attach the vacuum valve to the plate. With the vacuum attached check for leaks. You want the vacuum to be very strong as to push into all the different shapes of your plates or corrugated. If there are leaks, press on the gum tape to find the leaks and eliminate them. The vacuum line should be very difficult to move.

P11: Step 19

Set up the oven to cure the composites. At 5°F per minute rise, and a 250-degree dwell for 2 hours. Using the computer, load a program to engage vacuum and the proper timing for the cure per the manufacturer.

P12: Step 20

Once the cure is done, remove from the oven. Discarding all the vacuum bag material, keeping the breathers that are still in good condition.

P13: Step 21

Carefully remove all pieces from the form. With a strong constant force, the corrugated material should lift from the mold.

E1: Step 22

Once you have the two separate pieces for the sandwich, get construction adhesive epoxy two-part mixture. As per the instructions measure out the appropriate amount for each.

E1: Step 23

Spread the epoxy on the corrugated shapes, just the contact points in a thin uniform layer.

E1: Step 24

Put a layer of vacuum bag on the aluminum mold, place the corrugate in the mold with the epoxy on top, get a sheet of fiberglass and massage it onto the corrugated shape. Once it is massaged in, place a heavy distributed weight on top and let dry for time indicated on the epoxy.

E1: Step 25

Once the corrugated shape is dry, attach the other flat piece with construction adhesive in the same way.

E1: Step 26

Using a wet saw, or a water jet, cut the corrugated panels to the exact shape desired. Remember to add any holes or features in this step.

B1: Step 27

Make right angle corners of dimension desired. Following the previous curing cycle and style, make a form to keep a right angle of the desired shape.

B1: Step 28

Attach the right angles with epoxy to the corrugated shapes making the box shape at the desired dimension.

6.1.2 AEROGEL CORRUGATE WALL

After the corrugate structure was built using the glued corrugate panels and corners, the insulation needed to be installed. The aerogel-fiberglass composite came in a fabric-like sheet, making it easy to cut and install in the open spaces of the corrugate. The way the composite was manufactured was by placing powdered aerogel into woven fiberglass. During the installation process, however, visible particulates were coming loose from the fabric—meaning the composite was becoming a larger percentage of fiberglass in its original form and therefore reducing its insulative properties. The installed aerogel-fiberglass composite can be seen in Figure 6.2



Figure 6.2. Corrugate wall installed with aerogel fiberglass composite.

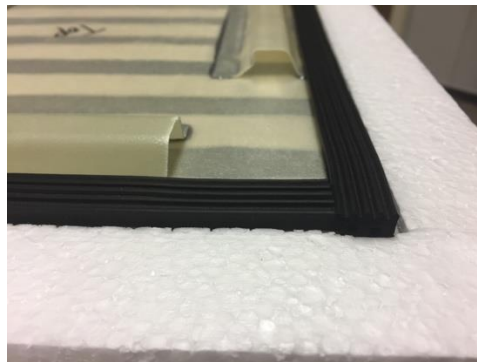
6.1.3 LID

The lid was designed out of the same corrugate structure as the walls of the refrigerator and filled with aerogel. The bottom view of the lid can be seen in Figure 6.3.



6.3. Bottom view of lid.

In order to seal the lid, rubber weather stripping was placed between the lid and the walls, and weight was added to the top to ensure a tight seal. The rubber used can be seen in a close up in Figure 6.4.



6.4. Rubber weather stripping used to seal the box.

6.2 PELTIER/HEATSINK STACK

Since the multi-stage Peltier module was purchased as well as the CPU cooler, all that was required was assembly. The cold side heat sink and fan were installed inside the refrigerator chamber, and the Peltier CPU assembly was mounted to the wall of the refrigerator, with the radiators perpendicular to the wall. A photo of the installed configuration is shown in Figure 6.5.



Figure 6.5. Top view of the Peltier module and heat transfer apparatuses. From left to right they are: CPU cooler (black), heat sink (silver), fan (black).

7.0 DESIGN VERIFICATION PLAN

To ensure the functionality of the final prototype each element was tested individually to determine its performance before the prototype was tested overall.

The testing for the design was split based upon the individual components of the refrigerator as discussed above. These include the corrugate, Peltier devices, heat dissipation from the Peltier, insulation, and the control unit. Having data for each component of the product enabled specific comparison between products and configurations. The initial theoretical calculations were used to narrow down the number of items in each design decision to be tested and then the results were used to make the final decisions for the prototype. For example, before choosing the type of insulation to use in the final design, panels of varied materials were tested to see how well they thermally insulate. Similarly, Peltier configurations were tested and compared as well as methods for dissipating heat from the hot side of the Peltier. The prototype was then tested at the end to ensure that the integration of all the design decisions produced the desired results.

7.1 STRENGTH TESTING

Compression and 3-point bend tests were conducted on sample pieces of corrugate wall. These results were then used to estimate the load that the overall walls can take once constructed as a structure.

A corrugated sample was made for a destructive test of size of 17.6 X 21.5 cm (2), and 33 X 5 cm (2). The smaller pieces were tested with a distributed load along the top as seen in Figure 7.1. Longer, narrower test sections were used for the three-point bend test. This test would mimic a person sitting on the lid of the refrigerator. The compressive test panel withstood 6000 lbs. of force, which is well above the threshold of 400 lbs. distributed and thus proving that the structure will be strong enough for the load of a human sitting on top of the refrigerator.



Figure 7.1. Corrugated panel under distributed vertical load, failure at 6000 lbs.

As seen in Figure 7.2, the load vs crosshead position can be seen to take the force.

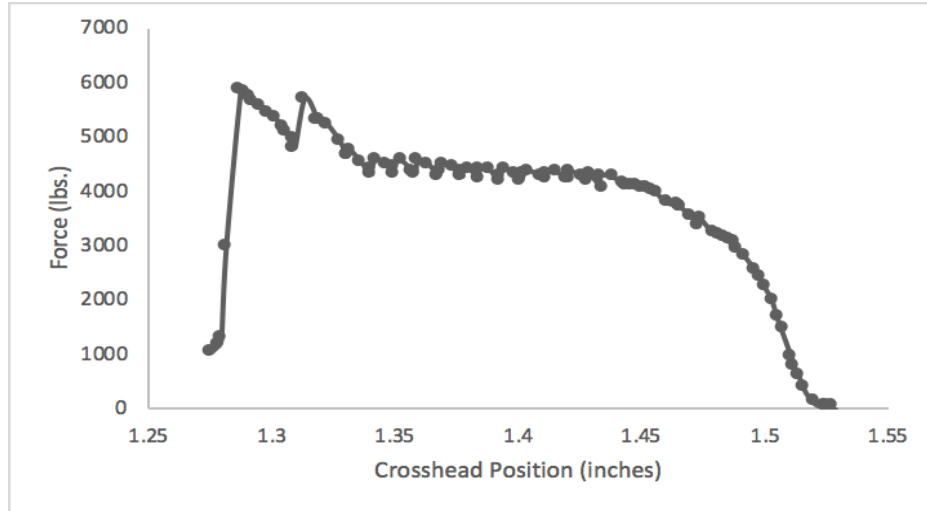


Figure 7.2. Corrugated Compression test.

Figure 7.3 shows a slim piece of corrugate subjected to a 3-point bend test. Since the piece was very thin, buckling happened almost immediately. The sample eventually failed in delamination. Delamination is the most common way composites fail, when the plates separate from the core due to the shear on the adhesive. Even though the 3-point bend test took very little load compared to the distributed load, it is still strong enough to hold a 400-pound person of the area of the corrugated plate that was made. Figure 7.4 shows the load-displacement data for this bending load.

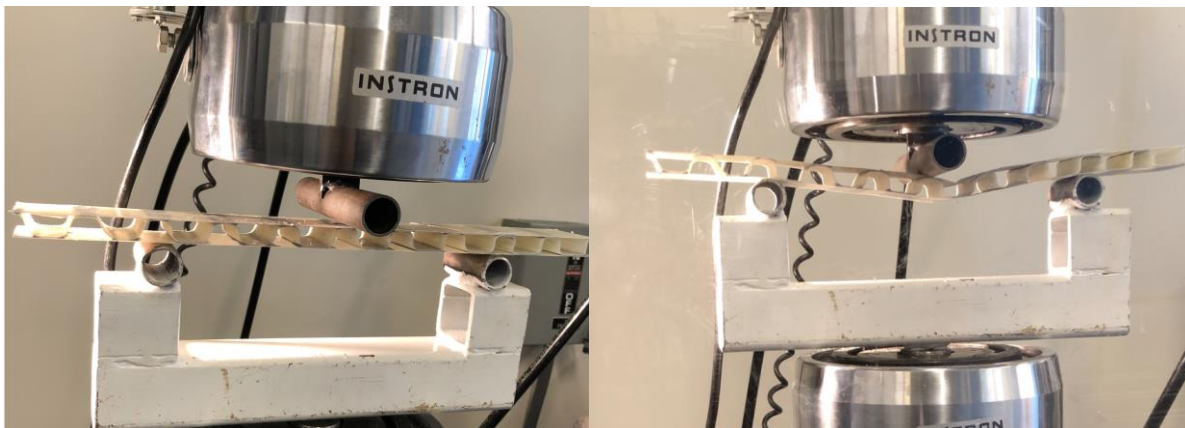


Figure 7.3. Three-point bend test on slim corrugated structure.

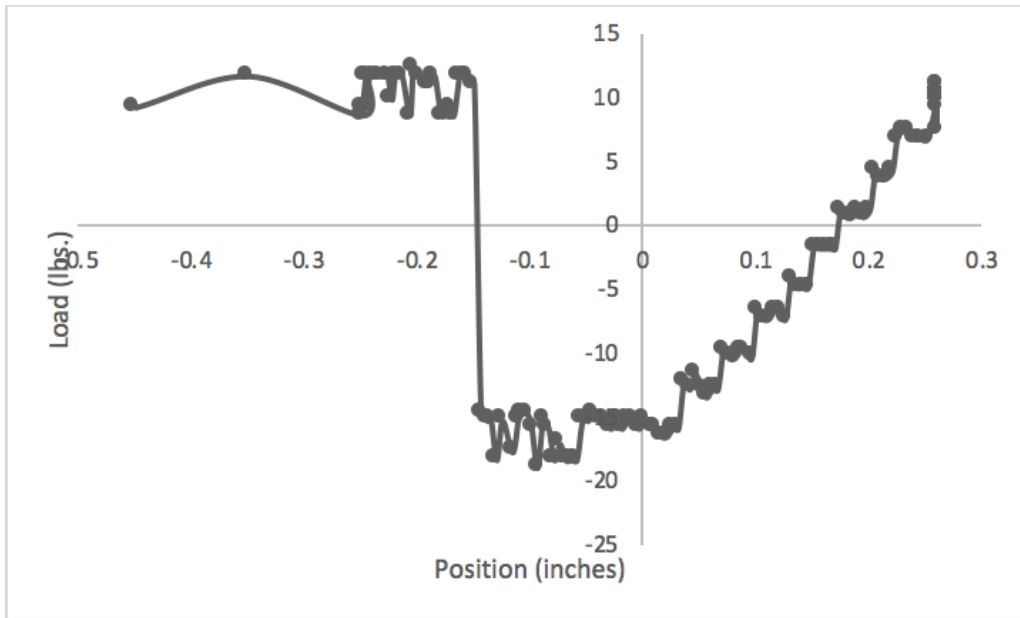


Figure 7.4. Three-point bend results.

Through this destructive testing, it was determined that two-layer fiberglass with a corrugated core will withstand the structure's maximum loading condition.

7.2 PELTIER ARRANGEMENT TESTING

After doing research into types of Peltier refrigerators that were on the market, several were ordered to baseline test. To understand the difference between the refrigerators tested, it is important to understand the Peltier types used in each test and how they differ. Peltiers are classified by a string of numbers and letters as seen in Figure 7.5. All Peltiers tested up to now have been standard "C" size with one stage and 127 couples. Where they differ is in the current rating, the Bestek has a current rating of 5A, the Igloo 6A, and the Peltiers used in series 15A.

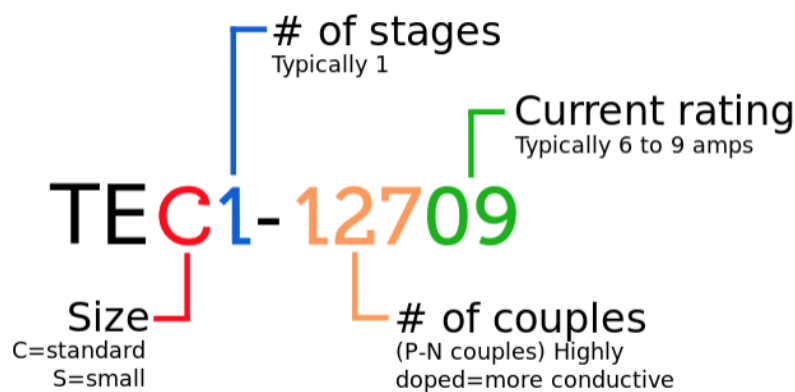


Figure 7.5. Nomenclature for Peltier designations.

Peltiers are still extremely misunderstood, and even though the Peltiers have different current ratings it is unclear how this corresponds to temperature difference. In research conducted by students under Pete Schwartz in the Physics department it was shown that the TEC06 performed better at the same currents than the TEC15, as seen in Figure 7.6. Data taken in Figures 7.7 and 7.8 show that TEC05 performs better

at the same currents than the TEC06. There appears to be a trend that lower rated amperage Peltiers produce a larger temperature difference. Another thing to note from this research is that there is a certain cutoff current where decreasing the amperage even more results in worse effects than the previous amperage. In other words, there is a distinct operating current for the Peltiers that will produce the best results.

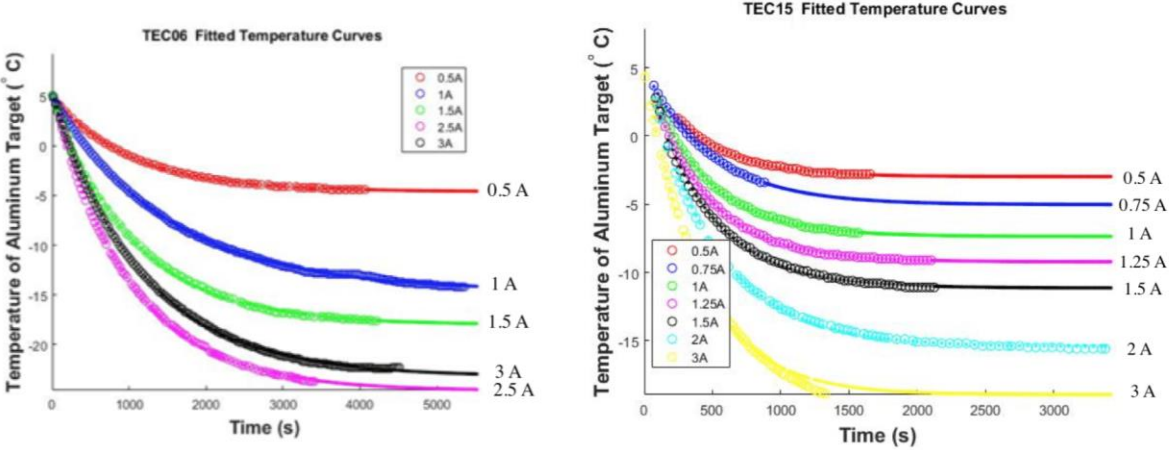


Figure 7.6. Temperature versus time curves for TEC06 and TEC15 Peltiers run at different currents. [5]

Baseline testing was done for the Bestek refrigerator using its stock Peltier (TEC1-12705) to determine how the refrigerator performed at different amperes. Figure 7.7 is just the temperature difference across the Peltier in the Bestek. The highest amperage run, 4.5, produced the largest temperature difference across the Peltier and the largest difference between room ambient and refrigerator chamber ambient. Other data was collected from the Bestek, most notably the chamber ambient temperature, however just the Peltier data is shown to highlight the difference between the 5A rated and 6A rated Peltiers as shown in the Bestek and Igloo respectively. How the amperage rating affects the temperature difference achievable is still unknown, but for this data the 5A rated Peltier outperformed the 6A. The 6A Peltier difference can be seen in Figure 7.8.

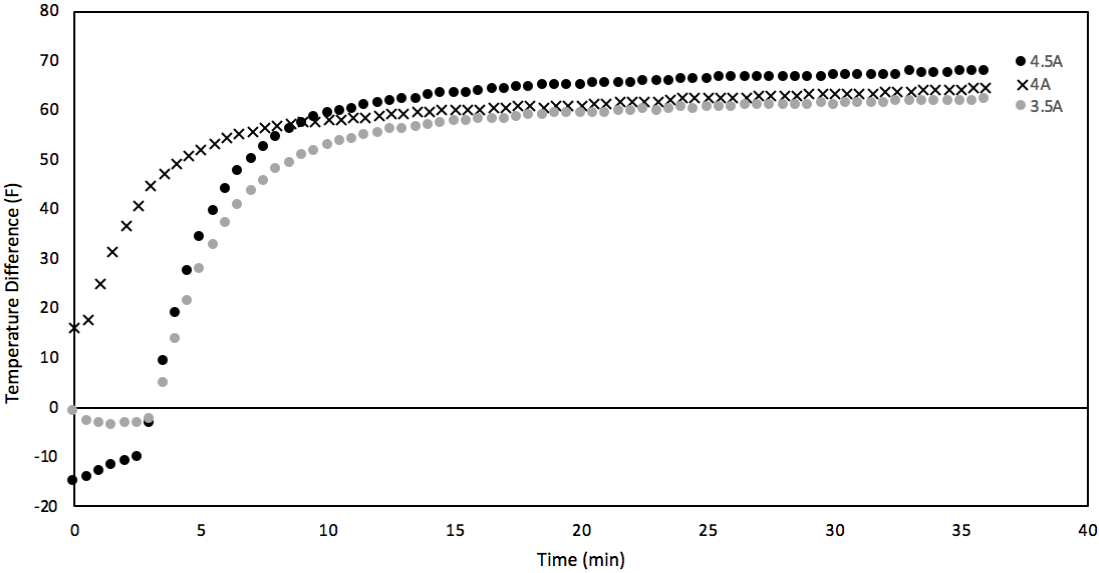


Figure 7.7. Plot of temperature difference across the Peltier in the Bestek (TEC1-12705) for varying currents versus time.

Baseline testing was done for the Igloo refrigerator with the commercial Peltier (TEC1-12706) to determine what the best current for the refrigerator was. The relationship between current and temperature difference, which can be seen in Figure 7.8, is a positive correlation, although clearly not a linear one.

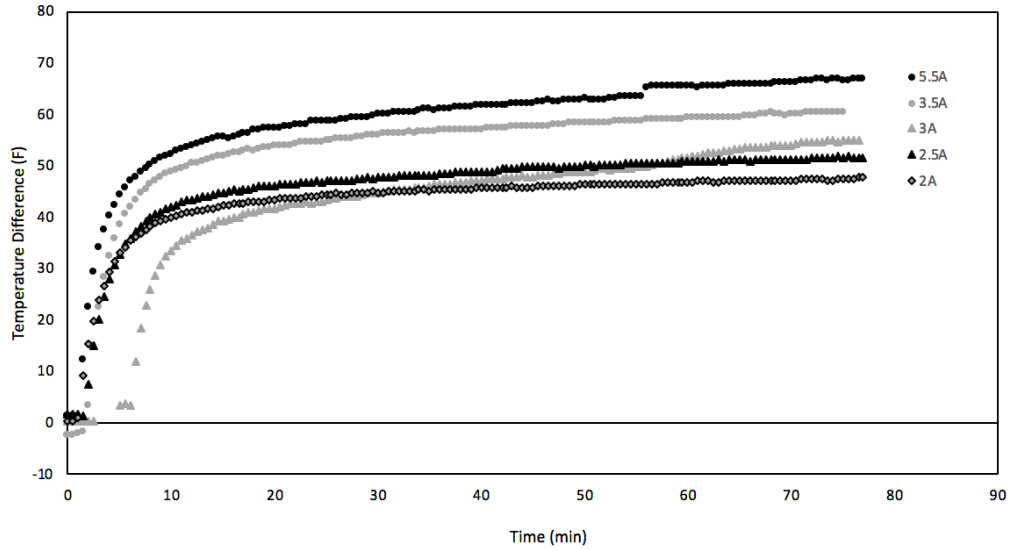


Figure 7.8. Plot of temperature difference across the Peltier in the Igloo (TEC1-12706) for varying currents versus time.

The “best” current was defined as the current that produced the largest temperature difference across the Peltier, which correlated to the largest temperature difference between ambient room temperature and the temperature inside the chamber. The chamber ambient temperature, however, does not respond as quickly or as dramatically as the Peltiers. In fact, a major limitation of the refrigerator is that although the temperature difference across the Peltiers is clearly exponential, the ambient temperature inside the refrigerator frequently looks linear. The refrigerator ambient temperature is limited by how well the air is circulated, and this is a variable that was investigated in the new design of the refrigerator to try and optimize the heat transfer to the air and create a curve that is more proportional to that of the Peltier surface temperature. The unoptimized relationships can be seen in Figure 7.9.

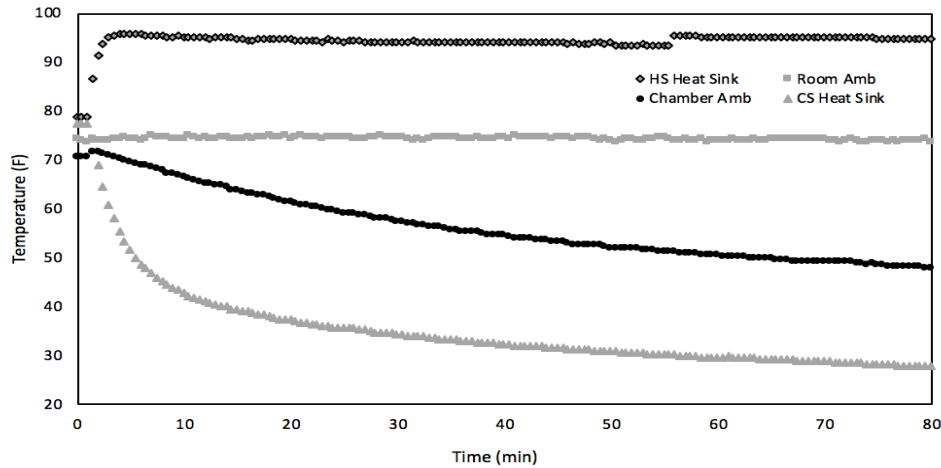


Figure 7.9. Temperatures measured during the Igloo test with a current of 5.5A. This current achieved the lowest ambient temperature inside the refrigerator during this test, 48 F. All the temperature readings for the varied currents showed these same trends.

Based upon Josh’s summer research the design goal is to use Peltiers in series to achieve a larger temperature difference faster. The same Peltiers that were used in the design seen in Figure 2.4 were used. These Peltiers are different from those used in the Igloo, so the temperature differences cannot be directly compared. The data from the Peltiers in series, however, shows that it is beneficial to run different currents through each of the Peltiers. This data is shown in Figure 7.10. Although a direct comparison cannot be made between the datasets because multiple variables changed, it is interesting to note that the temperature difference between the cold side heat sink and the chamber ambient temperature was halved when there were two Peltiers run in series. This helps justify using Peltiers in series as minimizing this difference is a design goal.

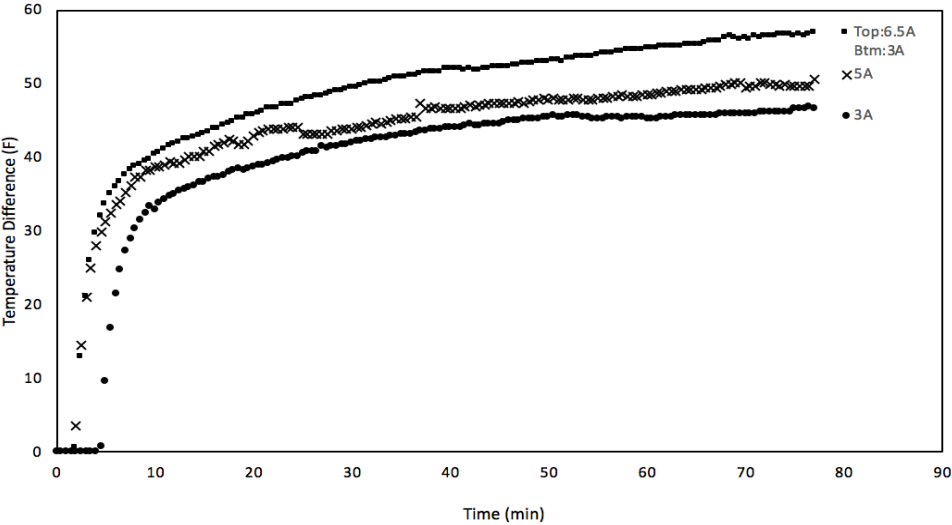


Figure 7.10. Plot of temperature differences across two Peltiers in series (TEC1-12715) and one Peltier run at 5A and 3A

Further experiments were conducted with three Peltiers in series. The team kept the cold side heat sink fan off and the hot side heat sink fan on. Since the only thermal resistance to the cold side heat sink is natural convection due to the fan being off, there is a much smaller load for the Peltier stack to work against. With only natural convection, the cold side heat sink can reach a much lower temperature. An experiment was conducted using the Igloo refrigerator with three 40x40mm Peltiers in series running at 2, 4, and 6 Amps. Figure 7.11 shows the data for this experiment.

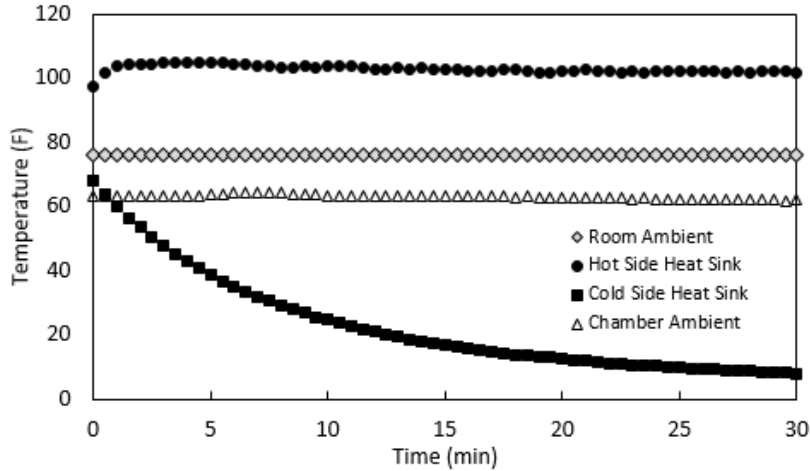


Figure 7.11. Three 40x40mm Peltiers with cold side fan off

Figure 7.11 shows how leaving the cold side heat sink fan off results in a very low cold side heat sink temperature of 8.1°F. This shows that the Peltier stack can reach a freezing temperature, but not yet as low as the goal of -10°F. Seeing as this is the closest temperature to the goal reached so far, the temperature goal was altered. The first temperature goal is 30°F, to show that the chamber can reach freezing, and then once that is reached the second target will be 10°F. To experiment and see how the cold side heat sink would react to suddenly having a forced convection load on the cold side heat sink, the team kept all parameters the same and turned on the cold side heatsink fan. This transient response can be seen in Figure 7.12.

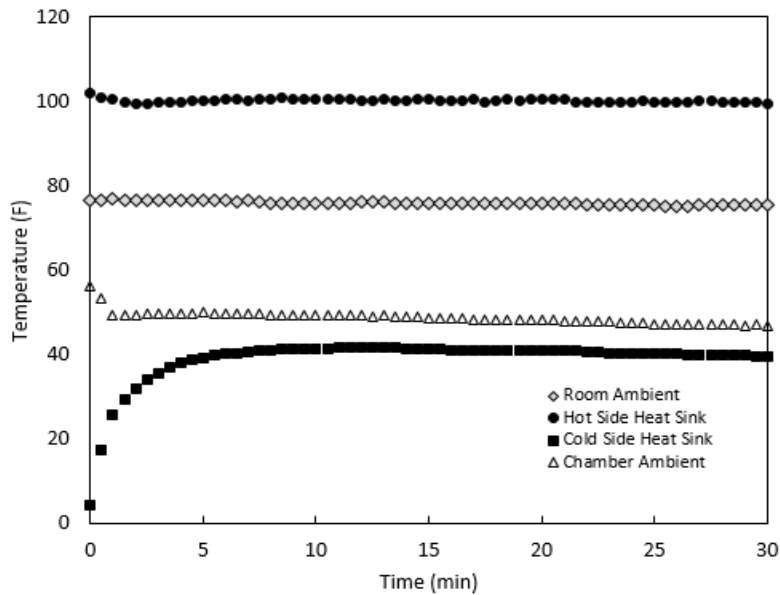


Figure 7.12. Transient response of cold side fan being turned on.

As seen in Figure 7.12, the cold side heat sink sucked in heat from the chamber within five minutes and reached a temperature of 41.7°F before decreasing again. After 30 min, the chamber temperature was 46.5°F, far away from either of the goal temperatures. The Peltier heat extraction is small enough (the team estimates less than 10W) that the heat leakage into the refrigerator was a significant concern. This is why it was helpful in the final design to use heat extraction data for tetch Peltiers ordered to develop a theoretical model of the refrigerator. This is how the team made the design choice of having two Peltier stacks. Table 7.1 shows how much power was consumed by the Peltier stack of three 40x40mm Peltiers.

Table 7.1. Power consumption of three 40x40mm Peltiers

Peltier	Current (A)	Voltage (V)	Power consumed (W)
Cold	2	2.3	4.6
Middle	4	5.2	20.8
Hot	6	8.0	48.0
TOTAL	12	15.5	73.4

The power consumed for more than one stack will only affect the voltage, since all the cold Peltiers will be running on the same current, along with all the middle Peltiers on their same current, and all the hot Peltiers on their own current. This means that for two Peltier stacks, the total power consumed will just equal the power consumed by one stack multiplied by two. So, in the above case, the power consumed by two Peltier stacks would be 146.8W. Testing has been performed for a pyramidal shape of Peltier stack, but the data above has been the most promising. The pyramidal stack did not get below 10°F even after turning off the cold side heat sink fan.

A stack of two Peltiers was shown to be the most promising design for this application. It provided the lowest temperatures with the least amount of power draw. It was determined that two stacks would be used for the chamber to get the temperature closer to the goals of 30°F and 10°F. The main limitation for the Peltier stack was the heat transfer between the two units, to resolve this issue a multi-stage Peltier was ordered.

7.3 PELTIER HEAT TRANSFER TESTING

To determine how much heat is being extracted by a Peltier stack, the team experimentally determined the thermal resistance of a polyethylene foam refrigerator (a cheap Styrofoam refrigerator from Home Depot) and then tested the Peltier stack. This enabled the team to determine whether the data given by tetch was accurate to what was experimentally measured by the team. Once this configuration reached steady state operation, the heat extracted by the Peltiers was equal to the heat leakage into the refrigerator. As mentioned in section 7.2, the Peltier heat flowrate needed to be known to determine how many Peltier stacks were necessary to overcome the heat leakage of the refrigerator and reach the temperature goal. This will justify the use of tetch data for Peltier selection in the refrigerator final design.

The first step in this process was to determine the thermal resistance (R value) of the Styrofoam being used. Figure 7.13 shows the experimental set up.

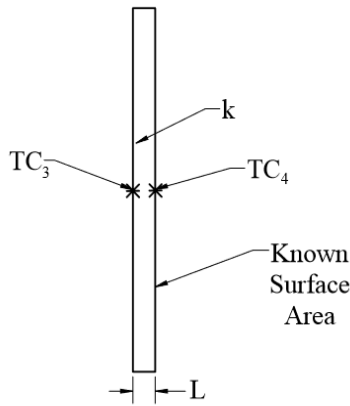


Figure 7.13. Experimental set up.

The calculated value for the Styrofoam was $R = 0.219 \frac{^{\circ}\text{C}\cdot\text{m}^2}{\text{W}}$. In order to determine the overall thermal resistance of the cooler the thermal resistance value was divided by the surface area of the cooler, 0.5977 m^2 to get $R_{tot} = 0.661 \frac{^{\circ}\text{F}}{\text{W}}$. In order to validate the theoretical models provided by tetch, the team then measured the temperature difference across one wall of the cooler and using the calculated R value in equation 7.1, the heat transfer was determined to be 27.45 W.

$$Q = \frac{1}{R_{wall}} (T_{out} - T_{in}) \quad (7.1)$$

This test was conducted at 12V and temperature difference of 18°F (7°C). The theoretical curve shown in Figure 7.14 predicts the heat transfer to be about 27 W, showing agreement between the theoretical and experimental results. This justified the use of Figure 7.14 in predicting the performance of the refrigerator overall.

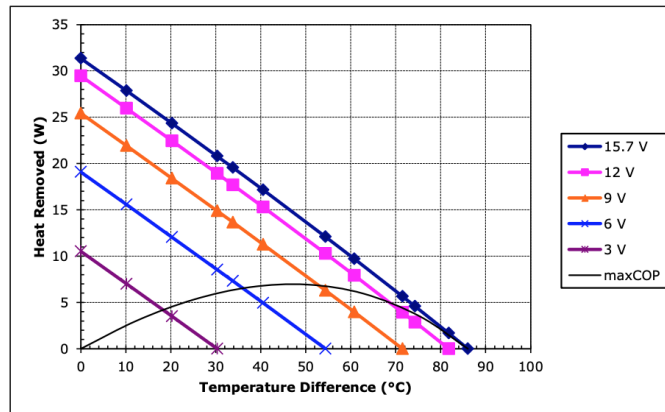


Figure 7.14. Data provided by tetch for Peltier modules used in final design.

The next step for the team was to determine the thermal resistance of the corrugate walls being used in the design. Using the same theoretical premise as with the Styrofoam wall, the corrugate-aerogel wall was determined to have a thermal resistance of $R = 0.0483 \frac{^{\circ}\text{C}\cdot\text{m}^2}{\text{W}}$. At this point, the team noted the large difference between the thermal resistance of the Styrofoam and the corrugate wall. Likely due to the difference in thickness and reduction in air gaps in the Styrofoam manufacturing. This discrepancy caused a change in design: the refrigerator would be tested with only the corrugate wall first to see how it performed, but ultimately at least one layer of Styrofoam would be added to the exterior to increase the insulation.

7.4 INSULATION TESTING

After the initial insulation heat transfer analysis, it was determined that the material properties of aerogel and rice hulls should be investigated further. These are relatively new materials for the application of insulation, so testing was required to determine their thermal conductivity to use in heat transfer calculations for the refrigerator. Little research has been done as to how these materials perform long term for insulation purposes. These two materials provide good options for very different markets, rice hulls would be beneficial in developing nations due to their wide accessibility, low cost, and low environmental impact. In addition to rice hulls, hemp was also investigated as a possible solution for the same market. Aerogel was also investigated as it was found to have the most potential for thermal isolation.

The goal of this experiment was to determine the thermal conductivity of each material given a heat flux and temperature difference. This enables quick calculation of temperature change across the walls of the refrigerator using the experimental thermal conductivity and measured heat flux. The walls used in the testing rig were aluminum. Metals have well recorded thermal properties; therefore, it was unnecessary to measure the thermal response of the wall in the test to determine an equation for the total heat transfer through the composite wall. To develop an equation that can predict future heat flux or temperature change, the thermal conductivities of the insulation materials were measured. Thermal conductivity is a function of temperature and pressure; therefore, the tests were all performed at the same temperature and operating pressure that were predicted for the thermoelectric refrigerator. All materials were tested in the same rig as discussed below.

7.4.1 Experimentation

A testing rig was designed specifically for the insulation experiments. The conditions for which all the thermal conductivities were measured was held constant to ensure comparable results.

7.4.1.1 Fabrication

To compare the thermal conductivities of each material, the thickness parameter was held constant for each material and therefore each testing section. The results of this were 6.5 ± 1.5 mm thick test sections. The aerogel was purchased in a 5 mm sheet, so to control the thickness parameter in the experiment, the hemp and rice hull samples were fabricated to be a similar thickness. The silicone and organic materials were mixed together and bonded for 24 hours in a wood frame 1-square-foot in area with a height of 5 mm. During the bonding process weight was added to the drying section to maintain a consistent thickness. Figure 7.15 shows the test section created for the rice hulls. The hemp test section was created in the same fashion.



Figure 7.15. Manufactured test specimen using rice hulls and silicone caulking.

To construct the hemp and rice hulls into panels with a given thickness, they were bonded with silicone caulking. Silicone was selected for its low thermal conductivity and bonding capabilities. The same fiber to silicone mass ratio was used for both samples, 20 % by weight fiber, to ensure a viable comparison. In addition, another test section was created in the same fashion out of silicone caulking for further analysis which will be discussed later. The measured mass and thickness for each test section is presented in Table 7.2.

Table 7.2. Measured mass and thickness of each material.

Material	Average Thickness (mm)	Weight (g)
Hemp Bio-Composite	7.81	357.5
(Hemp Alone)	(N/A)	(71.5)
Rice Hull Bio-Composite	6.66	345.0
(Rice Hulls Alone)	(N/A)	(69.0)
Aerogel Bio-Composite	4.92	130.0
Silicone Caulking	3.40	247.9

7.4.1.2 Experimental Setup

Since thermal conductivity is a function of temperature, the experiment was set to be as close to operating temperatures of the refrigerator as possible. The expected operating conditions of the refrigerator are -15 °C on the inner surface and 45 °C on the outer surface. To get the most representative thermal conductivity for the operating conditions, the testing rig needed to span almost the entire temperature range anticipated without overshooting it by too much. Three initial experiments were run to determine the best design for the testing rig. These initial tests varied the temperatures of the cold side or hot side.

The first experimental setup maintained the cold side temperature with dry ice on the cold side, and a low voltage input into the surface heater to maintain the hot side temperature. Once the data was collected, it was found that this setup was too cold, with the cold side being -73°C, and the hot side of the insulation stabilizing at 10 °C. While this setup achieved a large temperature change across the testing rig, most of the temperature measurements were below the threshold of temperatures anticipated for the refrigerator. Additionally, thermal conductivity increases with temperature, therefore this experimental setup would overpredict how the insulation would perform when applied to the refrigerator. The second experimental setup used ice on the cold side and the same low voltage input to the surface heater as used in the first setup. This produced a temperature range of 0°C to 22°C, which was a subset of the operating conditions. Although the temperature range of the second setup did not span the entire range of operation it gave a more accurate measurement for a subset of the conditions. The conclusion from the first two tests was that the experiment should be run with ice on the cold side and the heater on the hot side but supplied with a higher voltage to capture the higher range of temperatures within the operating conditions.

The third test was run without ice but supplying the rated voltage to the heater (120 VAC) to determine the highest possible temperature. The heater quickly went above 120 °C, far above the limit of the operating conditions, at which point a dimmer was wired in series with the heater to give control over the power supplied. Additionally, an insulating foam block and a weight was placed on top of the surface heater to ensure minimal heat loss to the surroundings. With higher voltage supplied to the heating element

coupled with ice maintaining the cold side of the rig, a temperature range of 0 °C to 60 °C was achievable. This experimental design as seen in Figure 7.16 was used to test each sample.

A higher temperature was maintained by the heater than was anticipated for the ambient operating conditions because of the added insulation of the heat flux sensor on the hot side of the testing rig. Although the recorded heater temperatures were almost double that of upper limit operating conditions, the hot side of the test section measured at an average of 30 °C. The cold side had a 5 °C temperature change across the aluminum plate, so 30 °C at the hot side of the insulation mimics the response of having the heater at 35 °C and only an aluminum plate between them.

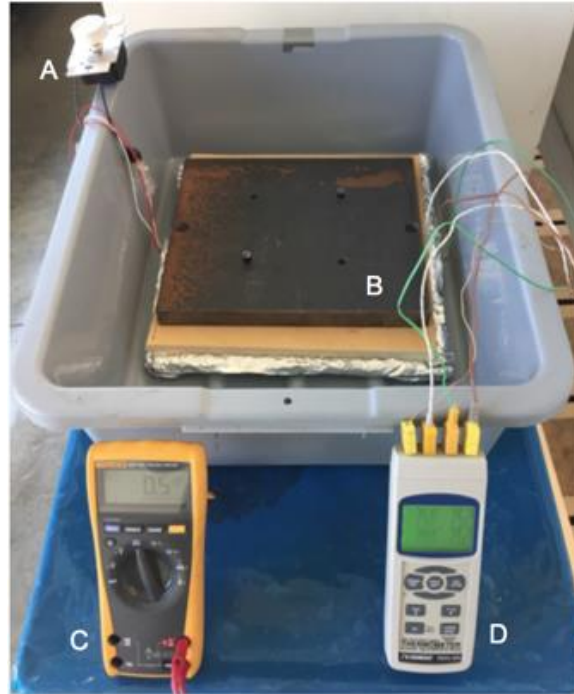


Figure 7.16. Experimental setup that was used to conduct the experiment. (A) Dimmer in series with heater. (B) Testing rig. (C) Voltmeter to read heat flux sensor data. (D) Thermocouple reader.

Each insulation material was assembled in the same rig as seen in Figure 7.18. The insulation on the sides of the testing rig serves to reduce losses due to convection out of the test section, assuming 1-D conduction in the direction of heat flow. The experiment was designed to measure the heat flux and temperatures in the direction of heat flow to calculate the thermal conductivity of the material in the test section. Figure 7.17 shows the insulated rig with the surface heater visible.



Figure 7.17. Insulated experimental rig used for testing whose interior is described by Figure 7.18.

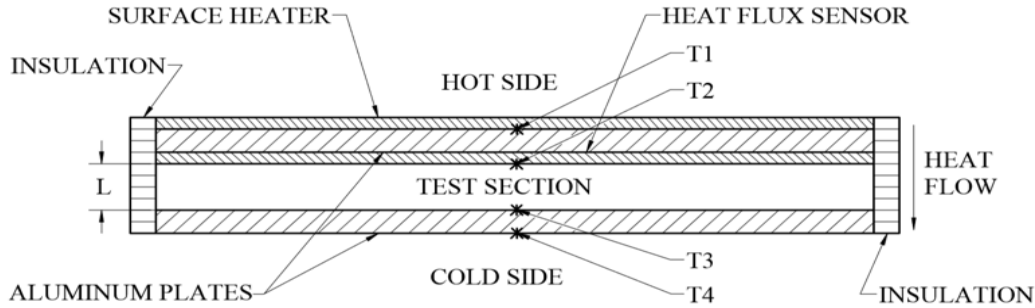


Figure 7.17. Schematic of the experimental test rig. The four type-K thermocouple locations are indicated by asterisks (*) and labeled as T1, T2, T3, and T4.

The hot side temperature was controlled by a silicone resistor-based surface heater and the cold side temperature was maintained with an ice bath. These set the boundary conditions for the experiment—constant heat flux on the hot side and the cold side maintained at a constant temperature. To control the power delivered to the heater a dimmer was wired in series with the surface heater, and each test was run with the dimmer set to approximately the same setting. Additional insulation was added to the silicone heater where it was in contact with ambient as to avoid heat loss to the surroundings, and a weight was placed on top of the testing rig to give the thermocouples good contact. To isolate the rig from any heat loss out of the sides of the testing rig, R-2 piping insulation was wrapped around the outer edges of the testing rig and sealed with aluminum tape. As the test section heated, each section came to equilibrium temperatures. Once steady state was reached data was collected for an additional 5-10 minutes. These values were then averaged to determine the experimental thermal conductivity of each material. Five tests were run for each insulation and the thermal conductivities averaged to determine the experimental values.

7.4.1.3 Experimental Results

The experimental data for the heat flux through the test section and the temperature difference between thermocouples T2 and T3 are presented in Figures 7.19, 7.20, 7.21, and 7.22 for the hemp, rice hulls, aerogel, and silicone caulking, respectively. Each test was conducted with the dimmer on the surface heater allowing for $\frac{1}{4}$ power. Data was collected until all the desired values were not changing with respect to time. The data collected when the system was at steady-state was used for determining the thermal conductivity of each material, but the transient responses of each test were included for completeness.

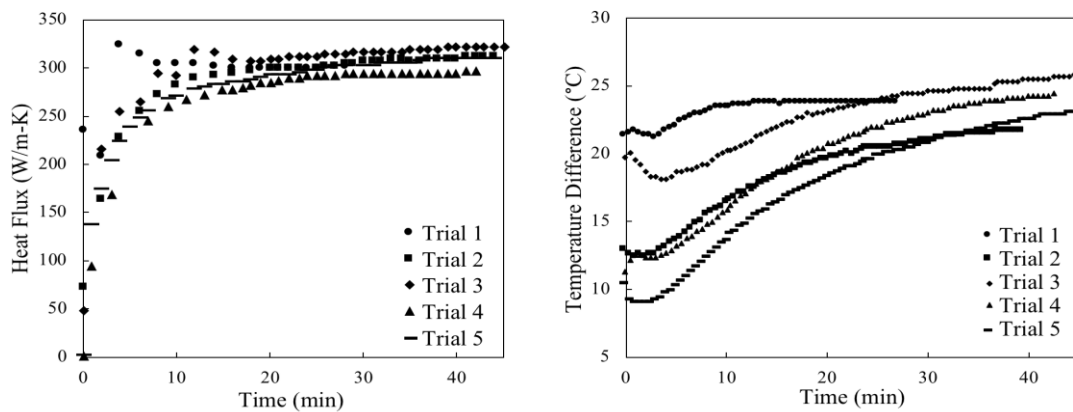


Figure 7.19. Results of the bio-composite hemp insulation testing. Experimental heat flux data (left) and temperature difference between thermocouples T2 and T3 (right).

As shown in Figure 7.19, the surface heater provided consistent heat flux values for each trial. The temperature difference across the test section provided sufficient steady-state data for determining the thermal conductivity of the hemp insulation. Trials 1 and 2 were ended early because the system reached steady-state faster than the other trials.

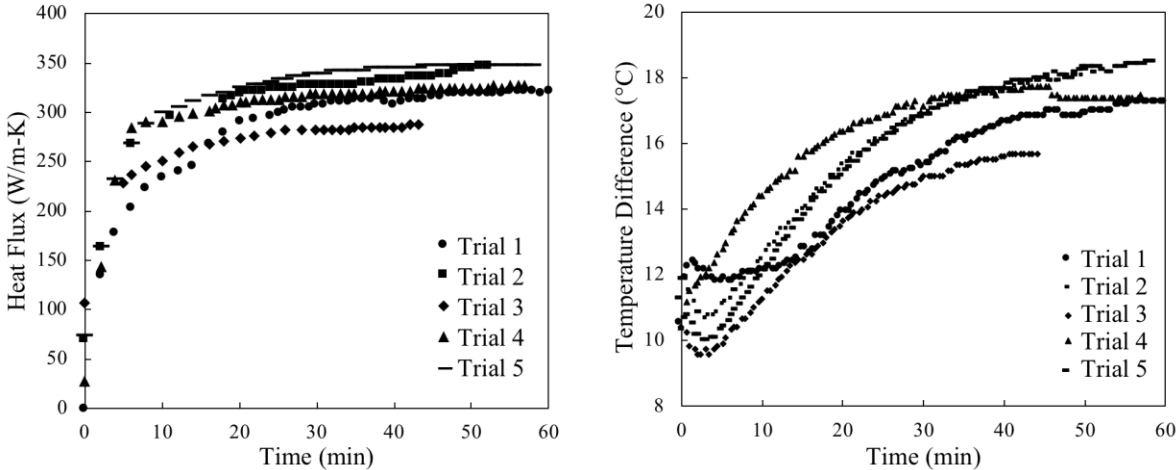


Figure 7.20. Results of the bio-composite rice hull insulation testing. Experimental heat flux data (left) and temperature difference between thermocouples T2 and T3 (right).

Like the hemp insulation tests, the heat flux provided by the surface heater was consistent for all trials as seen in Figure 7.20. However, with the same power settings on the surface heater, a smaller temperature difference was achieved for the rice hulls insulation. Again, trials 2 and 3 were ended earlier than the others due to the system reaching steady state faster.

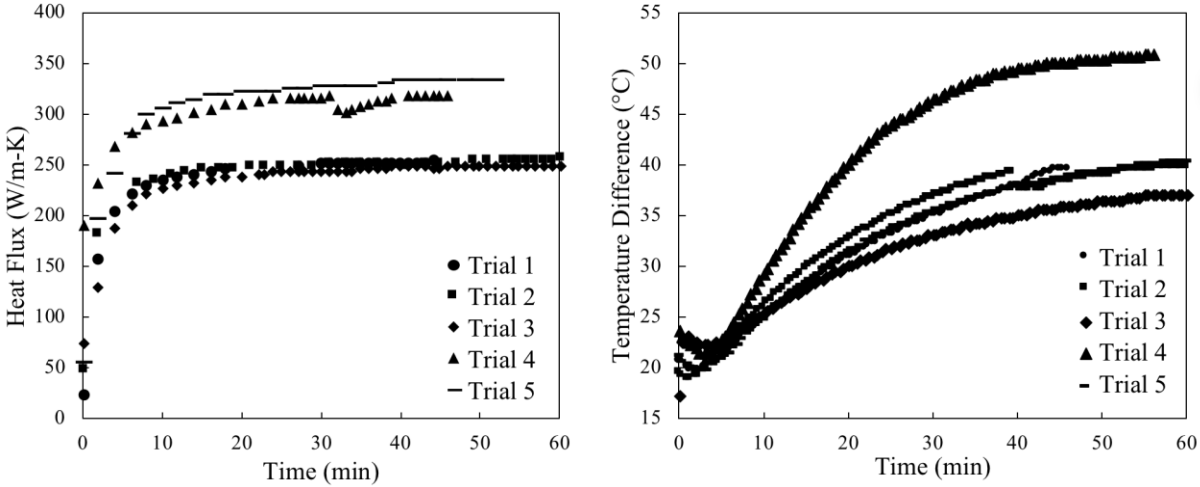


Figure 7.21. Results of the bio-composite aerogel insulation testing. Experimental heat flux results (left) and temperature difference between thermocouples T2 and T3 (right).

Shown in Figure 7.21, a much higher temperature difference was achieved during the aerogel insulation testing, with a slightly smaller heat flux for each trial. The trial 4 temperature difference and heat flux were significantly higher than the other trials. This is likely because the experimental setup used for this testing did not utilize a control circuit and thus had some fluctuations to the heat flux being supplied. Differences

in atmospheric conditions and the ambient temperature could also have affected the point at which steady-state was reached, as some trials were performed on different days.

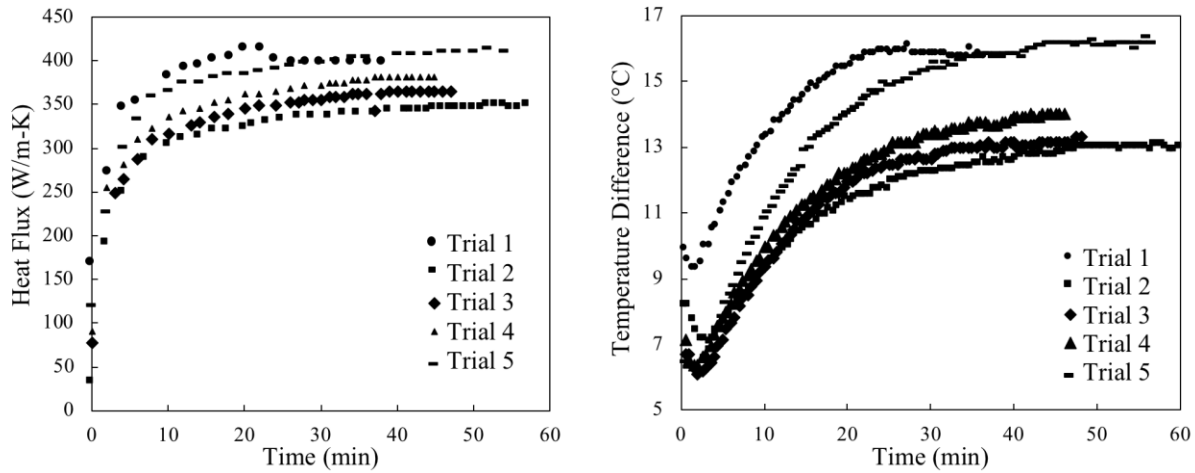


Figure 7.22. Results of the silicone caulking testing. Experimental heat flux data (left) and temperature difference between thermocouples T2 and T3 (right).

The experimental results for the silicone caulking testing, shown in Figure 7.22, indicate that the surface heater was able to provide a significantly higher heat flux for a lower temperature difference. This large heat flux compared to the other tests is likely due to the smaller thickness of the silicone caulking test section. Again, trials 1 and 5 had larger temperature differences compared to the other trials due to the uncontrolled heat flux being supplied, the difference in the steady-state heat flux of these trials can be observed in the left plot shown in Figure 7.22.

7.4.2 Results

The experimental data discussed above was used for further analysis to calculate the thermal conductivity of each testing material and the overall statistical and measurement uncertainty of each value presented. The values presented are accompanied by relevant theory and analysis to support the discussion of the results.

7.4.2.1 Thermal Analysis and Results

Fourier's equation was used to conduct a theoretical heat transfer analysis to determine the thermal conductivity of the materials being tested. For this analysis, the hot side temperature, cold side temperature, and the heat flux provided to the system were assumed to be at steady state, or invariable with time. In addition, the conduction through the test section occurred in one direction. Thus, the 1-D steady-state simplified Fourier's equation was employed for this analysis, shown in Equation 7.2,

$$q_x'' = -k\nabla T \quad (7.2)$$

where q_x'' is the heat flux in W/m^2 , k is the thermal conductivity in W/m-K , and T is the temperature in K. The system was assumed to be sufficiently insulated such that convection and radiation effects could be neglected, and the temperature gradient across the test section was constant. Equation 3.1 was then simplified further to yield Equation 7.3,

$$q_x'' = -\frac{k}{L} (T_C - T_H) \quad (7.3)$$

where L is the length of the test section in m, T_H is the hot side of the insulation temperature in K, and T_C is the cold side of the insulation temperature in K. Solving for the thermal conductivity k in Equation 7.4,

$$k = \frac{q_x'' L}{T_H - T_C} \quad (7.4)$$

the thermal conductivity of the test materials could be determined using the experimentally measured values. A detailed sample derivation can be found in Appendix C. Using Equation 3.3, the thermal conductivity of each material was calculated for the five trials. The average values of the steady-state temperature difference and heat flux data were used for each calculation. The average thermal conductivity and the standard deviation of the results for each material is presented in Table 7.3.

Table 7.3. Compiled thermal conductivity data for each material over five trials, averages and standard deviation calculated.

Experimental Thermal Conductivity (W/m-K)							
Hemp Bio-Composite		Rice Hull Bio-Composite		Aerogel Bio-Composite		Silicone	
Trial 1	0.098	Trial 1	0.124	Trial 1	0.0326	Trial 1	0.0859
Trial 2	0.113	Trial 2	0.126	Trial 2	0.0318	Trial 2	0.0910
Trial 3	0.098	Trial 3	0.122	Trial 3	0.0331	Trial 3	0.0946
Trial 4	0.098	Trial 4	0.125	Trial 4	0.0274	Trial 4	0.0931
Trial 5	0.106	Trial 5	0.126	Trial 5	0.0273	Trial 5	0.0868
Average	0.103	Average	0.125	Average	0.0305	Average	0.0903
Standard Deviation	0.00654	Standard Deviation	0.00147	Standard Deviation	0.00288	Standard Deviation	0.00381

To estimate the thermal conductivity of all samples, a statistical analysis was conducted to determine the 95 % confidence interval of the infinite population. The model shown in Equation 7.5 was used to predict the infinite population mean from the finite-population mean and standard deviation

$$\mu = \bar{x} \pm \frac{t s}{\sqrt{n}} \quad (7.5)$$

where μ is the infinite population mean, \bar{x} is the sample mean, t is the Student-t statistic variable, s is the standard deviation of the sample, and n is the sample size. The Student-t statistic variable was obtained from Student-t Statistic tables for a 95 % confidence interval [17].

The uncertainty of the thermal conductivity due to the resolution of the measuring devices used in this experiment was determined using uncertainty analysis. Equation 7.6 was used to determine the uncertainty of the thermal conductivity, taking Equation 7.4 as the function k ,

$$U_k = \sqrt{\left(\frac{\partial k}{\partial L} U_L\right)^2 + \left(\frac{\partial k}{\partial q_x''} U_{q_x''}\right)^2 + \left(\frac{\partial k}{\partial \Delta T} U_{\Delta T}\right)^2} \quad (7.6)$$

where U_k is the uncertainty of the thermal conductivity and U_x is the measurement uncertainty of each measured quantity. Defining $U_s = \frac{t_s}{\sqrt{n}}$ as the statistical uncertainty, the total uncertainty of the thermal conductivity can be found using Equation 7.7.

$$U_T = \sqrt{U_k^2 + U_s^2} \quad (7.7)$$

A detailed sample analysis can be found in Appendix C.

3.5.3.2.2 Results and Discussion

Table 7.4 presents the thermal conductivity of all testing materials and their uncertainties from the averages of the trials and the uncertainty analysis introduced above.

Table 7.4. Presented thermal conductivity of all tested materials and their uncertainties.

Experimental Thermal Conductivity and Uncertainties (W/m-K)			
Hemp Bio-Composite	Rice Hull Bio-Composite	Aerogel Bio-Composite	Silicone Caulking
0.103 ± 0.0081	0.125 ± 0.0019	0.0305 ± 0.0036	0.0903 ± 0.0048

The aerogel provides the best heat transfer resistance for conduction due to its low thermal conductivity value. The silicone caulking also has a low thermal conductivity, and thus can add a significant thermal resistance to a composite insulation. The hemp silicone and rice hull silicone bio-composites, while having less competitive thermal conductivity values, could provide an inexpensive alternative to more widely used insulation materials. Below, analysis is performed to calculate the equivalent thermal conductivity of hemp and rice hulls without the addition of silicone caulking.

A thermal resistance analogy was used to determine the thermal conductivity of the materials that were mixed with silicone caulking to form the test section. Using the experimentally determined thermal conductivity values of the silicone caulking and the bio-composite silicone material, the thermal conductivity of the testing material could be determined by employing Equation 7.8,

$$k_t = L_t \left(\frac{L_{total}}{k_{total}} - \frac{L_s}{k_s} \right)^{-1} \quad (7.8)$$

where k_t is the thermal conductivity of the testing material, k_{total} is the thermal conductivity of the bio-composite material, and k_s is the thermal conductivity of the silicone caulking, all in units of W/m-K. L_{total} , L_s , and L_t are the thicknesses in units of m of the bio-composite material, the silicone caulking test section, and the organic material, respectively. An analysis of the thermal resistance analogy can be found in Appendix C.

Table 7.5. Thermal conductivity values of the hemp and rice hulls alone.

Corrected Thermal Conductivity (W/m-K)			
Hemp		Rice Hulls	
0.115 ± 0.0094		0.206 ± 0.0051	
% Difference	10.6	% Difference	49.0

The thermal conductivity of the hemp and rice hulls without the silicone caulking are presented in Table 7.5. Removing the thermal resistance of the silicone caulking made the thermal conductivities of the organic materials higher, showing that silicone caulking is a better insulator than either of these materials alone. The difference between the original measured conductivity and the corrected conductivity was larger for the rice hulls than hemp as can be seen in Table 7.5. The drastic difference between the respective changes in thermal conductivity is likely due to two main factors: density and difference in thermal conductivity from silicone. Both materials' densities were measured, and it was found that the rice hulls were denser, and therefore for the same mass they would have taken up less space within the bio-composite section. This is important in the thermal resistance approximation of the materials because it is based upon the thickness of each material in the bio-composite section—not the mass, which was the factor kept constant in manufacturing. The hemp was 1 mm thicker than the rice hulls in the bio-composite section—approximately a 15% difference in thickness. The second factor that caused such a large discrepancy in percent difference was how different the thermal conductivities of the bio-composite sections were from the thermal conductivity of the silicone. The thermal conductivity of hemp is closer to that of silicone, so adding the silicone in the bio-composite section didn't change the bio-composite thermal conductivity by as drastic an amount as the rice hull bio-composite. Due to the rice hulls' thermal conductivity being much higher than that of silicone, adding silicone made the rice hull bio-composite significantly better at insulating.

The aerogel test section provided the most resistance to conduction with the lowest thermal conductivity of 0.0305 W/m-K. Typical refrigerators on the market use polystyrene or polyurethane as the insulation. The thermal conductivity of polystyrene is approximately 0.038 W/m-K, depending on the conditions, and polyurethane's thermal conductivity is approximately 0.034 W/m-K [18] [19]. Aerogel's thermal conductivity is better than these foams, and therefore is a competitive alternative to these other insulating materials. Aerogel is lightweight, and its premade sheets are very flexible making it a versatile option for thermal insulation. In contrast, aerogel is very expensive making it less accessible to a wide range of markets. Rice hulls and hemp, while an order of magnitude worse in terms of thermal conductivity, offer environmental and cost benefits if they can be tailored to the specific application. The plain hemp and plain rice hulls thermal conductivity values were not comparable to that of the aerogel or the silicone caulking test sections but could still have a wide range of uses for cheaper applications. Since these materials are green, cheap, and readily available, hemp and rice hulls are a viable option for food storage applications in developing nations.

7.5 CONTROLS TESTING

To test the controller and filter design, hardware such as a microcontroller, LCD screen, keypad, and current drivers were selected to control the Peltier and heatsink stacks. Using the control theory and simulation presented, a finite-state-machine program was written that controls the hardware. Using cooperative multitasking techniques, tasks will be designed that run simultaneously to implement the hardware and control the inner temperature of the refrigerator. The LCD screen and keypad serve as an interface to provide a way to select a specific desired temperature, as well as display other useful temperature values for testing. An app was developed as the user interface. Unfortunately, due to manufacturing issues the PCB board was unable to be completed although all the theory was designed and is detailed in Section 5.5.

7.6 PROTOTYPE TESTING

Once the prototype was built, the system was wired to a power supply to test the temperatures that could be reached within the chamber. A picture of first build of the refrigerator is shown in Figure 7.23



Figure 7.23. View of the first build stage of the refrigerator.

Figure 7.24 Shows a top view of the refrigerator. As you can see in both figures, there were many areas for improvement at this stage, particularly with respect to sealing of the lid and between the walls and bottom of the refrigerator.

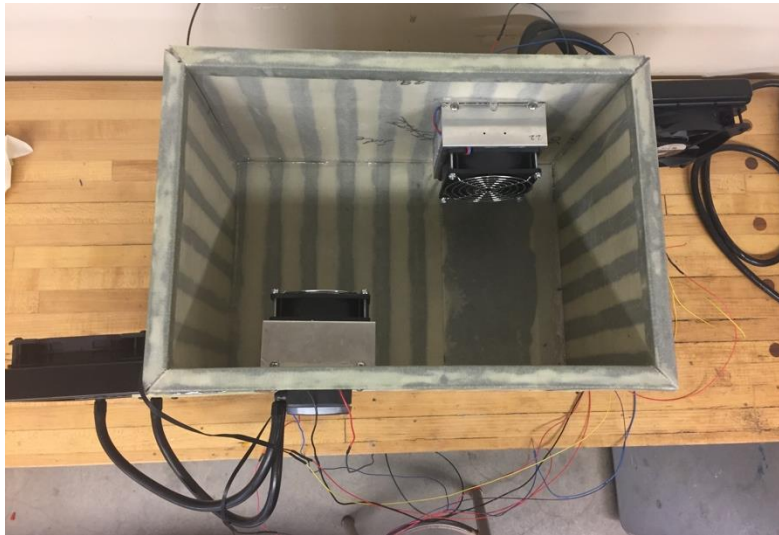


Figure 7.24. Top view of the first build stage of the refrigerator.

This build was tested with two power supplies as a preliminary test to PCB testing. The distribution of voltage and current to each device can be seen in Figure 7.25 The Peltiers were supplied by their own power supply.

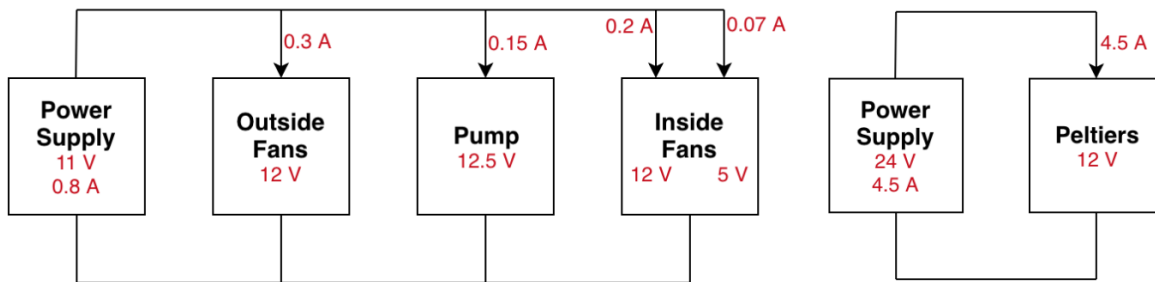


Figure 7.25. Current and voltage diagram for the test of the first build.

The test was run for one hour to see how the refrigerator performed at this stage. The results can be found in Figure 7.26.

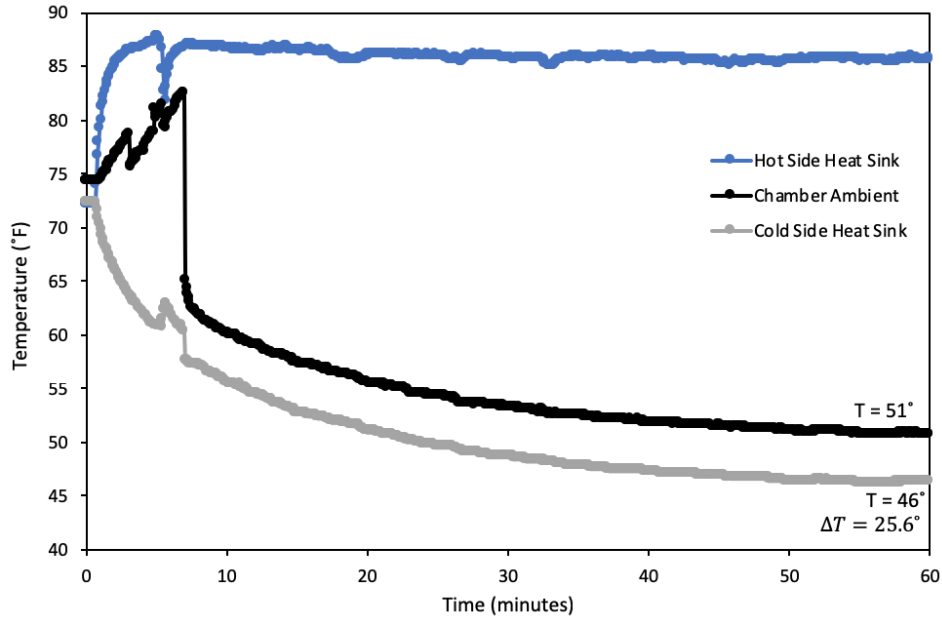


Figure 7.26. Temperature data for the test on the first build.

The results from this initial test were promising, however it did miss the critical mark of 30°F. In order to try and reach this critical temperature, silicone caulking was added inside the refrigerator to decrease losses between walls, and an additional 3/4 inch of Styrofoam was added to the outside of the refrigerator to increase insulation. After adding the Styrofoam to the outside, the data in Figure 7.27 was collected.

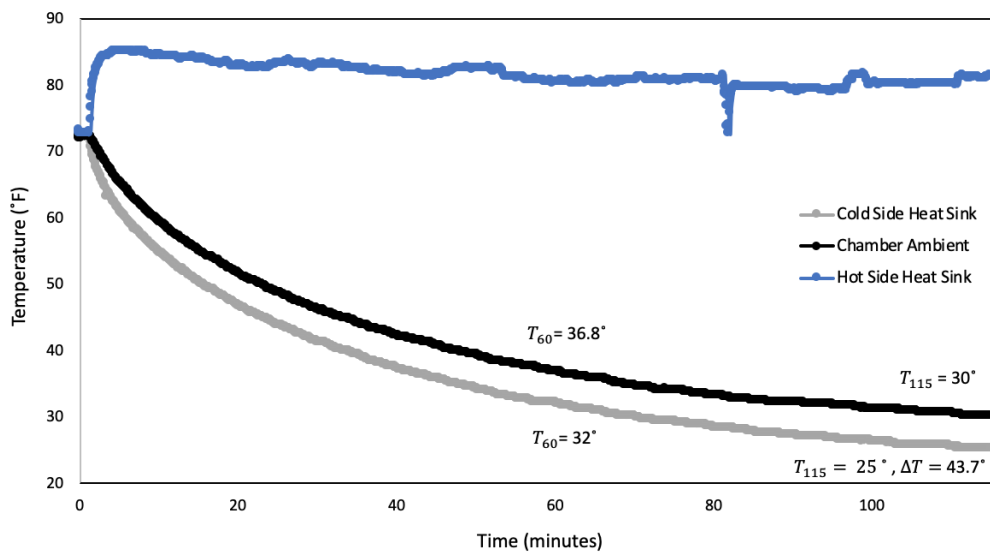


Figure 7.27. Data collected from the final build. Critical temperatures and times are noted on the plot.

Another test was run with the Peltiers at 13V and 5A, at 115 minutes the chamber ambient reached 29.9 °F, a negligible difference from the 12V and 4A condition, and therefore the power difference was unjustifiable. An additional test was run with the inside fans run at 5V instead of their previous 12V, and at 115 minutes the chamber reached 28.4 °F. This difference, although small, is beneficial and is the final voltage value decided for the inside fans. The goal chamber temperature of 30°F was reached at just over one and a half hours, beating the market competition, with freezing temperatures reached a full 30 minutes before this.

8.0 PROJECT MANAGEMENT

With a group of four Mechanical Engineering students and a previous example to start from, as well as plenty of current products on the market to benchmark from, the process of improving the current models was paramount. The full refrigerator has been designed, tested, and built with results achieving the design goals. In addition, a safety hazard checklist is presented in Appendix H explaining the safety hazards that for this project. Table 8.1 shows the key deliverables of the project and the quarter that they were completed.

Table 8.1. List of key deliverables for the project.

Quarter	Key Deliverables	Completed?
1st Quarter ME428	Letter of Introduction to Sponsor	Yes
	Team Contract	Yes
	Quality Function Deployment	Yes
	Scope of Work	Yes
	Concept Models and Concept Prototype	Yes
	Preliminary Design Review	Yes
	Failure Modes and Effects Analysis	Yes
2nd Quarter ME429	Interim Design Review	Yes
	Critical Design Review	Yes
	Risk Assessment	Yes
	Ethics Activities	Yes
	Manufacturing and Test Review	Yes

3rd Quarter ME430	Project Update Memo	Yes
	Hardware/Safety Demo	Yes
	Final Design Review	Yes

In addition to Table 5 above, a Gantt Chart can be found in Appendix L showing specific information regarding the deadlines of the deliverables listed.

9.0 CONCLUSION AND RECOMMENDATIONS

The purpose of this document is to outline the work done to create a versatile thermoelectric refrigerator. By disassembling and working to understand the limitations of existing products, a more robust and reliable product was designed. The final product reached freezing temperatures after approximately an hour, outperforming all of the tested competition. Research on existing patents utilizing Peltier devices has given us valuable insight on what is currently possible utilizing these devices. Based on research and communication with the customer, a list of customer needs and engineering specifications was developed. The chosen design is explained in the above text and was presented to peers in a Final Design Review presentation.

REFERENCES

- [1] Igloo Iceless Owner's Operating Manual, Igloo Products Corp, 2011
- [2] "BESTEK Electric Refrigerator with Wheels 30 Quart 12V for Travel." *Bestek Mall*, www.bestekmall.com/bestek-electric-refrigerator-refrigerator-with-wheels-30-quart-12v-for-travel.
- [3] Doman, Erin. "Wine Refrigerators: Thermoelectric vs. Compressor." *WineRefrigeratorDirect.com*, Dec. 2016, learn.winerefrigeratordirect.com/wine-refrigerators-thermoelectric-vs-compressor/.
- [4] "MLR102 Countertop Laboratory / Pharmacy Refrigerator." *Helmer Scientific | Countertop Lab Pharmacy Refrigerator*, Helmer Scientific, www.helmerinc.com/products/mlr102-countertop-lab-pharmacy-refrigerator.html.
- [5] Drake, *Investigation of Peltier Devices for Refrigeration*, Senior Project for Dr. Schwartz, Cal Poly, 2017
- [6] Liang, Yuying, et al. "Thermal Performance and Service Life of Vacuum Insulation Panels with Aerogel Composite Cores." *Energy and Buildings*, vol. 154, 1 Nov. 2017, pp. 606–617., doi:10.1016/j.enbuild.2017.08.085.
- [7] Gangåssæter, Haakon Fossen, et al. "Air-Filled Nanopore Based High-Performance Thermal Insulation Materials." *Energy Procedia*, vol. 132, Oct. 2017, pp. 231–236., doi:10.1016/j.egypro.2017.09.760.
- [8] Sajid, Muhammad, et al. "An Overview of Cooling of Thermoelectric Devices." *Renewable and Sustainable Energy Reviews*, vol. 78, Oct. 2017, pp. 15–22., doi:10.1016/j.rser.2017.04.098.
- [9] Gao, Yan-Wei, et al. "Enhanced Peltier Cooling of Two-Stage Thermoelectric Refrigerator via Pulse Currents." *International Journal of Heat and Mass Transfer*, vol. 114, June 2017, pp. 656–663., doi:10.1016/j.ijheatmasstransfer.2017.06.102.
- [10] Riley Hilliker, Jalen Mano, Isaac Blundell and Eltahry Elghandour, *Design optimization of corrugated aircraft structure panels to maximize compressive mechanical properties of various fiber reinforced composite materials*, Cal Poly, 2017
- [11] Haryati, Sri, et al. "Insulation Material from Rice Husk Granule ." *Chemical Engineering Transactions*, vol. 56, pp. 571–576., doi:10.3303/CET1756096.
- [12] Hurtado, Pablo Lopez, et al. "A Review on the Properties of Cellulose Fibre Insulation." *Building and Environment*, vol. 96, 2016, pp. 170–177., doi:10.1016/j.buildenv.2015.09.031.
- [13] Nguyen, Son T, et al. "Advanced Thermal Insulation and Absorption Properties of Recycled Cellulose Aerogels." *Colloids and Surfaces A: Physicochemical and Engineering Aspects*, vol. 445, 24 Jan. 2014, pp. 128–134. *Sciencedirect*, ac.els-cdn.com/S0927775714000545/1-s2.0-S0927775714000545-main.pdf?_tid=68af4c9a-4ae4-46df-9880-8749721d3480&acdnat=1520553729_6f55024b408845a812bf549799cbbfd8.
- [14] "Types of Insulation." *Department of Energy*, Office of Energy Efficiency & Renewable Energy, www.energy.gov/energysaver/weatherize/insulation/types-insulation.

- [15] “TE-2-(127-127)-1.15 Thermoelectric Module (Peltier Module) Specifications.” *Tetech*, TeTechnology.
- [16] “Hydro Series™ H60 High Performance Liquid CPU Cooler.” *Corsair*, Corsair, www.corsair.com/us/en/Categories/Products/Liquid-Cooling/Single-Radiator-Liquid-Coolers/Hydro-Series%E2%84%A2-H60-High-Performance-Liquid-CPU-Cooler/p/CW-9060007-WW.
- [17] Thorncroft, G.E. (2015). *Engineering Measurement and Data Analysis*, San Luis Obispo, Mechanical Engineering Department, California Polytechnic State University.
- [18] Jhy-Wen Wu, W.-F. S.-S (1998). Thermal conductivity of polyurethane foams. *International Journal of Heat and Mass Transfer*, 7.
- [19] *Expanded Polystyrene – Thermal Conductivity*. (n.d.). Retrieved from Netzsch: <https://www.netzsch-thermal-analysis.com/us/materials-applications/thermal-insulation/expanded-polystyrene-thermal-conductivity/>

APPENDIX A: QFD

QFD: House of Quality
 Project: Team Project
 Revision: 1
 Date: 1/27/2018

Correlations	
Positive	+
Negative	-
No Correlation	

Relationships	
Strong	●
Moderate	○
Weak	▽

Direction of Improvement	
Maximize	▲
Target	◇
Minimize	▼

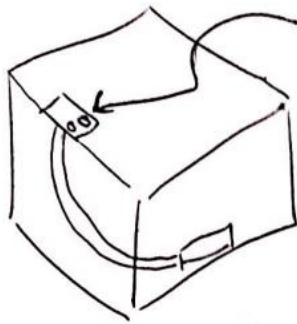
Row #	WHQ: Customer										HOW: Engineering Specifications																NOW: Current Product Assessment - Customer Requirements						Row #						
	Weight Chart	Relation Weight	How Often Weaken	Medical Industry	RV Owners	Truck Drivers	Third World	Outdoors	Office Employees	Maximum Relationship	WHAT: Customer Requirements (explicit & implicit)	Direction of Improvement	Column #	1	2	3	4	5	6	7	8	9	10	11	12	13	14	15	16	Our Current Product	Robtison	Vincomp VTI4TEBDS		Igloo Iceless	Domestic CFX				
1		3%	9	1	9	9	9	9	9	9	9	▲	1	2	3	4	5	6	7	8	9	10	11	12	13	14	15	16	5	4	1	1	4	3	15	1			
2		6%	9	9	3	3	3	3	3	3	3	▲	1	2	3	4	5	6	7	8	9	10	11	12	13	14	15	16	5	5	4	4	5	4	14	2			
3		3%	1	1	1	1	1	1	1	1	1	▲	1	2	3	4	5	6	7	8	9	10	11	12	13	14	15	16	5	1	1	1	1	1	14	4			
4		4%	3	9	9	9	9	9	9	9	9	▲	1	2	3	4	5	6	7	8	9	10	11	12	13	14	15	16	5	5	1	5	4	4	12	5			
5		4%	3	9	9	9	9	9	9	9	9	▲	1	2	3	4	5	6	7	8	9	10	11	12	13	14	15	16	5	1	5	2	5	4	10	6			
6		1%	1	1	1	1	1	1	1	1	1	▲	1	2	3	4	5	6	7	8	9	10	11	12	13	14	15	16	5	1	1	1	1	1	10	7			
7		6%	3	9	9	9	9	9	9	9	9	▲	1	2	3	4	5	6	7	8	9	10	11	12	13	14	15	16	5	1	1	1	2	2	8	8			
8		8%	3	9	9	9	9	9	9	9	9	▲	1	2	3	4	5	6	7	8	9	10	11	12	13	14	15	16	5	1	1	1	5	5	8	9			
9		4%	3	1	3	3	3	3	3	3	3	▲	1	2	3	4	5	6	7	8	9	10	11	12	13	14	15	16	5	1	1	1	1	1	6	10			
10		1%	1	1	1	1	1	1	1	1	1	▲	1	2	3	4	5	6	7	8	9	10	11	12	13	14	15	16	5	1	1	1	1	1	4	11			
11		4%	3	9	9	9	9	9	9	9	9	▲	1	2	3	4	5	6	7	8	9	10	11	12	13	14	15	16	5	5	3	5	4	4	12	12			
12		9%	9	9	9	9	9	9	9	9	9	▲	1	2	3	4	5	6	7	8	9	10	11	12	13	14	15	16	5	4	4	4	4	5	4	13			
13		6%	9	9	9	9	9	9	9	9	9	▲	1	2	3	4	5	6	7	8	9	10	11	12	13	14	15	16	5	4	2	4	3	3	2	14			
14		1%	1	1	1	1	1	1	1	1	1	▲	1	2	3	4	5	6	7	8	9	10	11	12	13	14	15	16	5	1	1	1	1	1	0	15			
15		1%	1	1	1	1	1	1	1	1	1	▲	1	2	3	4	5	6	7	8	9	10	11	12	13	14	15	16	5	1	1	1	1	1	0	16			
												HOW MUCH: Target	10 deg F	2 hours	100% AC, 15V DC Max Power	< 20 lbs	>= 39 quarts	< \$250	20 mins	200 lbs	10 - 40 deg F	100 deg F																	
												Max Relationship	9	9	9	9	9	9	9	9	9	9																	
												Technical Importance Rating	276.2	175.1	218.8	142.5	198.4	202.1	135.5	111.4	303.4	191.5																	
												Relative Weight	14%	9%	11%	7%	10%	11%	7%	6%	18%	7%																	
												Weight Chart	[Bar chart showing relative weights for each specification across various criteria]																										
												Our Product	5	5	5	5	5	5	5	5	5	5																	
												Competitor #1: BESTEK 30 quart	2	1	1	1	5	5	1	1	1	4																	
												Competitor #2: Igloo Iceless	3	0	1	5	4	5	1	1	1	1																	
												Competitor #3: Vincomp VTI4TEBDS	4	1	1	4	4	1	1	1	5	1																	
												Competitor #4: Domestic CFX	5	5	4	1	2	4	1	1	1	5	2																
												Current Product Assessment: Engineering Specifications	[Scatter plot showing performance of various products against engineering specifications]																										

APPENDIX B: Decision Matrices

PUGH MATRIX

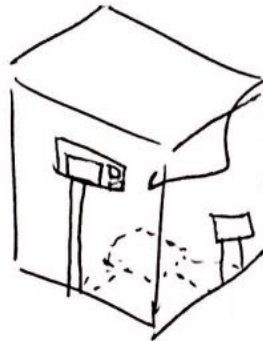
- SKETCH 4 IDEAS FOR CONTROL LOCATION/WIRING

(1)



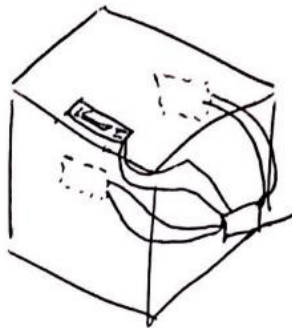
LCD SCREEN WITH
TEMPERATURE DISPLAYED
W/ KNOBS FOR ADJUSTING
TEMPERATURE

(2)



TEMPERATURE UP/DOWN
BUTTONS, CONTROL UNIT
ON BOTTOM

(3)



CONTROL UNIT ~~AND~~ ON
BOTTOM, WIRES GOING TO
PELTS AND LCD SCREENS
IN BETWEEN CORRUGATED
STRUCTURE

PUGH MATRIX (CONT'D)

21

CONCEPT	DATUM	1	2	3	4
USABILITY	S	+	+	+	+
REPAIRABILITY	S	S	S	S	-
ROBUSTNESS	S	-	+	+	+
USER-FRIENDLY	S	+	S	+	S
LIFE	S	-	+	-	-
RELIABILITY	S	+	+	S	S
AESTHETICS	S	+	+	+	+
COST	S	-	-	-	-
WEIGHT	S	-	+	-	-
$\Sigma +$	0	4	6	4	3
$\Sigma -$	0	4	1	3	4
ΣT	0	0	5	1	-1

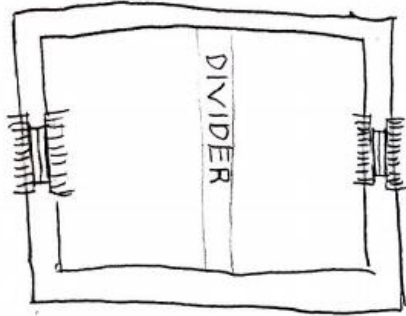
CONCEPT #2 IS THE WINNER

Pugh Matrix for Lid Design

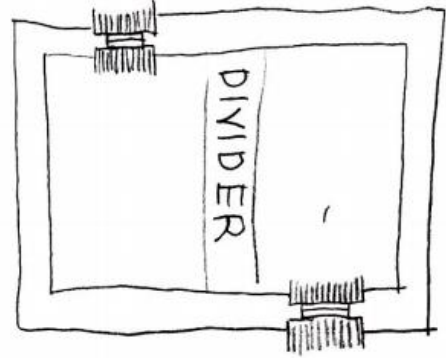
	hinged 1	slide 2	off 3	2 hinge 4
sealing	S	+	+	S
carry-ability	S	+	+	-
light	S	-	+	-
simple	S	-	+	-
insulation	S	S	S	-
strength	S	S	S	-
seal panel add-ability	S	-	-	-
wiring ease	S	-	-	S
$\Sigma +$	0	2	4	0
$\Sigma -$	0	4	2	6
ΣS	8	2	2	2

PELTIER PLACEMENT (2 STACKS)

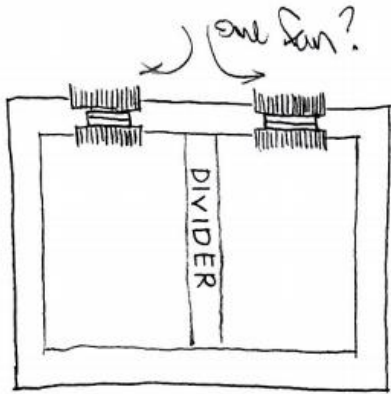
1:



2:

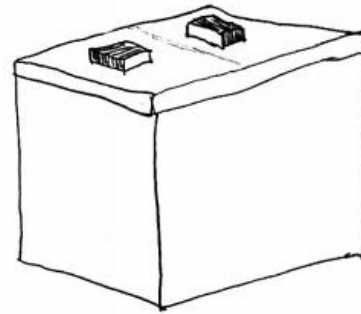


3:



4:

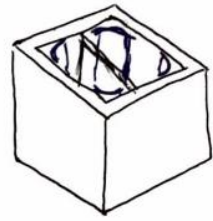
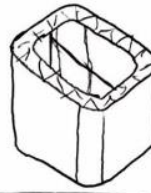
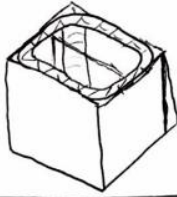
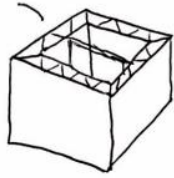
DATUM



	1	2	3	4
car compatibility	-	-	S	S
connection inside	-	-	-	S
capacity for 2 compartments	S	S	S	S
CG	+	+	+	S
wiring amount	-	-	S	S
interference	+	+	-	S
fan economic	-	-	S	S
ΣS	1	1	4	7
$\Sigma +$	2	2	1	0
$\Sigma -$	4	4	2	0

Pugh Matrix (structural)

2/19/18



size	S	S	S	+
weight	S	+	S	+
corrugation style	S	+	S	+
area for insulation	S	+	-	+
workability	+	-	-	-
pieces/steps to cure	+	-	-	-
strength	S	+	-	+
aesthetic	-	-	+	-
portability	S	-	+	-
car placement	-	-	+	-
radius	-	+	+	+
partition	S	S	S	S
handle	-	-	+	-
Σ-	3	6	4	6
ΣS	7	2	4	6
Σ+	1	5	4	6

PUGH MATRIX: INSULATION

CONCEPTS →

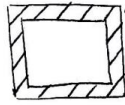
CATEGORIES ↓

① AEROGEL

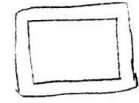
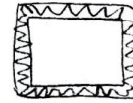
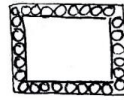
② RICE HULLS

③ FIBERGLASS

④ STYROFOAM



(DATUM)



NON-TOXIC

S

+

S

-

DENSITY

S

-

-

-

THERMAL CONDUCTIVITY

S

-

-

-

COST

S

+

+

+

WORKABILITY

S

+

S

+

LIFE

S

-

+

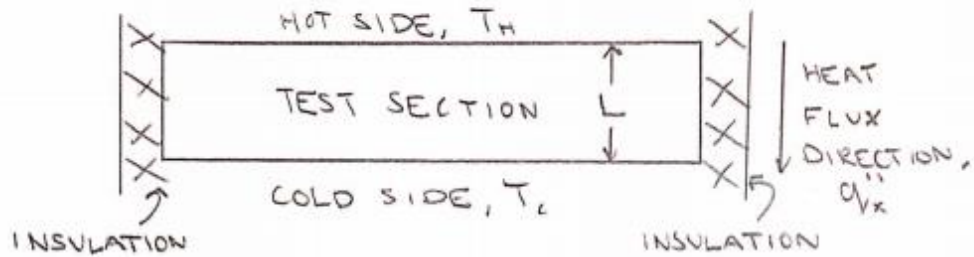
+

Σ -	3	2	4
Σ S	0	2	0
Σ +	3	2	2

APPENDIX C: Preliminary Insulation Hand Calculations

APPENDIX C

SCHEMATIC



ASSUMPTIONS

- 1) STEADY STATE
- 2) NEGLECT CONVECTION AND RADIATION
- 3) LINEAR TEMPERATURE DISTRIBUTION
- 4) 1-D CONDUCTION

ANALYSIS

STARTING WITH FOURIER'S LAW,

$$q''_x = -k \nabla T$$

WITH THE ASSUMPTIONS LISTED, THIS EQUATION BECOMES

$$q''_x = -\frac{k}{L} (T_c - T_H)$$

SOLVING FOR THE THERMAL CONDUCTIVITY k ,

$$\underline{\underline{k = \frac{q''_x L}{T_H - T_c}}}$$

APPENDIX C

TO ESTIMATE THE THERMAL CONDUCTIVITY K FOR ALL SAMPLES, THE MEAN OF THE FINITE SAMPLE OF K -VALUES WILL BE USED TO PREDICT THE INFINITE POPULATION MEAN.

MODEL:

$$M = \bar{X} \pm \frac{t S}{\sqrt{n}}$$

WHERE

M = POPULATION MEAN

\bar{X} = SAMPLE MEAN

n = SAMPLE SIZE

S = SAMPLE STANDARD DEVIATION

t = STUDENT t STATISTIC VARIABLE

FOR A SAMPLE SIZE OF $n=5$, THE DEGREES OF FREEDOM IS

$$v = n - 1 = 4$$

FROM STUDENT- t STATISTIC TABLES FOR $v=4$ AND 95% CONFIDENCE INTERVAL,

$$t = 2.776$$

EMPLOYING THESE VALUES IN THE MODEL EQUATION, THE INFINITE POPULATION MEAN CAN BE ESTIMATED.

$$M = \bar{X} \pm \frac{t S}{\sqrt{n}}$$

$$M = \bar{X} \pm \frac{(2.776) S}{\sqrt{5}}$$

$$\underline{M = \bar{X} \pm 1.24 S}$$

APPENDIX C

NEXT, THE UNCERTAINTY OF THE THERMAL CONDUCTIVITY DUE TO THE RESOLUTIONS OF THE MEASURING DEVICES USED IS CALCULATED BY:

$$U_k = \left[\left(\frac{\partial k}{\partial L} U_L \right)^2 + \left(\frac{\partial k}{\partial q''} U_{q''} \right)^2 + \left(\frac{\partial k}{\partial \Delta T} U_{\Delta T} \right)^2 \right]^{1/2}$$

WHERE

U_L = HALF-DIGIT RESOLUTION UNCERTAINTY OF THICKNESS MEASUREMENT

$$= \pm 0.025 \text{ mm}$$

$U_{q''}$ = HALF-DIGIT RESOLUTION UNCERTAINTY OF HEAT FLUX MEASUREMENT

$$= \pm 0.05 \text{ W/m}^2$$

$U_{\Delta T}$ = HALF-DIGIT RESOLUTION UNCERTAINTY OF TEMPERATURE MEASUREMENT

$$= \pm 0.05^\circ \text{C}$$

AND THE FUNCTION k IS DEFINED AS

$$k = \frac{q'' L}{\Delta T}$$

SIMPLIFYING,

$$U_k = \left[\left(\frac{q''}{\Delta T} U_L \right)^2 + \left(\frac{L}{\Delta T} U_{q''} \right)^2 + \left(\frac{L q''}{2 \Delta T^2} U_{\Delta T} \right)^2 \right]^{1/2}$$

FIND THE TOTAL UNCERTAINTY BY ROOT-SUM-SQUARING THE STATISTICAL AND MEASUREMENT UNCERTAINTIES WHERE $U_s = t_s/\sqrt{n}$

$$U_T = \sqrt{U_k^2 + U_s^2}$$

APPENDIX C

MODEL

THERMAL RESISTANCE IN SERIES:



R_t - THERMAL RESISTANCE OF TESTED MATERIAL

R_s - THERMAL RESISTANCE OF SILICONE EPOXY

$$R_t = \frac{L_t}{K_t A}$$

$$R_s = \frac{L_s}{K_s A}$$

ANALYSIS

FOR THERMAL RESISTANCES IN SERIES,

$$R_{\text{TOTAL}} = R_t + R_s$$

$$\frac{L_{\text{TOTAL}}}{K_{\text{TOTAL}} A} = \frac{L_t}{K_t A} + \frac{L_s}{K_s A}$$

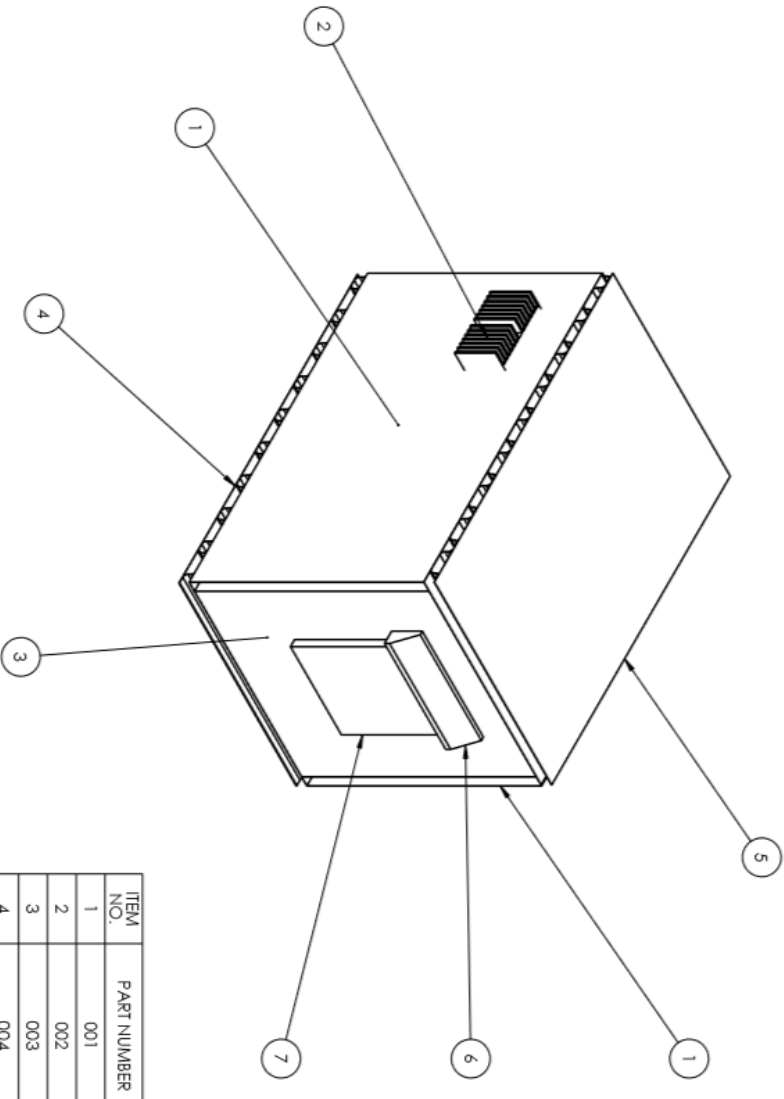
SOLVING FOR K_t , THE DESIRED THERMAL CONDUCTIVITY,

$$\frac{L_{\text{TOTAL}}}{K_{\text{TOTAL}}} = \frac{L_t}{K_t} + \frac{L_s}{K_s}$$

$$\frac{L_t}{K_t} = \frac{L_{\text{TOTAL}}}{K_{\text{TOTAL}}} - \frac{L_s}{K_s}$$

$$\underline{\underline{K_t = L_t \left(\frac{L_{\text{TOTAL}}}{K_{\text{TOTAL}}} - \frac{L_s}{K_s} \right)^{-1}}}$$

APPENDIX D: Drawing Package

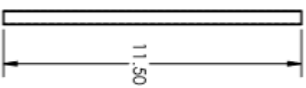
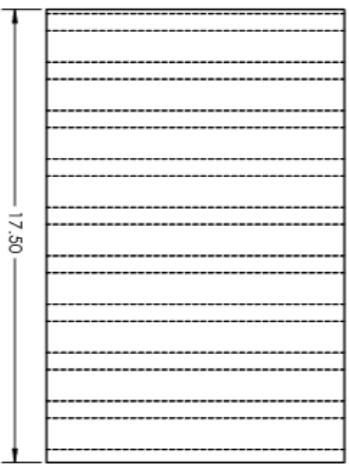


The drawing shows an exploded view of a cooler assembly. Callout 1 points to the top and bottom corrugated panels. Callout 2 points to the long side corrugation. Callout 3 points to the bottom side corrugation. Callout 4 points to the short side corrugation. Callout 5 points to the top corrugated lid. Callout 6 points to the felt device/heat sink. Callout 7 points to the LCD interface. Callout 8 points to the control module.

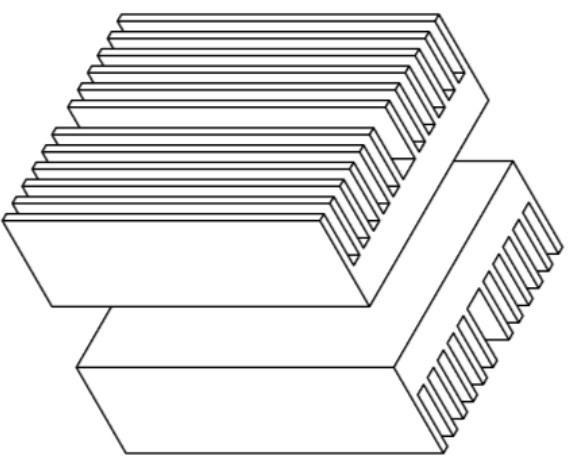
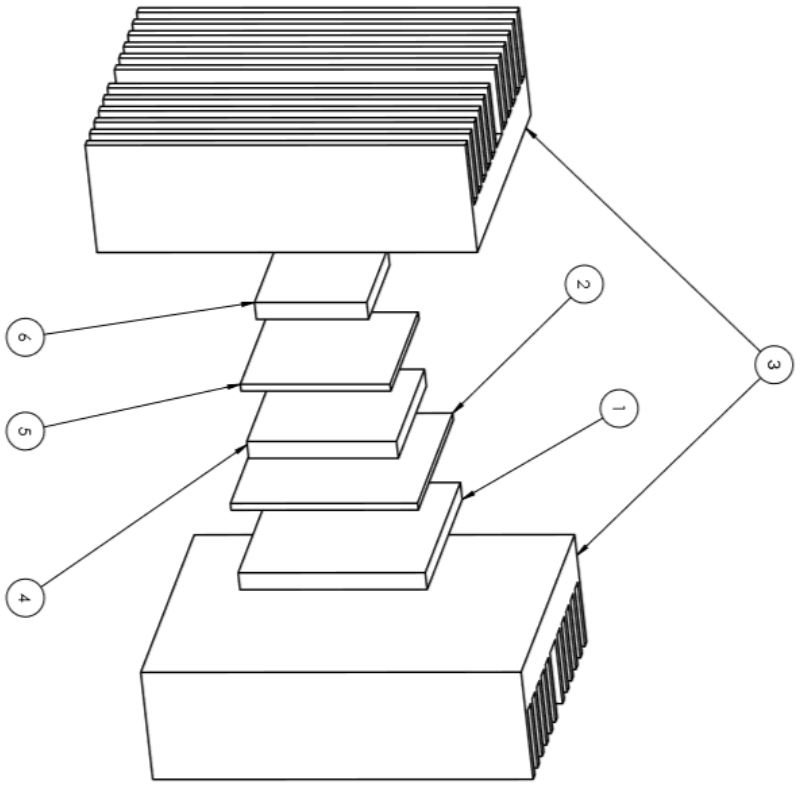
ITEM NO.	PART NUMBER	DESCRIPTION	QTY.
1	001	LONG SIDE CORRUGATION	2
2	002	PELTIER DEVICE/HEAT SINK	2
3	003	SHORT SIDE CORRUGATION	2
4	004	BOTTOM CORRUGATION	1
5	005	CORRUGATED LID	1
6	006	LCD INTERFACE	1
7	007	CONTROL MODULE	1
8	008	PARTITION	1

Col Poly Mechanical Engineering	Lab Section:	Assignment #	Title: COOLER ASSEMBLY	Dwn By: ZACH WILSON
ME 429 - SPRING 2018	Dwg #: 000	Nxt Asb:	Dte: 4/25/18	Scale: 1 = 4
				Chkd By: JOSH DIMAGGIO

- NOTES:**
 UNLESS OTHERWISE SPECIFIED:
 1) ALL DIMENSIONS IN INCHES
 2) MATERIAL = FIBERGLASS
 3) TRAPEZOIDAL CORRUGATION PATTERN
 4) XX TOLERANCE = ± .010
 5) DEBURK ALL EDGES .005 TO .015
 6) FIBERGLASS THICKNESS = 0.125



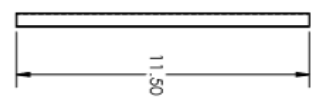
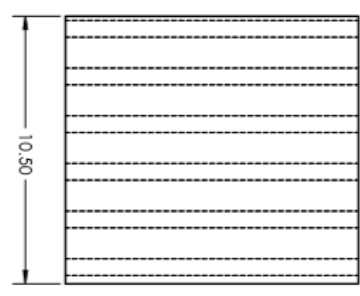
Cal Poly Mechanical Engineering	Lab Section:	Assignment #	Title: LONG SIDE CORRUGATION	Dwn. By: ZACH WILSON
ME 429 - SPRING 2018	Dwg. #: 001	Nxt. Ass:	Date: 4/25/18	Chkd. By: JOSH DIMAGGIO
			Scale: 1 = 4	



ITEM NO.	PART NUMBER	DESCRIPTION	QTY.
1	001	BASE PELTIER	1
2	002	BOTTOM ALUMINUM PLATE	1
3	003	HEAT SINK	2
4	004	MIDDLE PELTIER	1
5	005	TOP ALUMINUM PLATE	1
6	006	TOP PELTIER	1

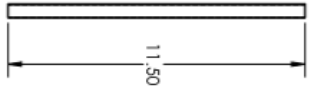
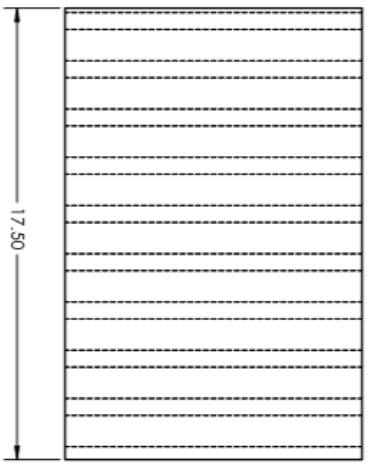
Cal Poly Mechanical Engineering
 MAE 429 - SPRING 2018
 Lab Section: Lab Section: Assignment # Title: PELTIER/HEAT SINK STACK
 Dwg. #: 002 Nxt Ass: Date: 4/25/18 Scale: 1 = 1
 Dwn. By: ZACH WILSON
 Chkd. By: CASSIE BECK

- NOTES:**
 UNLESS OTHERWISE SPECIFIED:
 1) ALL DIMENSIONS IN INCHES
 2) MATERIAL = FIBERGLASS
 3) TRAPEZOIDAL CORRUGATION PATTERN
 4) TOLERANCE ± .010
 5) DEBURR ALL EDGES .005 TO .015
 6) FIBERGLASS THICKNESS = 0.125



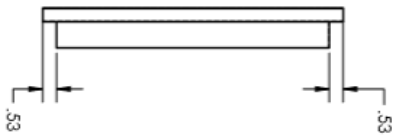
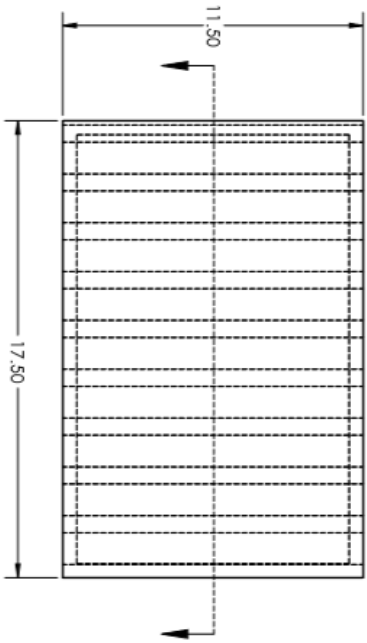
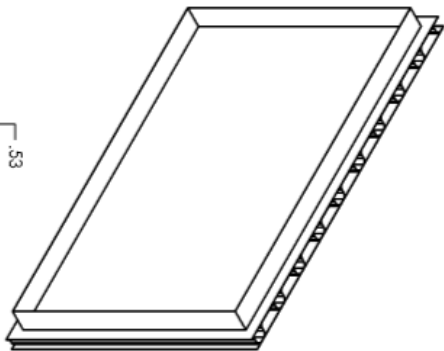
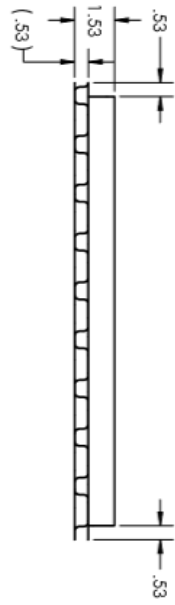
Cal Poly Mechanical Engineering	Lab Section:	Assignment #	Title: SHORT SIDE CORRUGATION	Dwn. By: ZACH WILSON
ME 429 - SPRING 2018	Dwg. #: 003	Nxt Asb:	Date: 4/25/18	Chkd. By: CASSIE BECK
			Scale: 1 = 4	

- NOTES:**
 UNLESS OTHERWISE SPECIFIED:
 1) ALL DIMENSIONS IN INCHES
 2) MATERIAL = FIBERGLASS
 3) TRAPEZOIDAL CORRUGATION PATTERN
 4) XX TOLERANCE = $\pm .010$
 5) DEBURR ALL EDGES .095 TO .015
 6) FIBERGLASS THICKNESS = 0.125



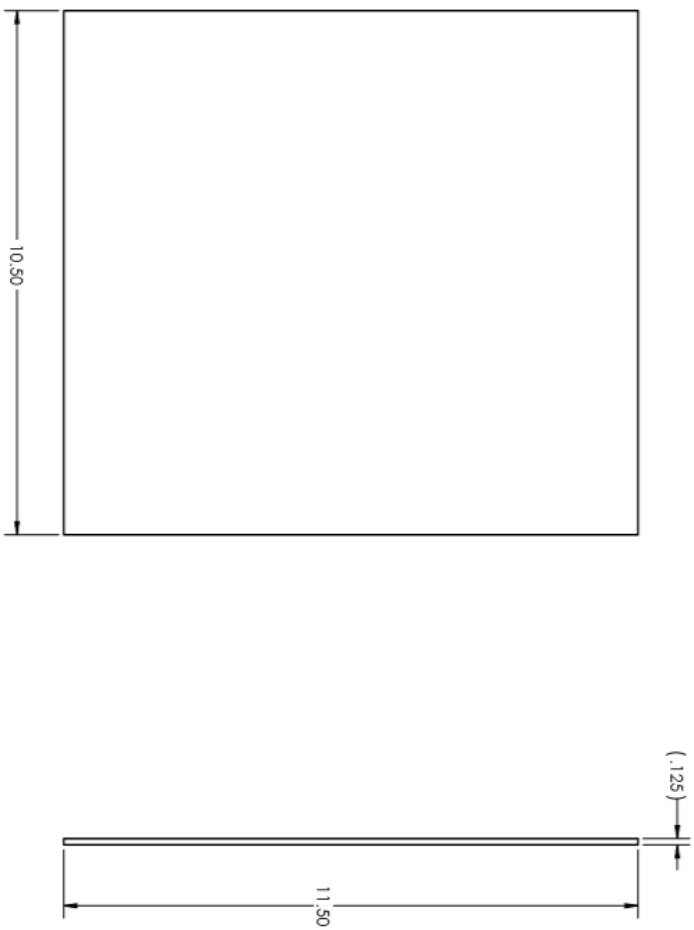
Col Poly Mechanical Engineering	Lab Section:	Assignment #	Title: BOTTOM CORRUGATION	Dwn. By: ZACH WILSON
ME 429 - SPRING 2018	Dwg. #: 004	Nrt Abo:	Date: 4/25/18	Chkd. By: RYAN GELINAS
			Scale: 1 = 4	

- NOTES:**
 UNLESS OTHERWISE SPECIFIED:
 1) ALL DIMENSIONS IN INCHES
 2) MATERIAL = FIBERGLASS
 3) TRAPEZOIDAL CORRUGATION PATTERN
 4) DEBURR ALL EDGES $\pm .005$ TO $.015$
 5) FIBERGLASS THICKNESS = 0.125



Cal Poly Mechanical Engineering	Lab Section:	Assignment #	Title: CORRUGATED LID	Dwn. By: ZACH WILSON
ME 429 - SPRING 2018	Dwg. #: 005	N/A	Date: 4/25/18	Scale: 1 = 4
				Chkd. By: RYAN GEUNAS

- NOTES:**
 UNLESS OTHERWISE SPECIFIED:
 1) ALL DIMENSIONS IN INCHES
 2) MATERIAL = FIBERGLASS
 3) XX TOLERANCE = ± .010
 4) DEBURR ALL EDGES .005 TO .015
 5) FIBERGLASS THICKNESS = 0.125



Col Poly/Mechanical Engineering	Lab Section:	Assignment #	Title: PARTITION	Drawn By: ZACH WILSON
ME 429 - SPRING 2018	Dwg. #: 008	NX# Atb:	Date: 4/25/18	Scale: 1 = 2
				Chkd By: JOSH DIMAGGIO

Peltier Controller Model

Table of Contents

.....	1
System Parameters	1
Model	2
Original Simulation	4
Simulation with Anti-Windup Scheme	6
Simulation with Digital Filter	7
Simulation with Kalman Filter, 1st Iteration	9
Simulation with Kalman Filter, 2nd Iteration	11
Comparison	13

Zach Wilson, 3/28/18

```
clear;
clc;
close all;
```

System Parameters

```
% Bestek Parameters
% Tau_peltier = 6.1667*60;      % Time constant of peltier temperature
%                               [s]
% Tau_chamber = 13.4167*60;    % Time constant of inner chamber
%                               temperature [s]
% K_peltier = 9.5667;          % Gain of peltier temperature
% K_chamber = 0.5234;         % Gain of inner chamber temperature

% Model Parameters
Tau_peltier = 6.1667*60;      % Time constant of peltier temperature
%                               [s]
Tau_chamber = 13.4167*60;    % Time constant of inner chamber
%                               temperature [s]
K_peltier = 18;              % Gain of peltier temperature
K_chamber = 0.75;           % Gain of inner chamber temperature
deltat = 0.5;               % Discrete timestep [s]
process_noise_variance = 0.001; % Process noise
rand_process = randi(40,1); % Random number process noise seed
Q = process_noise_variance; % Process noise matrix used in kalman
%                               filter algorithm
measure_noise_variance = 0.2; % Measurement noise
rand_measure = randi(40,1); % Random number measurement noise seed
R = measure_noise_variance; % Measurement noise matrix used in
%                               kalman filter algorithm
dead_sone_current = 6;      % Saturation current [A]
sim_time = 100*60;         % Timespan of simulation [s]
step_time = 3*60;          % Time of step input [s]
desired_temperature = 22;   % Desired chamber temperature [deg F]
```

Peltier Controller Model

```
initial_temperature = 90;      % Initial (ambient) temperature [deg
    F]

% Digital Filter parameters
Tau_filter = 5;                % Digital filter time
    constant [s]
C_previous = Tau_filter/(Tau_filter + deltat); % Previous filtered
    value gain
C_input = deltat/(Tau_filter + deltat);      % Filter input gain

% Kalman Filter Parameters
x0 = 0;                        % Initial condition of predicted state
Pk0 = 0.5;                    % Initial condition of predictor matrix

% Control parameters
Kp = 0.13;                    % Proportional gain
Ki = 0.00018;                % Integral gain
Kd = 0.0;                    % Derivative gain
Kb = 250;                    % Anti-windup gain

% Prompt for which kalman filter to be used
which_kalman = 2;
```

Model

```
% Peltier element system model
peltier_tf_c = tf(K_peltier, [Tau_peltier 1]); % Continuous transfer
    function
peltier_ss_c = ss(peltier_tf_c);             % Continuous state space
    model
peltier_ss_d = c2d(peltier_ss_c, deltat);    % Discrete state space
    model
Ap_c = peltier_ss_c.A;    % A matrix
Bp_c = peltier_ss_c.B;    % B matrix
Hp_c = peltier_ss_c.C;    % H matrix
Dp_c = peltier_ss_c.D;    % D matrix

% Chamber system model
chamber_tf_c = tf(K_chamber, [Tau_chamber 1]); % Continuous transfer
    function
chamber_ss_c = ss(chamber_tf_c);             % Continuous state space
    model
chamber_ss_d = c2d(chamber_ss_c, deltat);    % Discrete state space
    model
Ac_c = chamber_ss_c.A;    % A matrix
Bc_c = chamber_ss_c.B;    % B matrix
Hc_c = chamber_ss_c.C;    % H matrix
Dc_c = chamber_ss_c.D;    % D matrix
Ac_d = chamber_ss_d.A;    % A matrix
Bc_d = chamber_ss_d.B;    % B matrix
Hc_d = chamber_ss_d.C;    % H matrix
Dc_d = chamber_ss_d.D;    % D matrix
```

Peltier Controller Model

```
% Coupled system model
system_tf_c = tf((K_peltier*K_chamber), [Tau_peltier+Tau_chamber
    (Tau_peltier + Tau_chamber) 1]); % Continuous transfer function
system_ss_c = ss(system_tf_c); % Continuous state space
model
system_ss_d = c2d(system_ss_c,deltat); % Discrete state space model
A_d = system_ss_d.A; % A matrix
B_d = system_ss_d.B; % B matrix
H_d = system_ss_d.C; % H matrix
D_d = system_ss_d.D; % D matrix

% Original Simulation
%
set_param('System_Controller_Model_sim_original','MaxConsecutive2CsMsg','none');
sim('System_Controller_Model_sim_original')
tout_original = tout;

% Simulation with anti-windup
%
set_param('System_Controller_Model_sim_antiwindup','MaxConsecutive2CsMsg','none');
sim('System_Controller_Model_sim_antiwindup')
tout_antiwindup = tout;

% Simulation with digital filter
%
set_param('System_Controller_Model_sim_digital_filter','MaxConsecutive2CsMsg','nc
sim('System_Controller_Model_sim_digital_filter')
tout_digital = tout;

% Simulation with kalman filter
%
set_param('System_Controller_Model_sim_kalman','MaxConsecutive2CsMsg','none');
sim('System_Controller_Model_sim_kalman')
tout_kalman = tout;

%
set_param('System_Controller_Model_sim_kalman_2','MaxConsecutive2CsMsg','none');
sim('System_Controller_Model_sim_kalman_2')
tout_kalman_2 = tout;

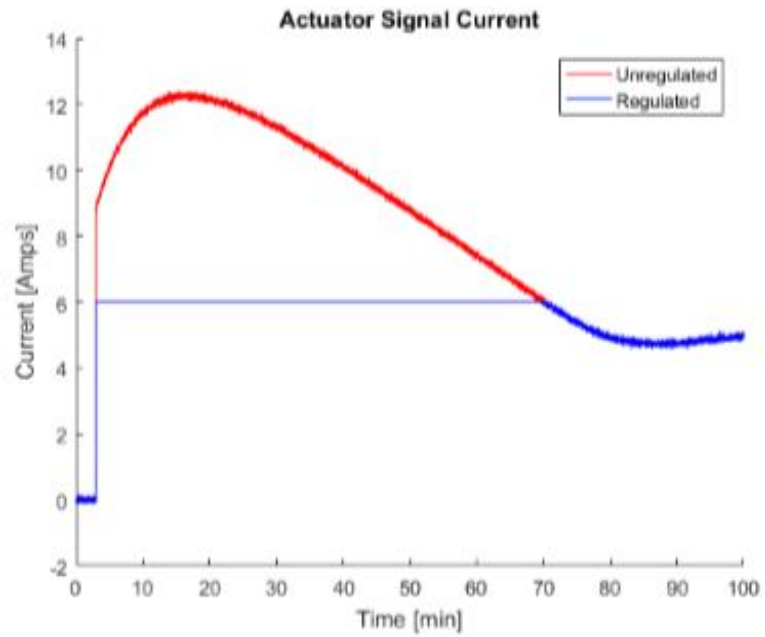
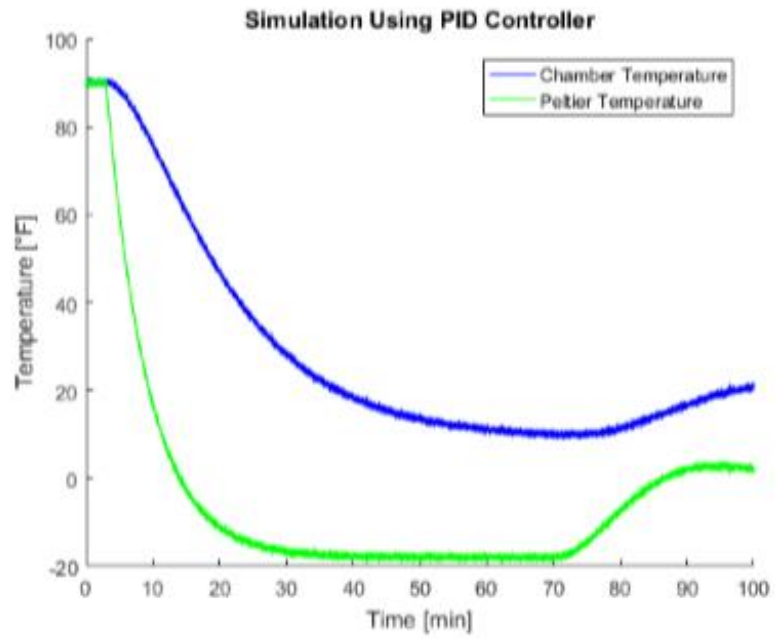
Warning: Convergence problem (mode oscillation) detected when solving
algebraic
loop containing 'System_Controller_Model_sim_antiwindup/PID
Controller/Derivative' at time 525.3311015220396. Simulink will try
to solve
this loop using Simulink 3 (R11) strategy. Use
feature('ModeIterationsInAlgLoops',0) to disable the strategy
introduced in
Simulink 4 (R12)
Warning: Convergence problem (mode oscillation) detected when solving
algebraic
loop containing 'System_Controller_Model_sim_digital_filter/PID
Controller/Derivative' at time 1019.0325257133484. Simulink will try
to solve
```

```
this loop using Simulink 3 (R11) strategy. Use
feature('ModeIterationsInAlgLoops',0) to disable the strategy
introduced in
Simulink 4 (R12)
```

Original Simulation

```
% Plot of inner chamber temperature
figure;
hold on
title('Simulation Using PID Controller')
plot(tout_original/60,chamber_temp_original,'color','blue')
plot(tout_original/60,peltier_temp_original,'color','green')
xlabel('Time [min]')
ylabel('Temperature [°F]')
legend('Chamber Temperature','Peltier Temperature')
hold off

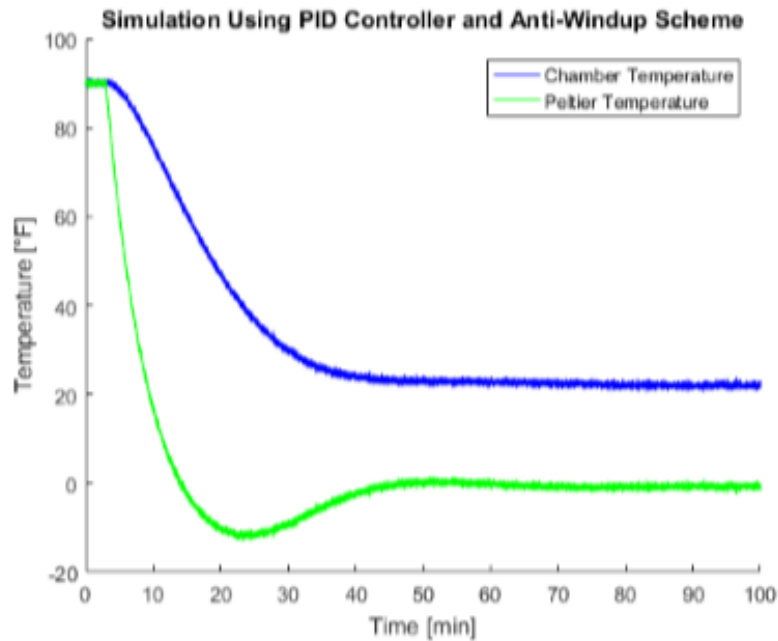
% Plot of actuator signal
figure;
hold on
title('Actuator Signal Current')
plot(tout_original/60,actuator_signal_original,'color','red')
plot(tout_original/60,actuator_signal_sat_original,'color','blue')
xlabel('Time [min]')
ylabel('Current [Amps]')
legend('Unregulated','Regulated')
hold off
```

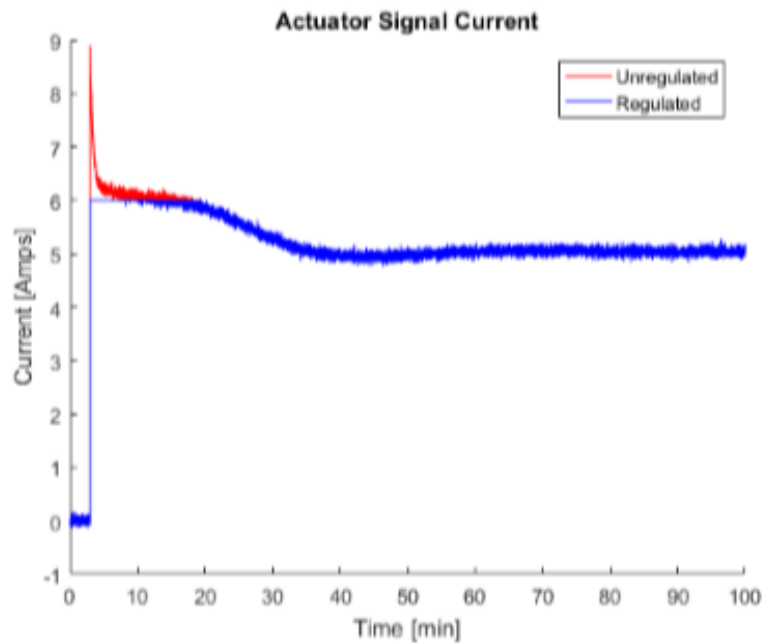


Simulation with Anti-Windup Scheme

```
% Plot of inner chamber temperature
figure;
hold on
title('Simulation Using PID Controller and Anti-Windup Scheme')
plot(tout_antiwindup/60, chamber_temp_antiwindup, 'color', 'blue')
plot(tout_antiwindup/60, peltier_temp_antiwindup, 'color', 'green')
xlabel('Time [min]')
ylabel('Temperature [°F]')
legend('Chamber Temperature', 'Peltier Temperature')
hold off

% Plot of actuator signal
figure;
hold on
title('Actuator Signal Current')
plot(tout_antiwindup/60, actuator_signal_antiwindup, 'color', 'red')
plot(tout_antiwindup/60, actuator_signal_sat_antiwindup, 'color', 'blue')
xlabel('Time [min]')
ylabel('Current [Amps]')
legend('Unregulated', 'Regulated')
hold off
```





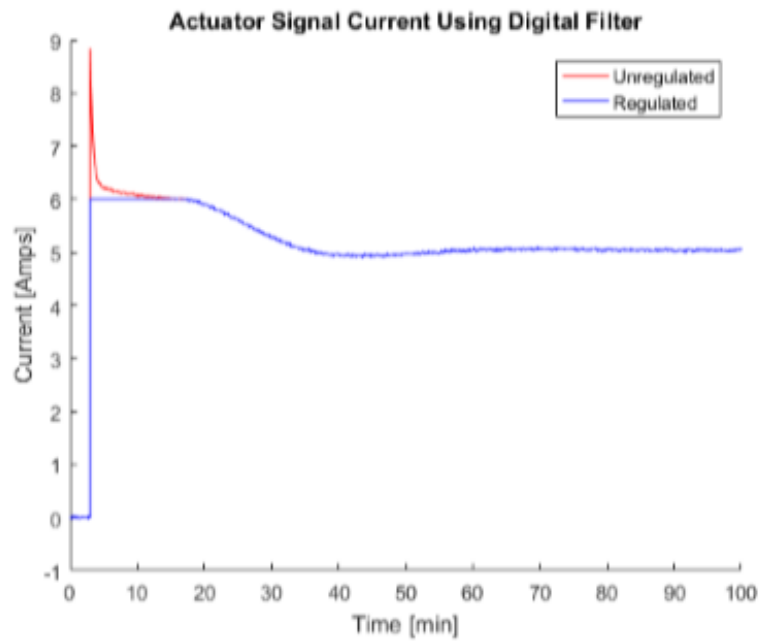
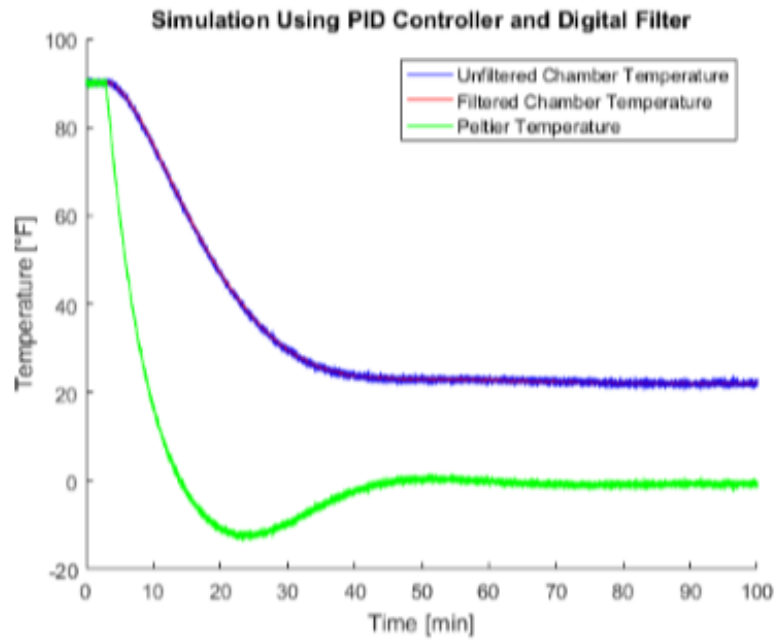
Simulation with Digital Filter

```

% Plot of inner chamber temperature
figure;
hold on
title('Simulation Using PID Controller and Digital Filter')
plot(tout_digital/60,chamber_temp_digital,'color','blue')
plot(tout_digital/60,filtered_temp_digital,'color','red')
plot(tout_digital/60,peltier_temp_digital,'color','green')
xlabel('Time [min]')
ylabel('Temperature [°F]')
legend('Unfiltered Chamber Temperature','Filtered Chamber
Temperature','Peltier Temperature')
hold off

% Plot of actuator signal
figure;
hold on
title('Actuator Signal Current Using Digital Filter')
plot(tout_digital/60,actuator_signal_digital,'color','red')
plot(tout_digital/60,actuator_signal_sat_digital,'color','blue')
xlabel('Time [min]')
ylabel('Current [Amps]')
legend('Unregulated','Regulated')
hold off

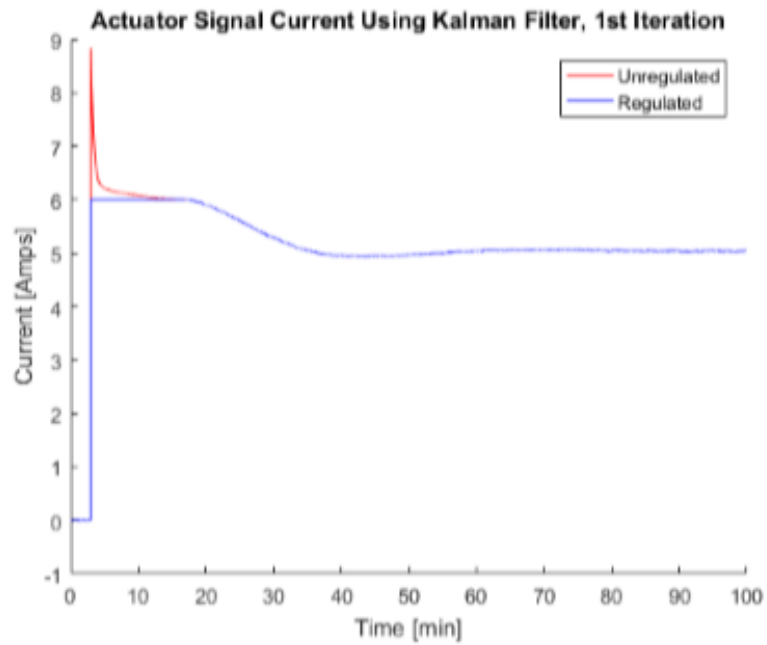
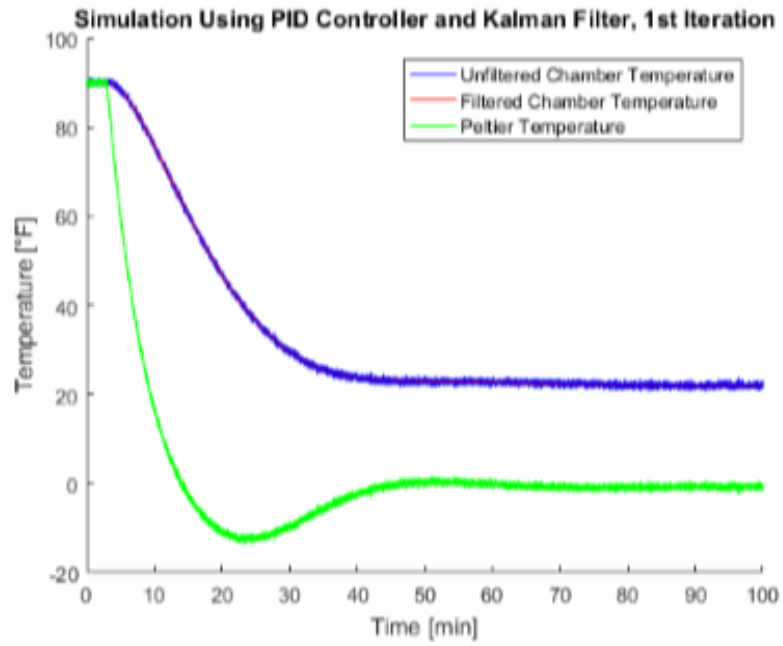
```

Simulation with Kalman Filter, 1st Iteration

```
% Plot of inner chamber temperature
figure;
hold on
title('Simulation Using PID Controller and Kalman Filter, 1st
Iteration')
plot(tout_kalman_2/60, chamber_temp_kalman_2, 'color', 'blue')
plot(tout_kalman_2/60, filtered_temp_kalman_2, 'color', 'red')
plot(tout_kalman_2/60, peltier_temp_kalman_2, 'color', 'green')
xlabel('Time [min]')
ylabel('Temperature [°F]')
legend('Unfiltered Chamber Temperature', 'Filtered Chamber
Temperature', 'Peltier Temperature')
hold off

% Plot of actuator signal
figure;
hold on
title('Actuator Signal Current Using Kalman Filter, 1st Iteration')
plot(tout_kalman_2/60, actuator_signal_kalman_2, 'color', 'red')
plot(tout_kalman_2/60, actuator_signal_sat_kalman_2, 'color', 'blue')
xlabel('Time [min]')
ylabel('Current [Amps]')
legend('Unregulated', 'Regulated')
hold off
```



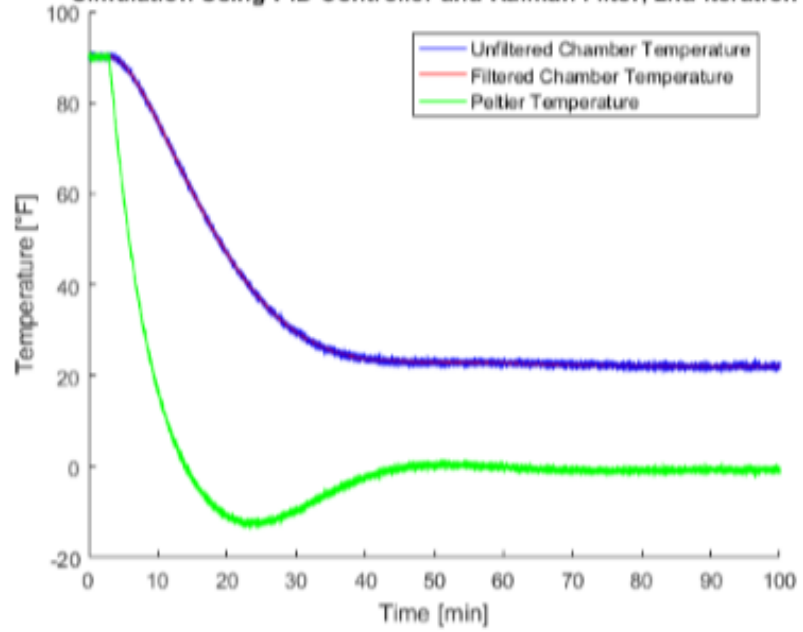
Simulation with Kalman Filter, 2nd Iteration

```
% Plot of inner chamber temperature
figure;
hold on
title('Simulation Using PID Controller and Kalman Filter, 2nd
Iteration')
plot(tout_kalman/60, chamber_temp_kalman, 'color', 'blue')
plot(tout_kalman/60, filtered_temp_kalman, 'color', 'red')
plot(tout_kalman/60, peltier_temp_kalman, 'color', 'green')
xlabel('Time [min]')
ylabel('Temperature [°F]')
legend('Unfiltered Chamber Temperature', 'Filtered Chamber
Temperature', 'Peltier Temperature')
hold off

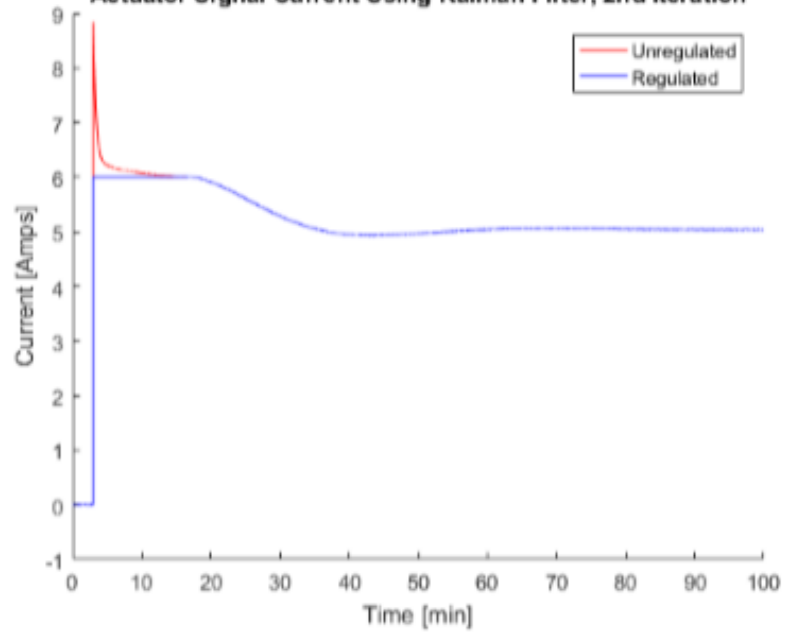
% Plot of actuator signal
figure;
hold on
title('Actuator Signal Current Using Kalman Filter, 2nd Iteration')
plot(tout_kalman/60, actuator_signal_kalman, 'color', 'red')
plot(tout_kalman/60, actuator_signal_sat_kalman, 'color', 'blue')
xlabel('Time [min]')
ylabel('Current [Amps]')
legend('Unregulated', 'Regulated')
hold off

% Plot of kalman gain and predictor gain
% figure;
% hold on
%
% subplot(2,1,1)
% plot(tout_kalman/60, P_k_kalman, 'color', 'red')
% title('Kalman Filter Predictor Gain (P_k)')
% xlabel('Time [min]')
% ylabel('Gain [-]')
%
% subplot(2,1,2)
% plot(tout_kalman/60, K_k_kalman, 'color', 'blue')
% title('Kalman Filter Gain (K_k)')
% xlabel('Time [min]')
% ylabel('Gain [-]')
%
% hold off
```

Simulation Using PID Controller and Kalman Filter, 2nd Iteration



Actuator Signal Current Using Kalman Filter, 2nd Iteration



Comparison

```

% % Comparison between feedback signals subplots
% figure;
% hold on;
%
% subplot(2,2,1)
% plot(tout_original/60,chamber_temp_original,'color','magenta')
% title('Original Feedback Signal')
% xlabel('Time [min]')
% ylabel('Temperature [°F]')
%
% subplot(2,2,2)
% plot(tout_antiwindup/60,chamber_temp_antiwindup,'color','green')
% title('Feedback Signal using Anti-Windup')
% xlabel('Time [min]')
% ylabel('Temperature [°F]')
%
% subplot(2,2,3)
% plot(tout_digital/60,filtered_temp_digital,'color','blue')
% title('Feedback Signal using Digital Filter')
% xlabel('Time [min]')
% ylabel('Temperature [°F]')
%
% subplot(2,2,4)
% plot(tout_kalman/60,filtered_temp_kalman,'color','red')
% title('Feedback Signal using Kalman Filter')
% xlabel('Time [min]')
% ylabel('Temperature [°F]')
%
% hold off;

% Comparison between feedback signals stacked
figure;
hold on
title('Comparison Between Feedback Signals')
plot(tout_original/60,chamber_temp_original,'color','magenta')
plot(tout_antiwindup/60,chamber_temp_antiwindup,'color','green')
plot(tout_digital/60,filtered_temp_digital,'color','blue')
plot(tout_kalman_2/60,filtered_temp_kalman_2,'color','red')
plot(tout_kalman/60,filtered_temp_kalman,'color','black')
xlabel('Time [min]')
ylabel('Temperature [°F]')
legend('Original Feedback signal','Feedback signal using anti-windup
scheme','Feedback signal using digital filter','Feedback signal using
kalman filter, 1st iteration','Feedback signal using kalman filter,
2nd iteration')
hold off

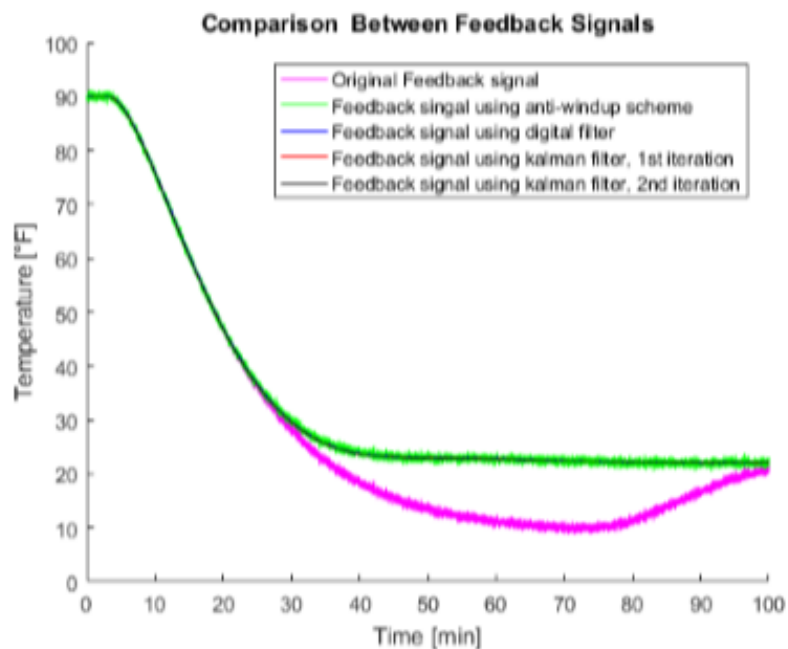
% Comparison between feedback signals stacked zoomed in
figure;
hold on
title('Comparison Between Feedback Signals')

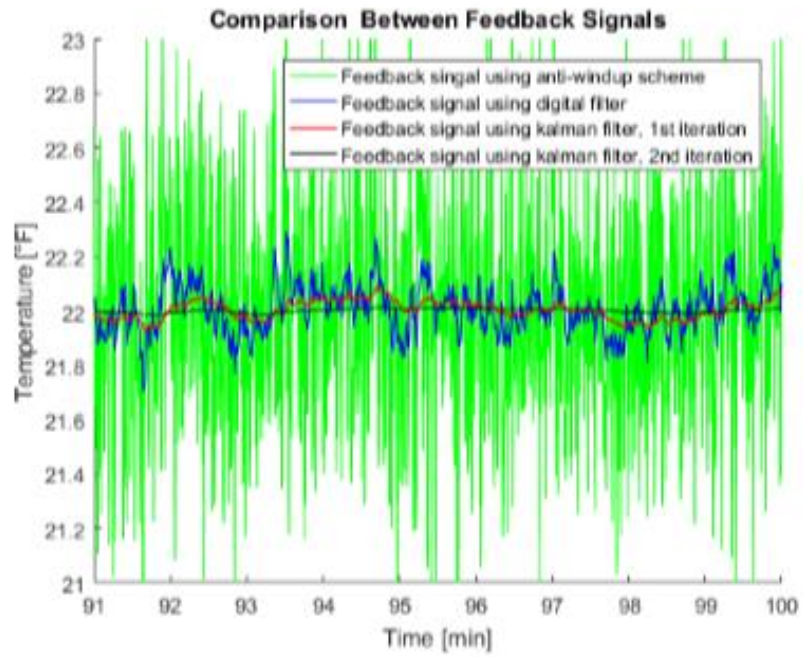
```

```

plot(tout_antiwindup/60, chamber_temp_antiwindup, 'color', 'green')
plot(tout_digital/60, filtered_temp_digital, 'color', 'blue')
plot(tout_kalman_2/60, filtered_temp_kalman_2, 'color', 'red')
plot(tout_kalman/60, filtered_temp_kalman, 'color', 'black')
xlabel('Time [min]')
ylabel('Temperature [°F]')
xlim([(sim_time/60 - 9), (sim_time/60)])
ylim([(desired_temperature - 1), (desired_temperature + 1)])
legend('Feedback singal using anti-windup scheme', 'Feedback signal
using digital filter', 'Feedback signal using kalman filter, 1st
iteration', 'Feedback signal using kalman filter, 2nd iteration')
hold off

```





Published with MATLAB® R2016b

APPENDIX G: FMEA

System / Function	Potential Failure Mode	Potential Effects of the Failure Mode	Severity	Potential Causes of the Failure Mode	Current Preventative Activities	Occurrence	Current Detection Activities	Detection	Priority	Recommended Action(s)	Responsibility	Action Results			
												Actions Taken	Severity	Occurrence	Criticality
Structure / support acts as a seat	Frame ruptures or buckles	User injury from falling over	4	Frame experiences stress greater than rated	robust structure design	1	Structure is no longer sturdy	1	4	Design frame to withstand the average weight of a user	Ryan Gelinias	Tested, structure is sound	4	3	6
Control Module / Spinning Fans	somebody sticks their fingers into the path of the rotating fan blade	injury to fingers or hands	2	easy access to spinning fan blades, room for fingers to interfere	add vent so fingers can't get in	4	Measurement techniques	3	24	Design so intentional injury is impossible	Ryan Gelinias	Tested, nobody has fingers small enough to get into the fan blades. Team will ensure safety by not wearing any dangling jewelry or hood strings.	2	1	4
Structure / Holds entire system in place and portable	Puncture	Cutting and Splintering	8	Stuff falling, or dropping onto structure	make 2 layer walls	1	have a test sample experimented for breakage modes	5	40	Using a test panel and breaking it	Josh DiMaggio	Tested, structure is sound enough to not be prone to break. Styrofoam added to outside, minimizes exposure to corrugate walls in event of failure.	8	3	6
Structure / Holds entire system in place and portable	Lid breakage	Trip and fall over broken lid	6	Hinge mechanism malfunction	Make sure hinge is robust enough	2	sample hinge for breakage	7	84	make an extra handle and break it for testing	Ryan Gelinias	Designed without a hinge.	6	1	1

APPENDIX H: Safety Hazard Checklist

DESIGN HAZARD CHECKLIST

Team: TEAM FREEZE 2-1 Advisor: ELGHANDOUR Date: 3-1-18

- | Y | N | |
|-------------------------------------|-------------------------------------|--|
| <input type="checkbox"/> | <input checked="" type="checkbox"/> | 1. Will the system include hazardous revolving, running, rolling, or mixing actions? |
| <input type="checkbox"/> | <input checked="" type="checkbox"/> | 2. Will the system include hazardous reciprocating, shearing, punching, pressing, squeezing, drawing, or cutting actions? |
| <input type="checkbox"/> | <input checked="" type="checkbox"/> | 3. Will any part of the design undergo high accelerations/decelerations? |
| <input checked="" type="checkbox"/> | <input type="checkbox"/> | 4. Will the system have any large (>5 kg) moving masses or large (>250 N) forces? |
| <input type="checkbox"/> | <input checked="" type="checkbox"/> | 5. Could the system produce a projectile? |
| <input type="checkbox"/> | <input checked="" type="checkbox"/> | 6. Could the system fall (due to gravity), creating injury? |
| <input type="checkbox"/> | <input checked="" type="checkbox"/> | 7. Will a user be exposed to overhanging weights as part of the design? |
| <input type="checkbox"/> | <input checked="" type="checkbox"/> | 8. Will the system have any burrs, sharp edges, shear points, or pinch points? |
| <input type="checkbox"/> | <input checked="" type="checkbox"/> | 9. Will any part of the electrical systems not be grounded? |
| <input type="checkbox"/> | <input checked="" type="checkbox"/> | 10. Will there be any large batteries (over 30 V)? |
| <input type="checkbox"/> | <input checked="" type="checkbox"/> | 11. Will there be any exposed electrical connections in the system (over 40 V)? |
| <input type="checkbox"/> | <input checked="" type="checkbox"/> | 12. Will there be any stored energy in the system such as flywheels, hanging weights or pressurized fluids/gases? |
| <input type="checkbox"/> | <input checked="" type="checkbox"/> | 13. Will there be any explosive or flammable liquids, gases, or small particle fuel as part of the system? |
| <input type="checkbox"/> | <input checked="" type="checkbox"/> | 14. Will the user be required to exert any abnormal effort or experience any abnormal physical posture during the use of the design? |
| <input checked="" type="checkbox"/> | <input type="checkbox"/> | 15. Will there be any materials known to be hazardous to humans involved in either the design or its manufacturing? |
| <input type="checkbox"/> | <input checked="" type="checkbox"/> | 16. Could the system generate high levels (>90 dBA) of noise? |
| <input checked="" type="checkbox"/> | <input type="checkbox"/> | 17. Will the device/system be exposed to extreme environmental conditions such as fog, humidity, or cold/high temperatures, during normal use? |
| <input type="checkbox"/> | <input checked="" type="checkbox"/> | 18. Is it possible for the system to be used in an unsafe manner? |
| <input checked="" type="checkbox"/> | <input type="checkbox"/> | 19. For powered systems, is there an emergency stop button? |
| <input type="checkbox"/> | <input checked="" type="checkbox"/> | 20. Will there be any other potential hazards not listed above? If yes, please explain on reverse. |

For any "Y" responses, add (1) a complete description, (2) a list of corrective actions to be taken, and (3) date to be completed on the reverse side.

Description of Hazard	Planned Corrective Action	Planned Date	Actual Date
THE STRUCTURE NEEDS TO SUPPORT AT LEAST 400lb.	THE STRUCTURE WILL BE MADE OUT OF CORRUGATED FIBERGLASS THAT CAN SUPPORT ~ 250,000 lbs.	5-15-18	
ORGANIC MATERIALS MAY BE USED TO MAKE THE STRUCTURE, WHICH CAN BE TOXIC	THE CORRUGATION PROCESS WILL MAKE THE TOXIC MATERIALS SAFE FOR THE USER AND THE ENVIRONMENT.	5-15-18	
HIGH ELECTRIC CURRENTS WILL BE INVOLVED IN THE DESIGN,	A SAFETY TASK WILL BE INCLUDED IN THE CONTROL TO STOP THE CURRENT FLOW.	5-15-18	
THE HEAT SINKS COULD BECOME VERY HOT.	CPU FANS WILL BE USED TO COOL THE HEAT SINKS TO PREVENT INJURY.	5-15-18	

APPENDIX I: Risk Assessment

designsafe Report

Application: Thermoelectric Cooler Risk Assessment
 Description:
 Product Identifier:
 Assessment Type: Detailed
 Limits:
 Sources:
 Risk Scoring System: ANSI B11.0 (TR3) Two Factor
 Guide sentence: When doing [task], the [user] could be injured by the [hazard] due to the [failure mode].

Analyst Name(s): Zach Wilson, Josh Dimaggio, Ryan Gelinás, Cassie Beck
 Company: California Polytechnic State University
 Facility Location: 1 Grande Ave, San Luis Obispo, CA

Item Id	User / Task	Hazard / Failure Mode	Initial Assessment		Risk Reduction Methods /Control System	Final Assessment		Status / Responsible /Comments /Reference
			Severity Probability	Risk Level		Severity Probability	Risk Level	
1-1-1	operator Common tasks	electrical / electronic : energized equipment / live parts Exposed wires	Catastrophic Unlikely	Medium	Insulate all wires and properly wire components to ground	Catastrophic Remote	Low	TBD [6/11/2018] Zach Wilson
1-1-2	operator Common tasks	electrical / electronic : overvoltage /overcurrent power surge	Catastrophic Unlikely	Medium	Insulate all wires and properly wire components to ground	Catastrophic Remote	Low	TBD [6/11/2018] Zach Wilson
1-1-3	operator Common tasks	fire and explosions : hot surfaces Heat sinks reach unsafe temperatures	Moderate Unlikely	Low	Properly cover heat sinks	Moderate Remote	Negligible	TBD [6/11/2018] Ryan Gelinás
1-1-4	operator Common tasks	heat / temperature : severe cold Heat sinks reach unsafe temperatures	Moderate Unlikely	Low	Properly cover heat sinks	Moderate Unlikely	Low	TBD [6/11/2018] Cassie Beck
1-2-1	operator normal operation	electrical / electronic : overvoltage /overcurrent Power surge	Moderate Unlikely	Low	Pick reliable current drivers	Moderate Unlikely	Low	In-process Zach Wilson
1-3-1	operator clean up	electrical / electronic : water / Minor wet locations Cooler not perfectly sealed	Minor Likely	Low	Seal composites thoroughly with epoxy	Minor Remote	Negligible	In-process Ryan Gelinás
1-4-1	operator load / unload materials	mechanical : crushing Structural failure	Serious Remote	Low	Design structure with a high factor of safety	Serious Remote	Low	In-process Josh Dimaggio

Item Id	User / Task	Hazard / Failure Mode	Initial Assessment		Risk Reduction Methods /Control System	Final Assessment		Status / Responsible /Comments /Reference
			Severity Probability	Risk Level		Severity Probability	Risk Level	
1-4-2	operator load / unload materials	mechanical : cutting / severing Sharp edges	Minor Likely	Low	Deburr all edges, smooth surfaces	Minor Likely	Low	In-process Josh Dimaggio
2-1-1	electrician / controls technician repair / replace wiring / systems	electrical / electronic : improper wiring Wires not wired up correctly	Catastrophic Remote	Low	Wire the electronics properly	Catastrophic Remote	Low	TBD [6/11/2018] Cassie Beck
2-1-2	electrician / controls technician repair / replace wiring / systems	electrical / electronic : overvoltage /overcurrent Wrong wire connected to ground or power surge	Catastrophic Unlikely	Medium	Wire electronics properly, pick reliable current drivers	Catastrophic Unlikely	Medium	TBD [6/11/2018] Ryan Gelinás
2-2-1	electrician / controls technician troubleshooting	electrical / electronic : unexpected start up / motion Improper control law	Catastrophic Unlikely	Medium	Design proper control law and finite-state-machine	Catastrophic Unlikely	Medium	TBD [6/11/2018] Zach Wilson
2-3-1	electrician / controls technician grounding panels / controls / machinery	electrical / electronic : energized equipment / live parts Exposed wires	Catastrophic Unlikely	Medium	Insulate all wires and properly wire components to ground	Catastrophic Unlikely	Medium	TBD [6/11/2018] Zach Wilson
2-3-2	electrician / controls technician grounding panels / controls / machinery	electrical / electronic : shorts / arcing / sparking Exposed wires	Serious Unlikely	Medium	Insulate all wires properly	Serious Unlikely	Medium	TBD [6/11/2018] Cassie Beck
2-4-1	electrician / controls technician install / test / repair circuit	electrical / electronic : lack of grounding (earthing or neutral) Improper wire connection	Catastrophic Remote	Low	Properly solder wires and ensure that wires are connected properly	Catastrophic Remote	Low	TBD [6/11/2018] Josh Dimaggio
2-5-1	electrician / controls technician adjust controls	heat / temperature : severe heat Fan failure	Moderate Likely	Medium	Design automatic shutoff for when components fail	Moderate Likely	Medium	TBD [6/11/2018] Cassie Beck
3-1-1	passer by / non-user walk near machinery	slips / trips / falls : trip Cooler is placed in busy location	Minor Likely	Low	Design structure so the cooler is stable and will not topple over	Minor Likely	Low	In-process Ryan Gelinás

APPENDIX J: Operators' Manual

Portable Thermoelectric Refrigerator Operator's Manual

This refrigerator has been designed to plug into a 24 volt DC power supply. This cooler should not be used with a power supply that is providing more than 24 volts rated at 20 amps. The power supply can be seen in Figure 1.



Figure 1. Picture of the power supply.

The refrigerator can be controlled with an app on your phone. The user interface can be seen in Figure 1. The refrigerator is turned on using the "toggle" button and the temperature can be changed using the "+/-" buttons on the screen. The lowest selectable temperature for the cooler is 22 degrees Fahrenheit, as limited by the peltier efficiency. Download the Simblee app that is available for both iOS and Android systems. To connect to the cooler, open the Simblee app and select the sketch labeled "TEC".

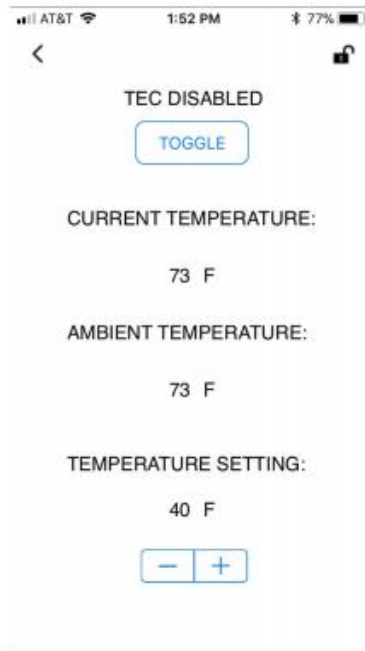


Figure 2. Picture of user interface within app.

APPENDIX K: Design Verification Plan & Report

Senior Project DVP&R													
Date: 10/17/18		Team: Team Freeze		Sponsor: Monaero		Description of System: Thermoelectric Freezer				DVP&R Engineer: Cassie Beck, Josh Diamglio, Ryan Gelinas, Zach Wilson			
TEST PLAN							TEST REPORT						
Item No	Specification #	Test Description	Acceptance Criteria	Test Responsibility	Test Stage	SAMPLES TESTED		TIMING		Test Result	TEST RESULTS		NOTES
						Quantity	Type	Start date	Finish date		Quantity Pass	Quantity Fail	
1	N/A	Thermal conductivity test for various insulation materials	<0.05W/m-K	Zach and Cassie	Complete	4	Rice Fluffs, Foam, Aerogel, Silicone epoxy	4/4/18	5/1/18	0.03W/m-K for aerogel	1	3	
2	N/A	Thermal Conductivity test of composite wall	<0.035W/m-K	Zach	Complete	2	Air and Aerogel	5/24/18	5/24/18	Aerogel Better	1	1	
3	N/A	Compression test on corrugated structure	>300lbs	Josh	Complete	2	Compression and Bending	4/30/18	4/30/18	6000lb compression 40lb bending	1	1	
4	N/A	Electronics Testing	Accurate temperature control	Zach	Planned	1	Circuitboard	11/12/18	11/26/18	Short Detected	0	1	Final Design run without PCB. Attached to 2 power supplies and
5	N/A	Overall Cooler Testing	Inner chamber can reach 32°F	All	Complete	1	Refrigerator	11/14/18	11/16/18	28°F reached	1	0	

APPENDIX L: Gantt Chart

